ANL-HEP-PR-99-102
October 26, 1999

THE TRIANGLE ANOMALY IN TRIPLE-REGGE LIMITS *

Alan. R. White†

High Energy Physics Division
Argonne National Laboratory
9700 South Cass, Il 60439, USA.

Abstract

Reggeized gluon interactions due to a single quark loop are studied in the full triple-regge limit and in closely related helicity-flip helicity-pole limits. Triangle diagram reggeon interactions are generated that include local axial-vector effective vertices. It is shown that the massless quark U(1) anomaly is present as an infra-red divergence in the interactions generated by maximally non-planar Feynman diagrams.

A multi-regge asymptotic dispersion relation formalism is developed which provides a systematic counting of anomaly contributions. The 48 triple discontinuities in the dispersion relation are of two kinds. The first kind are to one-particle inclusive cross-sections. The second kind contains the anomaly and the multi-regge theory has some special features, including a signature conservation rule. It is shown that the anomaly is present only in multiple discontinuities obtained from the maximally non-planar diagrams and that in the scattering of elementary quarks or gluons the signature and color parity of the exchanged reggeon states are such that the anomaly cancels.

In more complicated scattering processes the anomaly need not cancel. Color parity is not conserved by vertices containing the anomaly and only anomalous color parity reggeon states are coupled. The extraction of a potential hadronic regge region S-Matrix, via the infra-red divergent amplitudes that appear when an anomalous color parity regggeon condensate is introduced, is briefly discussed.

*Work supported by the U.S. Department of Energy, Division of High Energy Physics, Contracts W-31-109-ENG-38 and DEFG05-86-ER-40272

†arw@hep.anl.gov

1. INTRODUCTION

The purpose of this paper is to demonstrate that in massless QCD certain reggeized gluon interactions contain an infra-red divergence that can be understood as the infra-red appearance[1] of the U(1) quark anomaly. Although, of course, QCD contains only vector interactions, in multi-regge limits effective vertices are generated by quark loops which involve products of γ-matrices. The full triple-regge limit[‡] is sufficiently intricate (as are the helicity-flip helicity-pole limits that we also study) that both the axial-vector couplings and the orthogonal momenta, needed to generate the triangle anomaly, are present. Since triple-regge vertices appear as components in a wide array of multi-regge reggeon diagrams[3], this is a potential new infra-red manifestation of the U(1) anomaly, in a dynamical role !

We present direct calculations showing that the anomaly is indeed present in the (six-reggeon) triple-regge interaction vertex obtained from particular "maximally non-planar" Feynman diagrams that appear in three-to-three quark scattering[§]. However, since the infra-red anomaly is produced by chirality violating massless quark states, we expect that it will cancel, as a single reggeon interaction, in any scattering process that is helicity conserving and has only perturbative QCD ingredients for all accompanying interactions. Therefore, a first step in determining the possible dynamical role of the anomaly has to be a general understanding of such cancelations. In effect, this is the major focus of this paper.

Since multi-reggeon "states" are virtual, exchanged, configurations that do not directly produce particle states, the chirality violation associated with the anomaly does not produce any immediate conflict that requires a cancelation within a reggeon vertex. Rather such cancelations are secondary effects within the full scattering process that have to be traced. The number of Feynman diagrams contributing to even the lowest-order three-to three quark scattering processes of the kind we study is very large ($O(100)$). Therefore, even though we make no attempt to calculate the full reggeon interaction vertex, a-priori, understanding diagrammatically when the anomaly appears, and how and when the necessary cancelations take place, appears difficult, if not impossible. Fortunately, we are able to systematically count all anomaly contributions by using the multi-regge asymptotic dispersion relation formalism developed in [5] and [6]. This formalism allows us to reconstruct the full amplitude as a relatively simple sum over triple-regge multiple discontinuities.

[‡]This is a limit of three-to-three scattering amplitudes[2], not to be confused with the incorrectly named "triple-regge" limit of the one-particle inclusive cross-section that is actually a "non-flip helicity-pole" limit.

[§]In a companion paper[4] we present an abbreviated version of the central calculation together with a very brief overview of other arguments in this paper.

We then determine that the anomaly can only be present in multiple discontinuities obtained from the maximally non-planar diagrams. In addition, the multiple discontinuities in which the anomaly appears form only signatured amplitudes that satisfy an important signature conservation rule. (In the final Section we discuss why we expect this rule to lead, in hadronic reggeon diagrams, to the even signature of the pomeron.) Consequently, the study of cancelations reduces to a straightforward discussion of signature and the symmetry properties of color factors. We can then show that, in general, when the initial and final states are elementary quarks or gluons, the quantum numbers of the exchanged reggeized gluon states, in the triple-regge limit, are such that the anomaly does indeed cancel. (At lowest-order it actually cancels in individual diagrams after the transverse momentum integrations are performed.)

Because the reggeon vertices containing the anomaly satisfy a signature conservation rule, the presence of chirality violation within a vertex requires an accompanying non-conservation of color parity. In the low-order case we study, and we expect generally, for the anomaly to not cancel each of the coupled reggeon states must carry "anomalous" color parity (i.e. not equal to the signature). This places extensive restrictions on the amplitudes in which the anomaly vertices can appear. Cancelation can be avoided if additional particles are produced in each of the scattering states. In this case, and more generally, the presence of reggeon Ward identity zeroes in the external reggeon couplings compensates for the divergent anomaly vertices and prevents the divergence of the full amplitude. The anomaly does produce divergences if some external couplings are chosen so that corresponding Ward identity zeroes are absent. An anomalous color parity "reggeon condensate" (with the quantum numbers of the winding-number current[¶]) can be introduced this way in initial reggeon scattering states. A major component of the program we previously outlined[3] was to show that, in a color superconducting phase, such a condensate is consistently reproduced in all produced reggeon states by the anomaly infra-red divergences. In [3] we assumed the existence of the anomaly that, in this paper, we demonstrate the existence of. While the properties we assumed were essentially correct there are (as we briefly touch upon in Section 7) significant differences. Once we have understood the full structure of the anomaly we hope to implement our previously outlined program in detail, in future papers.

Regge limits have the virtue that, since high-energy is involved, they are a-priori close to perturbation theory at large transverse momentum. Conversely, in the infra-red transverse momentum region, the constraints imposed by analyticity and t-channel unitarity are very strong[5, 7]. In this region we might well expect the need for a non-perturbative modification of the theory to become apparent as well as, perhaps, the form this modification should take. Many calculations[8]-[14]

[¶]Note that this "condensate" is actually a "wee-parton" contribution in a physical reggeon state, rather than a vacuum condensate. Consequently, it need not be parity violating, as a true vacuum winding-number condensate surely would be.

have shown that in perturbation theory (when gluons and quarks are massive) these constraints are satisfied in an elegant and minimal manner by reggeon diagrams in which gluons and quarks are reggeized. In essence, our program is to start with the perturbative regge region solution of unitarity and show that, in the massless theory, infra-red divergences produce a transition to reggeon diagrams containing hadrons and the Reggeon Field Theory (RFT) critical pomeron[15]. As an intermediate stage, we construct a color superconducting phase (with the gauge symmetry broken from SU(3) to SU(2)) in which the reggeon condensate is present. Since the chirality violation involved in the anomaly divergence is qualitatively the same as that occurring in instanton interactions, it is clear that this divergence can anticipate the presence of "non-perturbative" physics in regge region interactions. Nevertheless if we successfully obtain a unitary (reggeon) S-Matrix, as we hope, it will be very close to perturbation theory, with the non-perturbative properties of confinement and chiral symmetry breaking a consequence of the anomaly only.

We give a brief description of our program at the end of Section 7, together with some short remarks on the physics that might be involved in Section 8. Apart from this we will not discuss at all the dynamical role of the anomaly divergences in this paper. Instead we will focus entirely on the technical problem of studying the asymptotic behavior of Feynman diagrams, setting up the necessary multi-regge formalism, and isolating the occurrence of the anomaly. We would like to emphasize that we have organized the paper in a manner that we hope will allow a reader to extract some general understanding of our results without necessarily absorbing all of the underlying multi-regge theory. Section 2 is a general outline of the purpose of the paper and a summary of it's contents that, as far as possible, avoids technical language. Section 3 describes the triple-regge and related helicity-pole limits in terms of light-cone variables. Section 4 is devoted to the calculation, using light-cone coordinates, of triple-regge contributions from three specific diagrams. This allows us to illustrate how the anomaly occurs as an infra-red divergence of reggeon vertices. We concentrate on the kinematic structure of diagrams and ignore color factors until we have set up the necessary machinery to discuss cancelations. We study one diagram that obviously does not contain the anomaly, one that might have anomaly contributions but actually does not and one, a maximally non-planar diagram, that does. At the end of the Section we discuss how the anomaly contributions from maximally non-planar diagrams cancel in various circumstances. In Section 5 we begin the development of the asymptotic dispersion relation and multi-regge formalism that ultimately allows us to systematically discuss all anomaly contributions. In Section 6 we study the complete set of double discontinuities and conclude that only those originating from maximally non-planar diagrams contain the anomaly. We finally discuss the role of color factors in cancelations in Section 7. We then briefly discuss diagrams which contain anomaly contributions that we do not expect to be canceled and outline how divergences can be produced.

2. OUTLINE AND SUMMARY

The triple-regge limit[2] (and closely related helicity-flip helicity-pole limits) can be formulated as the high-energy, near-forward, scattering of three particles carrying light-like momenta P_1, P_2 and P_3 whose spacelike components are orthogonal to each other. This limit (defined precisely in the next Section) is discussed in [3] for some simple diagrams but otherwise has not been discussed in QCD. In this paper we will study Feynman diagrams of the kind illustrated in Fig. 2.1 in which the three particles scatter via gluon interactions involving a single quark loop - the solid circle.

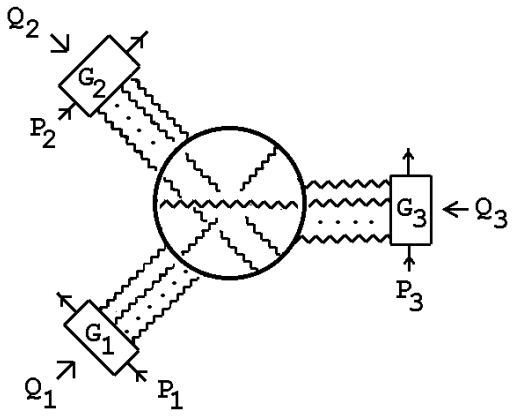

Fig. 2.1 The Class of Feynman Diagrams Studied

In most of our discussion the scattering particles will be single quarks and the couplings G_1, G_2 and G_3 will be the lowest-order elementary couplings. However, in discussing anomaly cancelations we will also allow these couplings to have more general properties, including the production (or absorption) of additional particles.

The quark loop initially contains a sufficiently large number of quark propagators that there are no ultra-violet divergences. At finite momentum, this loop also has no infra-red divergences, even when the quark mass is zero. The triangle Landau singularities that play a role in our discussion of the anomaly will be present but, because of the absence of local axial vector couplings in the finite momentum theory, will not produce divergences. If the gluons are massive, the gluon loops also have no divergence problems. For simplicity, we will set the gluon mass to zero. (This means that the diagrams we study will formally have infra-red divergences at zero gluon transverse momentum. These divergences are only relevant when we discuss our dynamical program at the end of Section 7. We will ignore them in the main body of the paper.)

In the triple-regge limits we consider the most important contributions come

from regions of the gluon loop integrations where a number of the propagators in the quark loop, and the scattering quark systems, are (to logarithmic accuracy) on-shell. Using the poles in these propagators to carry out light-cone (longitudinal) momentum integrations the integrals over gluon loop momenta reduce to two-dimensional "transverse momentum" integrals. (Alternatively, as we will discuss in later Sections, in a dispersion relation calculation the propagators are put on-shell by taking a multiple discontinuity.)

We will be particularly interested in those diagrams for which, with appropriate quantum numbers in the t_i $(= Q_i^2)$ channels, all the relevant quark lines are precisely on-shell in the leading contribution (i.e. the longitudinal integrations do not generate any logarithms of the large momenta.) In this case the leading contribution has the form

$$P_{1+}\ P_{2+}\ P_{3+}\ \prod_{i=1}^{3}\int \frac{d^2k_{i1}d^2k_{i2}\ \cdots\delta^2(Q_i-k_{i1}-k_{i2}-\cdots)\ G_i(k_{i1},k_{i2},\cdots)}{k_{i1}^2k_{i2}^2\ \cdots} \times\ R(Q_1,Q_2,Q_3,k_{11},k_{12},\cdots) \tag{2.1}$$

If we rewrite the large momentum factor as

$$P_{1+}\ P_{2+}\ P_{3+}\ \sim\ S_{12}^{1/2}\ S_{23}^{1/2}\ S_{31}^{1/2} \tag{2.2}$$

where $S_{ij} = (P_i+P_j)^2$, this is the lowest-order triple-regge behavior for the amplitudes that interest us (and, in particular, contain the anomaly) when the regge singularities in each channel have unit intercept. Consequently, the transverse momentum integrations, together with the gluon propagators and the external couplings G_i, are straightforwardly interpreted as the leading-order contribution of multi-reggeon states in which each gluon is regarded as a lowest-order reggeon. As illustrated in Fig. 2.2 for scattering quarks,

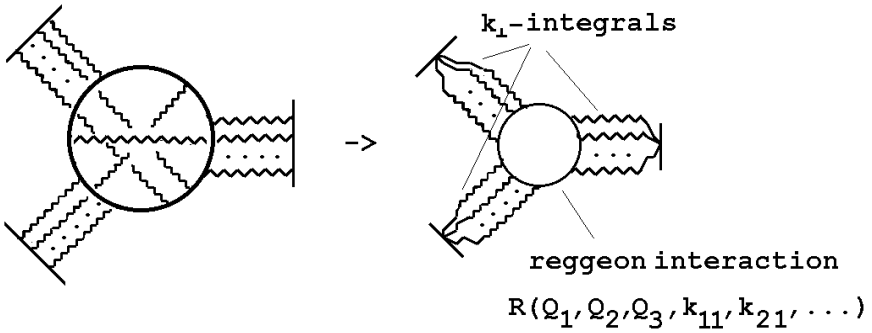

Fig. 2.2 Generation of a Reggeon Vertex

$R(Q_1, Q_2, Q_3, k_{11}, k_{21}, \cdots)$ can then be extracted[‖] as a "reggeon interaction vertex". This vertex will appear in the reggeon diagrams describing a wide range of high-energy multi-regge processes[3]. Therefore it's general structure is very important. In particular any divergences that are present may have a dynamical significance going far beyond the circumstances in which they are initially discovered.

When logarithms of the P_{i+} are absent, one propagator in the quark loop is placed on-shell for each gluon loop integration. As a result, the reggeon vertex contains a reduced quark loop in which only three of the original loop propagators are off-shell. The effective vertices (produced by the longitudinal integrations) in general contain local and non-local components. The local components are products of γ matrices that, in some cases, reduce to $\gamma_5\gamma$ couplings. Clearly, if there is an odd number of γ_5's then, a-priori, the U(1) triangle anomaly could be present in the reduced loop. Intrinsically, reggeon diagrams are most unambiguously defined at low transverse momentum. Therefore, we look for the infra-red manifestation of the anomaly as a divergence that is present when the quark mass vanishes[1]. Such a divergence indicates that the triangle Landau singularities of the quark loop are enhanced by the triple-regge limit.

Analyticity properties of reggeon vertices imply that if the anomaly is present as an infra-red effect then it should also be present as an ultra-violet effect when the quark mass is non-zero. This is potentially a more serious problem. As discussed in [3], the presence of the ultra-violet anomaly implies that the power behavior of diagrams is enhanced beyond the naive power counting arising from gluon exchange, ultimately giving a violation of unitarity. To remove this problem additional non-perturbative (instanton?) interactions must be present. In fact, as also outlined in [3], we believe that the presence of such interactions can be anticipated by Pauli-Villars regularization of the ultra-violet anomaly. We expect that, with the regularizing massive fermions present, a unitary physical theory can be constructed in the zero quark mass limit, from reggeon diagrams that contain an overall infra-red divergence due to anomaly interactions. We give some brief details of this procedure[**] at the end of Section 7. A full description, utilizing properties of the anomaly described in this paper, will be the subject of future papers. Our purpose in this paper is simply to demonstrate the presence of the anomaly and to study when it does or does not cancel. The ultra-violet region of the integrals in reggeon vertices is surely a very complicated place to look for the anomaly. Consequently, we will look only for it's presence in the infra-red region.

[‖] We should mention that the absence of logarithms of the P_{i+} (and fixing color quantum numbers) does not always determine the reggeon states involved. In particular, a pair of gluons in a t-channel color octet state may give the lowest-order contribution of either a two reggeized gluon state or an even signature reggeon.

[**] Note that this procedure would explicitly break supersymmetry if it were applied to a SUSY gauge theory.

Gauge-invariance will, of course, relate diagrams of the form of Fig. 2.1 to other diagrams involving the triple-gluon coupling. Although we will make brief references to such diagrams, we will make no attempt to give complete expressions for reggeon vertices corresponding to the set of all diagrams of a fixed-order. Rather we will concentrate first on demonstrating the presence of the anomaly in contributions from particular diagrams and then on finding circumstances in which it does not cancel. Since the infra-red divergence we are looking for requires[1] a triangle Landau singularity generated by a quark loop, diagrams of the kind we have isolated are the important ones. Most of our discussion will be concerned with the simplest diagrams of this kind, i.e. those of the form of Fig. 2.1 in which, as illustrated in Fig. 2.3, the particle states that are scattering are quarks and there are just two-gluons exchanged in each t-channel.

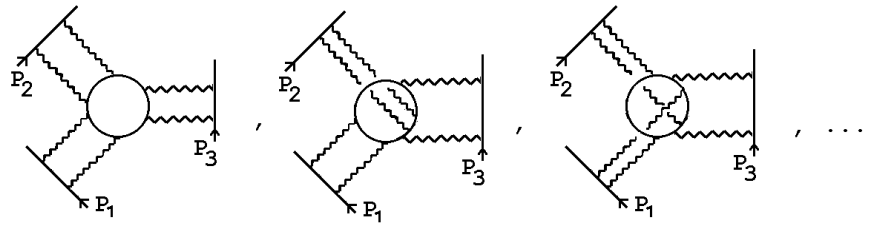

Fig. 2.3 Quark Scattering Diagrams with Two Gluons in each t_i-channel.

This simplest set already contains $O(100)$ distinct diagrams and so it is clear that even if we limit ourselves to searching for particular kinds of contributions, it is likely that counting all possibilities will be a very difficult thing to do unless we have a very systematic procedure.

The use of light-cone co-ordinates, together with the evaluation of longitudinal integrals by putting propagators on-shell, is the most popular method for studying regge limits. In practise, the justification for which propagators are put on-shell requires a careful discussion of the closing of integration contours in the complex plane. In fact many Feynman diagrams give interaction vertices which will vanish as higher-order reggeization effects appear because an integration contour, for which all singularities of the integrand lie in a half-plane, can be closed to zero. (We are referring here to diagrams which have insufficient non-planarity to produce the relevant "double-spectral function" property that is needed for regge cut couplings.) A well-known alternative procedure is to use a dispersion relation formalism[8] which begins with discontinuities in which many of the relevant lines are specifically on-shell. The dispersion relation formalism generally has the advantage (particularly in a gauge theory) that fewer diagrams need to be calculated. Also, once the regge behavior of the gauge theory is established, the close relationship between the structure of regge amplitudes and unitarity can be exploited[13] to short-cut direct calculations. The dispersion relation approach has the disadvantage that a cancelation which manifests

itself via the closing of a contour in the direct diagrammatic approach can appear as a more elaborate cancellation between different discontinuities, dependent on signature and quantum number properties.

In lowest-order there is usually a close and obvious relationship between the two methods. In higher orders the relationship is more subtle. Logarithms of external large momenta are produced by lines that are close to on-shell (rather than on-shell) in the light-cone method whereas in the dispersion method they are produced by the divergence of dispersion integrals. In our case we are interested in the low-order behavior of a large number of relatively complicated diagrams. A complete analysis based on the the closing of longitudinal momentum contours would be very difficult, if not impossible, given the complexity of the diagrams and the number involved. Fortunately, a generalization of the dispersion method can be used. The asymptotic dispersion relation formalism developed in [5] and [6] provides a fundamental basis for calculating triple discontinuities and assembling them to form the complete amplitude. We will see that the structure of multiple discontinuities is relatively simple and that the problem of counting contributions from all diagrams becomes straightforward. Also, when the amplitude is Regge-behaved the relationship between discontinuities and the full amplitude involves only (multiple) signature factors. If we are not interested in isolating the logarithms which build up the full multi-Regge behaviour, but only interested in isolating components of the lowest-order reggeon interaction vertices, it is relatively simple to use multiple discontinuities directly.

As we stated in the Introduction, we have tried to organize the paper in a manner which will allow a reader to extract some general understanding of our results without necessarily absorbing all of the underlying multi-regge theory. Consequently we begin, in Section 3, by formulating the triple-regge limits we discuss in terms of light-cone kinematics. As a result, we are able, in Section 4, to initially discuss some diagrams directly in terms of light-cone co-ordinate calculations without developing the multiple discontinuity formalism. This allow us to illustrate how the anomaly occurs. We study all three diagrams shown explicitly in Fig. 2.3. As described in Appendix A, the anomaly appears as an infra-red divergence of the triangle diagram when an odd number of axial-vector couplings is present and a combination of one lightlike momentum and additional spacelike momenta flow through the diagram - with the spacelike momenta scaled uniformly to zero. The first diagram of Fig. 2.3, fairly obviously, does not contain the anomaly since it generates only vector effective vertices. The second diagram contains a γ_5 effective vertex, but the necessary light-like momentum can not flow through the diagram. This illustrates the general point that, while several diagrams generate quark triangle reggeon vertices with the necessary effective axial-vector couplings, in most cases the longitudinal integrations produce additional effects that either prevent the occurence of the divergence, or lead to a cancelation.

The third diagram of Fig. 2.3 actually gives more than one reggeon interaction

contribution containing the anomaly. When this diagram is redrawn as in Fig. 2.4, it is clear that it has a "maximally non-planar" property.

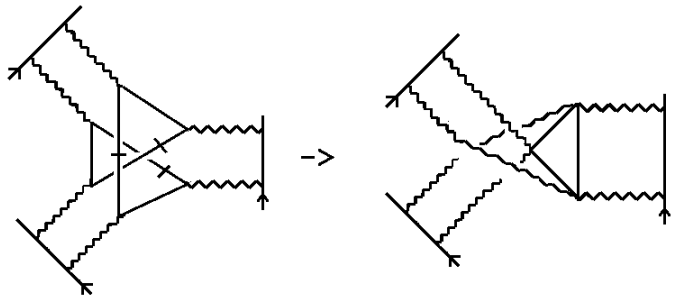

Fig. 2.4 The Simplest Diagram with an Anomaly Contribution.

(The couplings to the quark loop by the two gluons in the same t-channel are separated, in both directions around the loop, by couplings to gluons in the other two t-channels.) As we already alluded to above, this non-planarity property is ncessary to ensure that such diagrams unambiguously contribute to regge cut vertices and do not cancel as higher-order reggeization effects are included. When the hatched lines are placed on-shell by the gluon loop longitudinal integrations a reggeon interaction is generated as shown. The local coupling component of the interaction vertex obtained (using special light-cone co-ordinates of the kind discussed in Appendix B) is shown in Fig. 2.5.

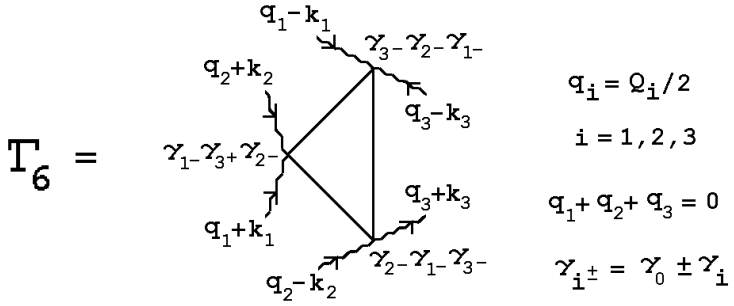

Fig. 2.5 A Triangle Diagram Reggeon Interaction.

It is straightforward (if lengthy) to show that the necessary γ_5 couplings are present in the products of γ-matrices shown and that the necessary light-like momentum flows through the diagram if the limit

$$(q_1+k_1+q_2+k_2)^2 \ \sim \ (q_2-k_2+q_3+k_3)^2 \ \sim \ (q_1-k_1+q_3-k_3)^2 \ \sim \ \mathbf{q}^2 \ \to 0 \quad (2.3)$$

is taken with

$$(q_1-k_1)^2 \ \sim \ (q_2-k_2)^2 \ \to \ 0 \ , \qquad (2.4)$$

and

$$(q_1 + k_1)^2 \ \rightarrow \ (q_2 + k_2)^2 \ \neq \ 0 \ , \quad (q_3 - k_3)^2 \ \rightarrow \ 2(q_3 + k_3)^2 \ \neq \ 0 \qquad (2.5)$$

The anomaly divergence has the form

$$\Gamma_6 \ \sim \ \frac{q_3^2}{q} \qquad (2.6)$$

The kinematics (2.3) and (2.5) are sufficient for the divergence to appear in the full triple-regge vertex. For it to appear in the single helicity-amplitude that is isolated by an additional helicity-flip helicity-pole limit it is necessary to take $(q_1 + k_1)^2 = (q_2 + k_2)^2 \ \rightarrow 0$.

That the divergences occurs at $(q_1 - k_1)^2 \ = \ (q_2 - k_2)^2 \ = \ 0$ implies that it will mix with other infra-red divergence effects. However, as we noted above and discuss further in Appendix A, an infra-red "non-renormalization theorem" implies that it can only be canceled by interactions that also contain the same quark loop anomaly divergence. The effects of the reggeon interaction divergence can also be modified by the occurrence of reggeon Ward identity zeroes[3] in the external couplings G_1,G_2 and G_3 since these occur at $(q_1 - k_1)^2 \ = \ 0 \ , \ (q_2 - k_2)^2 \ = \ 0 \ , \ \ldots$.

Note that, in the diagram of Fig. 2.4, we could equally well place on-shell the lines that are hatched in the diagram of Fig. 2.6.

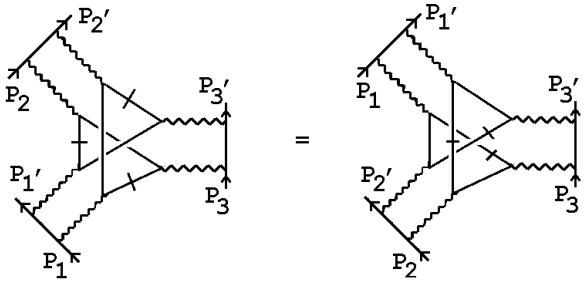

Fig. 2.6 An Alternative Set of On-shell Lines.

As we have shown in the figure, this new set of hatched lines can be related back to the original set simply by interchanging the role of P_1 and P_2. Obviously, this configuration must also give a reggeon interaction containing the anomaly. As we discuss in Appendix A, the interchange of the roles of 1 and 2 leads to a change of sign of the anomaly (due to the antisymmetry of the ϵ-tensor produced by the chirality violation). Since the large momentum factors do not change sign in going from Fig. 2.4 to Fig. 2.6, if the color factors are appropriately symmetric then we expect a cancelation between the two anomaly contributions. In fact the remaining gluon loop integrations also have some symmetry. When the external couplings G_1,

G_2 and G_3 are the lowest-order couplings that appear in the diagrams of Figs. 2.4 and 2.6, the appropriate symmetries are present in individual diagrams. More generally, we can allow the G_1, G_2 and G_3 couplings to have higher-order corrections. To obtain the additional symmetries, it is then necessary to add together all maximally non-planar diagrams, i.e. we must add to the contributions of Fig. 2.4 and 2.6 (with external couplings G_1, G_2 and G_3 replacing the elementary couplings), the analagous contributions from diagrams of the form of Fig. 2.7, obtained by making a twist in the 1, 2 or 3 channel,

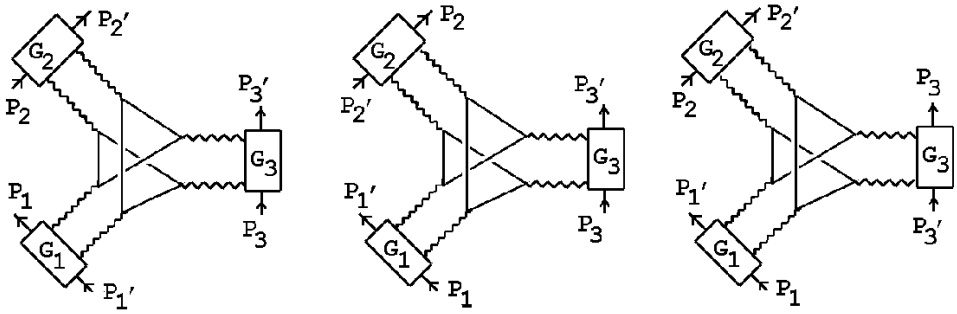

Fig. 2.7 Twisted Disgrams

In Section 5 we describe the asymptotic dispersion relation, for a three-to-three amplitude, that holds in the triple-regge limit. The physical-region triple discontinuities that appear are relatively simple. In terms of tree diagrams, in which an internal line represents a channel discontinuity, all the triple discontinuities are of one of the two forms illustrated in Fig. 2.8.

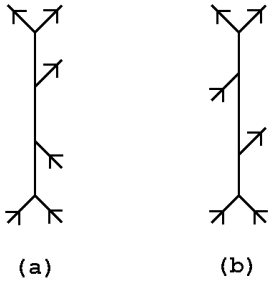

Fig. 2.8 Tree Diagrams for Triple Discontinuities

There are a total of 24 of each kind. Both contain initial and final state subenergy discontinuities and are distinguished by whether the third discontinuity is in the total energy (Fig. 2.8(a)) or in a cross-energy (Fig. 2.8(b)). The second kind of triple discontinuity is related to the one-particle inclusive cross-section via the appropriate

optical theorem. For kinematical reasons discussed at the end of Section 5, the anomaly can appear only in triple discontinuities of the first kind.

The multi-regge Sommerfeld-Watson representations are quite different for the two kinds of triple discontinuities. For those containing the anomaly there is a signature rule that the product of signatures in the three regge channels must be positive. This rule is superficially the same as the usual Gribov signature rule for the triple-regge vertices appearing in reggeon diagrams. However, it's origin is quite different. We suspect that this signature rule will ultimately lead to the even signature property of the pomeron when we finally extract the physical S-Matrix from reggeon diagrams. The analytic properties leading to this signature rule also imply that for the lowest-order amplitudes containing the anomaly, triple and double discontinuities are trivially related.

A major part of Section 5 is devoted to the hexagraph notation for counting the contribution of multiple discontinuities to the asymptotic dispersion relation. The hatched amplitudes of Fig. 2.4 and Fig. 2.6 correspond to distinct triple discontinuities and to distinct hexagraphs. We explain how the special nature of the triple-regge kinematics allows both triple discontinuities to appear in the same physical region, even though they are related by signature transformations. This property is crucial for the anomaly cancelation.

Section 6 has a very simple purpose and result. We study all contributions of diagrams of the form of Fig. 2.3 to a particular hexagraph (i.e. to a particular physical region double discontinuity) and look for the anomaly in the contributions to six-reggeon interactions. We show that only the double discontinuities originating from a maximally non-planar diagram contain the anomaly. This implies that to fully discuss the cancelation of the anomaly we only have to add a relatively simple discussion of color factors to our discussion at the end of Section 4. This we do in Section 7. In this Section, we also discuss processes in which the anomaly does not cancel. We also briefly describe the amplitudes that we expect to be selected by the anomaly infra-red divergence.

3. KINEMATICS - TRIPLE-REGGE LIMITS

In order to extract the asymptotic behavior of Feynman diagrams using familiar light-cone techniques, we begin by formulating the triple-regge limits we study using light-cone momenta. In Section 5 we will relate this formulation of limits to the usual description of multi-regge limits in terms of angular variables.

3.1 Light-Cone Description of the Triple-Regge Limit

We consider the three-to-three scattering process illustrated in Fig. 3.1(a) and define momentum transfers Q_1, Q_2 and Q_3 as in Fig. 3.1(b).

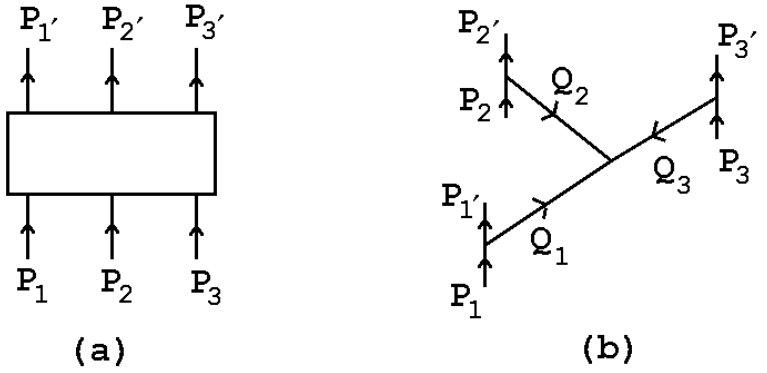

Fig. 3.1 Three-to-Three Scattering.

Consider first the "full triple-regge limit" in which each of $P_1,\ P_2$ and P_3 are taken large along distinct light-cones, with Q_1, Q_2 and Q_3 fixed, i.e.

$$\begin{array}{lllll} P_1 \to P_1^+ = (p_1, p_1, 0, 0)\ , & p_1 \to \infty & \qquad Q_1 \to (\hat{q}_1, \hat{q}_1, q_{12}, q_{13}) \\ P_2 \to P_2^+ = (p_2, 0, p_2, 0)\ , & p_2 \to \infty & \qquad Q_2 \to (\hat{q}_2, q_{21}, \hat{q}_2, q_{23}) \\ P_3 \to P_3^+ = (p_3, 0, 0, p_3)\ , & p_3 \to \infty & \qquad Q_3 \to (\hat{q}_3, q_{31}, q_{32}, \hat{q}_3) \end{array} \tag{3.1}$$

Momentum conservation requires that

$$\hat{q}_1 + \hat{q}_2 + \hat{q}_3 = 0,\ \hat{q}_1 + q_{21} + q_{31} = 0,\ \hat{q}_2 + q_{12} + q_{32} = 0,\ \hat{q}_3 + q_{13} + q_{23} = 0 \tag{3.2}$$

and so there are a total of five independent q variables which, along with P_1, P_2 and P_3, give the necessary eight variables. (Obviously $P_{i'} = P_i - Q_i,\ i = 1, 2, 3$. Also we omit light-cone components of both the P_i and the Q_i that go to zero asymptotically, but are necessary to put the initial and final particles on mass-shell.)

In terms of invariants, writing $s_{ij} = (P_i + P_j)^2$, $s_{ij'} = (P_i - P_{j'})^2$ and $s_{i'j'} = (P_{i'} + P_{j'})^2$, the limit (3.1) gives

$$\begin{aligned} s_{12} &\sim s_{1'2'} \sim -s_{12'} \sim -s_{1'2} \to 2p_1p_2 \ , \\ s_{23} &\sim -s_{2'3} \to 2p_2p_3 \ , \quad s_{31} \sim s_{3'1} \to 2p_3p_1 \ , \end{aligned} \tag{3.3}$$

while for invariants of the form $s_{122'} = (P_1 + Q_2)^2 = (P_1 + P_2 - P_{2'})^2$

$$\begin{aligned} s_{122'} &\sim 2P_1.Q_2 \to 2p_1(\hat{q}_2 - q_{21}) \ , \\ s_{133'} &\sim 2P_1.Q_3 \to 2p_1(\hat{q}_3 - q_{31}) \ , \\ s_{233'} &\to 2p_2(\hat{q}_3 - q_{32}) \ , \quad s_{311'} \to 2p_3(\hat{q}_1 - q_{13}) \ , \ \cdots \end{aligned} \tag{3.4}$$

Note that there is no constraint on the relative magnitudes of the Q_i. They can lie in either a spacelike plane ($s - s$ in the notation of [2] and of Appendix D) or in a plane with a timelike component ($s - t$ in the same notation).

3.2 Light-Cone Description of Helicity-Flip Helicity-Pole Limits

We can take a "helicity-flip helicity-pole limit", in addition to the triple-regge limit, by also taking

$$\frac{s_{31}}{s_{133'}\ s_{311'}} \sim \frac{1}{(\hat{q}_3 - q_{31})(\hat{q}_1 - q_{13})} \to \infty \tag{3.5}$$

$$\frac{s_{32}}{s_{233'}\ s_{322'}} \sim \frac{1}{(\hat{q}_3 - q_{32})(\hat{q}_2 - q_{23})} \to \infty \tag{3.6}$$

Introducing the notation of Appendix B, this limit is therefore equivalent to taking

$$q_{21^-} = \hat{q}_2 - q_{21} = q_{31} - \hat{q}_3 \to 0 \tag{3.7}$$

$$q_{12^-} = \hat{q}_1 - q_{12} = q_{32} - \hat{q}_3 \to 0 \tag{3.8}$$

With this additional limit taken

$$\begin{aligned} P_1 &\to P_1^+ = (p_1, p_1, 0, 0) \ , \quad p_1 \to \infty \qquad Q_1 \to (q_{112^-}, q_{112^-}, q_{112^-}, q_{13}) \\ P_2 &\to P_2^+ = (p_2, 0, p_2, 0) \ , \quad p_2 \to \infty \qquad Q_2 \to (q_{212^-}, q_{212^-}, q_{212^-}, q_{23}) \\ P_3 &\to P_3^+ = (p_3, 0, 0, p_3) \ , \quad p_3 \to \infty \qquad Q_3 \to (q_{33}, q_{33}, q_{33}, q_{33}) \end{aligned} \tag{3.9}$$

where now the constraints of momentum conservation are

$$q_{112^-} + q_{212^-} + q_{33} = 0 \ , \quad q_{13} + q_{23} + q_{33} = 0 \tag{3.10}$$

giving three independent q variables. As our notation indicates, the helicity-flip limit is naturally expressed in terms of the light-cone variables introduced in Appendix B.

We can obviously also define additional helicity-pole limits by taking

$$q_{32^-} \;=\; \hat{q}_3 - q_{32} \;=\; q_{23} - \hat{q}_1 \;\to\; 0 \tag{3.11}$$

$$q_{23^-} \;=\; \hat{q}_2 - q_{23} \;=\; q_{13} - \hat{q}_1 \;\to\; 0 \tag{3.12}$$

or

$$q_{13^-} \;=\; \hat{q}_1 - q_{13} \;=\; q_{23} - \hat{q}_2 \;\to\; 0 \tag{3.13}$$

$$q_{31^-} \;=\; \hat{q}_3 - q_{31} \;=\; q_{21} - \hat{q}_2 \;\to\; 0 \tag{3.14}$$

corresponding to further sets of light-cone co-ordinates defined as in Appendix B. Note that for all three helicity-pole limits, the Q_i must lie in the $s-s$ region, i.e. a spacelike plane in which the euclidean constraint

$$|Q_i| \;+\; |Q_j| \;\geq\; |Q_k| \qquad\qquad \forall\; i,j,k \tag{3.15}$$

is satisfied. This is necessary for the helicity-flip limit to be a physical region limit. In fact the Q_i lie in the $s-s$ region provided only that q_{ij^-} are sufficiently small.

4. Calculation of Feynman Diagrams

In this Section we calculate directly contributions to the triple-regge limit from selected diagrams. We will show how the triangle anomaly appears in the contributions of maximally non-planar diagrams. We will not attempt to be complete in our discussion and will not include color factors. The counting of all contributions from all diagrams has to be done via the multiple discontinuity asymptotic dispersion relation formalism that we develop in Section 5.

4.1 The Simple Planar Diagram

We begin with the first diagram of Fig. 2.3, which is also discussed in [3]. This planar diagram (almost obviously) contains no anomaly and, as we discuss shortly, will not contribute at all to the six-reggeon interaction once reggeization effects for both quarks and gluons are included. Nevertheless, we begin with it since it is the simplest to evaluate and to use to illustrate our general methods. The notation we use is illustrated in Fig. 4.1.

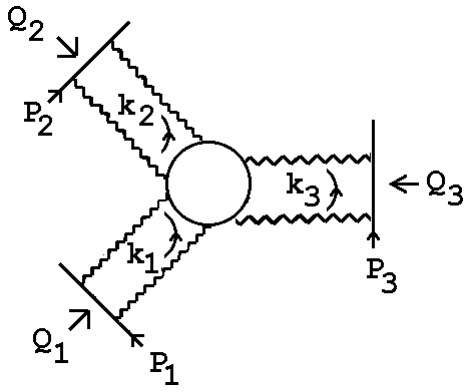

Fig. 4.1 The Simple Planar Diagram.

We will not specify the direction of the quark line but rather sum over both possibilities in the diagrams we discuss.

Because we are interested in infra-red contributions from the central quark loop we can suppose that large momenta do not flow through this loop. We can then use directly, for each scattering quark, arguments (reviewed in Appendix C) that apply when a fast quark scatters off a slow system. We begin by reducing each loop integral involving gluon propagators to a "transverse momentum" integral by carrying out longitudinal integrations. For a general diagram there will be an ambiguity as to which light-cone co-ordinates to use and also which quark propagators to use to

perform longitudinal integrations. For Fig. 4.1, however, each gluon loop momentum passes through only one line of the quark loop and there is no ambiguity as to how to proceed.

If we draw Fig. 4.1 as describing a physical scattering process with time in the upward vertical direction, as in Fig. 4.2,

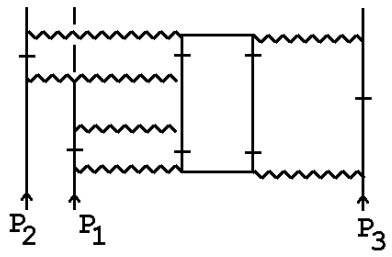

Fig. 4.2 A Physical Scattering Process.

it is clear that each of the quark propagators marked with a hatch can be naturally close to mass-shell as part of the scattering process. Since we are only looking for interesting contributions in this Section, we will not give a complete contour-closing argument as to whether a particular on-shell configuration is definitively present asymptotically. Rather if propagators are close to mass-shell during a scattering process we will take this as an indication that a leading asymptotic contribution may be obtained if these propagators are put on-shell by performing corresponding longitudinal momentum integrations. Also, since we are not interested in logarithms of the P_i (for reasons discussed in Section 2) we do not distinguish between "close to mass-shell" and "on mass-shell". (Note that when we evaluate multiple discontinuities in Section 6, we will automatically put the hatched lines on mass-shell.)

Each loop integral has the form I_i illustrated in Fig. 4.3.

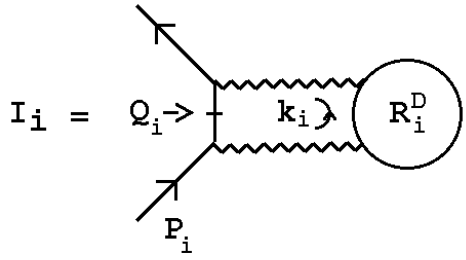

Fig. 4.3 The One Loop Integral I_i.

R_i^D denotes the remainder of the diagram besides the two gluon propagators shown. We choose a combination of conventional light-cone co-ordinates for each loop, i.e.

(in the notation of Appendix B) k_{ii^+}, k_{ii^-} and $k_{i\perp}$, $i = 1, 2, 3$. In the limit $P_{i^+} \to \infty$, we can use (C.2) - (C.7) to approximate the initial and final state spinors by $\not{p}_{ii^+}/m$ and so write each of the three I_i (in Feynman gauge) in the form

$$I_i \;=\; g^2 \int d^4k_i \left[\frac{\not{p}_{ii^+}}{m}\right] \gamma_\mu \, [\not{p}_i - \not{k}_i + m]^{-1} \, \gamma_\nu \left[\frac{\not{p}_{ii^+}}{m}\right] \left[\frac{g_{\mu\alpha}}{k_i^2}\right]\left[\frac{g_{\nu\beta}}{(Q_i - k_i)^2}\right] R^D_{i\alpha\beta}$$

$$\to \quad g^2 \, \frac{p_{i^+}}{m} \int d^4k_i \; \delta\Big(k_{ii^-} - (k^2_{ii\perp} - m^2)/2p_{ii^+}\Big) \, \frac{1}{k_i^2 \; (Q_i - k_i)^2} \;\; R^D_{i \; i^-,i^-} \qquad (4.1)$$

As discussed above, we have replaced the hatched quark propagator of Fig. 4.3 by a δ-function. Using this δ-function to perform the k_{ii^-} integration we obtain

$$I_i \;=\; g^2 \, \frac{p_{ii^+}}{m} \int d^2k_{ii\perp} dk_{ii^+} \;\; \frac{1}{k^2_{ii\perp} \; (Q_{ii\perp} - k_{ii\perp})^2} \;\; R^D_{i \; i^-,i^-} \qquad (4.2)$$

where we have used $k_{ii^-} \sim 1/p_{ii^+} \;\to 0$, together with $Q_{ii^-} = 0$, to eliminate the longitudinal momentum components in the gluon propagators.

For Fig. 4.1 the remaining k_{ii^+} integrations can be performed very simply. As illustrated in Fig. 4.4,

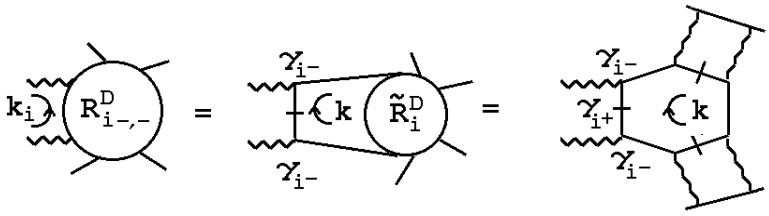

Fig. 4.4 $R^D_{i\;-,-}$ for Fig. 4.1.

the two gluons in I_i are separated by the single quark line within R^D_i that carries the only dependence on k_{ii^+}. We again replace the hatched propagator for this line by the corresponding δ-function and use it to carry out the k_{ii+} integration, i.e. we write

$$\begin{aligned}
\int dk_{ii^+} \; R^D_{i\;-,-} \;&=\; g^2 \int dk_{ii^+} \; \delta\Big((k_i + k)^2 - m^2\Big) \; \gamma_{i^-} \; [\; \gamma \cdot (k_i + k) \;] \; \gamma_{i^-} \; \tilde{R}^D_i \\
&=\; g^2 \int dk_{ii^+} \; \delta\Big(k_{ii^+}k_{i^-} + k_{i^+}k_{i^-} - (k_{i\perp} + k_{ii\perp})^2 - m^2\Big) \\
&\qquad \times \; \gamma_{i^-} \; [\gamma_{i^+} \cdot k_{i^-} + \cdots] \; \gamma_{i^-} \; \tilde{R}^D_i \\
&=\; g^2 \; \gamma_{i^-} \; \gamma_{i^+} \; \gamma_{i^-} \; \tilde{R}^D_i \;\; = \;\; g^2 \; \gamma_{i^-} \; \tilde{R}^D_i
\end{aligned} \qquad (4.3)$$

Using (4.1) - (4.3) for each of the k_i integrations, Fig. 4.1 gives the asymptotic amplitude

$$g^{12}\ \frac{p_{11^+}p_{22^+}p_{33^+}}{m^3}\ J_1(Q_1^2)J_1(Q_2^2)\ J_1(Q_3^2)\ \Gamma^v_{1^-2^-3^-}(Q_1,Q_2,Q_3) \tag{4.4}$$

where $J_1(Q^2)$ is the familiar two-dimensional integral (C.9) and $\Gamma^v_{1^-2^-3^-}(Q_1,Q_2,Q_3)$ can be identified with a particular component of the tensor that the triangle diagram contributes to the three-point function of three vector currents, i.e.

$$\Gamma^v_{1^-2^-3^-}(Q_1,Q_2,Q_3,m) = i\int \frac{d^4k\ Tr\{\gamma_{1^-}\ (\not{k}+m)\gamma_{2^-}(\not{k}+\not{Q}_2+m)\gamma_{3^-}(\not{k}+\not{Q}_1+m)\}}{(k^2-m^2)([k+Q_2]^2-m^2)([k+Q_1]^2-m^2)} \tag{4.5}$$

Note that (4.4) has been derived in the full triple Regge limit (3.1) in which the Q_i do not lie entirely in the $k_{i\perp}$ plane. While the J_1 factors depend only on the corresponding Q_i^2, the triangle diagram factor $\hat{\Gamma}^v_{1^-2^-3^-}(Q_1,Q_2,Q_3,m)$ will have a dependence on the light-like momenta $\hat{q}_1,\hat{q}_2$ and $\hat{q}_3$ of (3.1). In the helicity-pole limit (3.9) the magnitudes of the light-like momenta are identified with one of the spacelike components of the Q_i. This limit can clearly be taken smoothly within $\hat{\Gamma}^v$.

A-priori, it is straightforward to choose the quantum numbers of the Q_i-channels so that the lowest-order contribution is associated with two-reggeon exchange in each channel (color zero would be the simplest). In this case, the $J_1(Q_i^2)$ factors would be associated with the two-reggeon state. However, as we remarked at the beginning of this sub-section, since Fig. 4.1 is planar, we expect that as reggeization effects are added it ultimately does not provide a coupling for two-reggeon states. We can briefly describe how this happens as follows.

We performed the k_{11^+}-integration by using the hatched propagator contained in $R^D_{1^-,^-}$ as illustrated in Fig. 4.4. This integration can instead be written as an integral over the "missing mass" cross-energy

$$M^2\ =\ (k_1+Q_2)^2 \tag{4.6}$$

The singularities of $R^D_{1^-,^-}$ are all on the positive axis in the M^2-plane and so the contour integration over M^2 could be closed to zero if the large M^2 behavior were appropriate. In the lowest-order diagram we are discussing this is provided by quark-antiquark exchange which is just divergent enough to prevent the contour closing. In higher-orders the quark-antiquark reggeization illustrated in Fig. 4.5

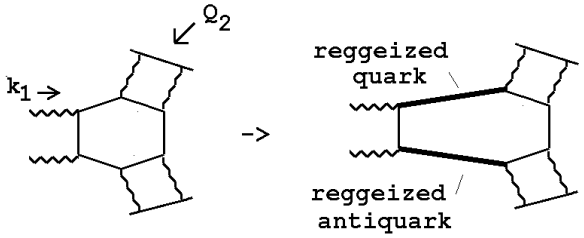

Fig. 4.5 Quark-Antiquark Reggeization

allows the closing of the contour. Consequently the analytic structure of the triangle reggeon interaction we have extracted will disappear as higher-order contributions are included (in parallel with the well-known AFS cancelation[16]). Nevertheless, (4.4) and (4.5) demonstrate how, at lowest-order, the full four-dimensional triangle diagram can appear as an effective interaction in the triple-Regge limit. Of course, in this case only vector couplings, i.e. the γ_{i-}, appear and this ensures that there is no possibility for the anomaly infra-red divergence discussed in Appendix A.

We must proceed further to find diagrams that generate a reggeon interaction containing the effective γ_5 coupling necessary to produce the anomaly. For the next diagram we study a γ_5 coupling does appear. However, we then find that the correct tensor and momentum structure for the full anomaly divergence is still absent.

4.2 A Diagram With Some Non-planarity.

In all other diagrams besides that of Fig. 4.1 (apart from those that are simply twisted versions of this diagram) one or more of the gluon loop momenta flows through more than one line of the quark loop. This introduces an extra complexity in carrying out the integrations over the longitudinal gluon momenta. The next diagram we consider, the second shown in Fig. 2.3, introduces the minimal complexity of this kind. This diagram can be redrawn as in Fig. 4.6(a), or as in Fig. 4.6(b).

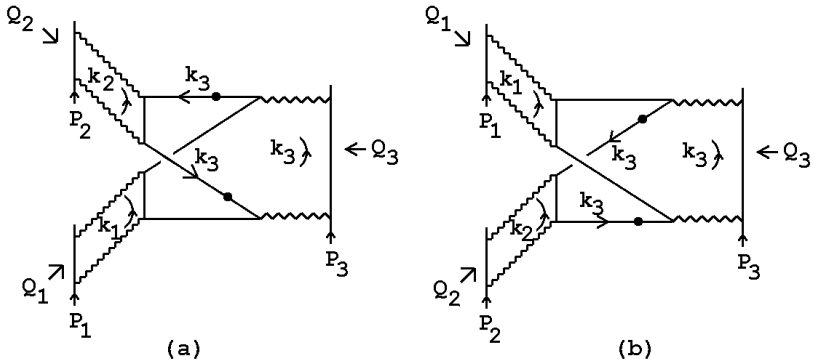

Fig. 4.6 (a) A Diagram With Some Non-planarity (b) The Same Diagram Redrawn.

There is just one gluon loop momentum, i.e. k_3, that flows through more than one line

of the internal quark loop. The k_1 and k_2 longitudinal integrations are straightforward and can be performed in the same way as we did for the longitudinal integrations of Fig. 4.1. For k_3 there are two possible routes. The first is shown in Fig. 4.6(a). The second would be that shown in Fig. 4.6(b) if the external momentum flow was kept as in Fig. 4.1(a).

If we route k_3 as in Fig. 4.6(a), then there are two possible quark propagators, each marked with a dot, that could be used to perform the k_{3^+}-integration. If we envisage the time-ordering of the scattering process as essentially represented by Fig. 4.6(a), then it would appear that only the lower dotted propagator describes a quark state that can be close to mass-shell during the scattering. The upper dotted propagator appears to describe a virtual exchange that will be a long way from mass-shell. However, when the diagram is redrawn as in Fig. 4.6(b), in the scattering process now described, the role of the two propagators is interchanged. It is now the lower propagator that is virtual and far from mass-shell. Clearly we have to add the two contributions obtained by using the two possible propagators to perform the k_{3^+}-integration.

Consider first the contribution of the upper dotted propagator in Fig. 4.6(a). After the longitudinal k_1 and k_2 integrations have been performed we will be left with the box-diagram integral illustrated in Fig. 4.7.

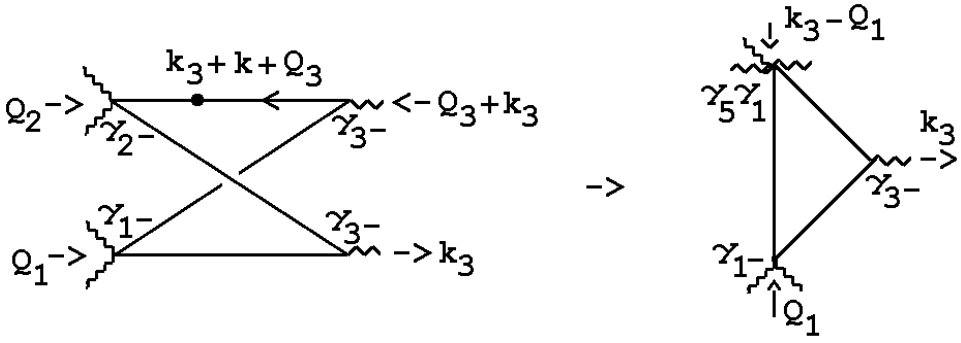

Fig. 4.7 The Box and Triangle Diagrams Generated by Fig. 4.6.

The k_{33^-} integration can be done by again utilising the evaluation of Fig. 4.3. With the dotted propagator replaced by a δ-function, the relevant factors in the k_{33^+} integration

are

$$\begin{aligned}
&\int dk_{33^+}\ \delta\Big((k_3+k+Q_3)^2-m^2\Big)\ \gamma_{2^-}\ \Big((k_3+k+Q_3)\cdot\gamma+m\Big)\ \gamma_{3^-}\\
&\quad=\ \int dk_{33^+}\ \delta\Big((k_{3^-}+Q_{33^-})k_{33^+}+\cdots\Big)\\
&\qquad\quad\times\gamma_{2^-}\ \Big((k_{3^-}+Q_{33^-})\cdot\gamma_{3^+}+\cdots\Big)\ \gamma_{3^-}\\
&\quad=\ \gamma_{2^-}\gamma_{3^+}\gamma_{3^-}\ \ +\ \ \cdots\\
&\quad=\ 2\ (\gamma_0-\gamma_2-\gamma_3)\ +\ 2\ i\gamma_5\gamma_1\ \ +\ \ \cdots
\end{aligned}\tag{4.7}$$

where, in the last line, we have used (C.21) to show that an axial γ_5-coupling is produced by the product of three γ-matrices. The omitted terms generate only what we call "non-local couplings". As elaborated in Appendix C, a non-local coupling is generated whenever the momentum dependence of the integrated propagator does not simply scale out of the integral, as it does for the part of (4.7) that we have written explicitly.

Focussing on the γ_5-interaction produced by (4.7), the asymptotic amplitude, with all longitudinal integrations performed, can be written as

$$\begin{aligned}
&g^{12}\ \frac{p_{11^+}p_{22^+}p_{33^+}}{m^3}\ \int\frac{d^2\underline{k}_{11\perp}}{\underline{k}^2_{11\perp}(Q_1-\underline{k}_{11\perp})^2}\ \int\frac{d^2\underline{k}_{22\perp}}{\underline{k}^2_{22\perp}(Q_2-\underline{k}_{22\perp})^2}\ \int\frac{d^2\underline{k}_{33\perp}}{\underline{k}^2_{33\perp}(Q_3-\underline{k}_{33\perp})^2}\\
&\int d^4k\ \ \frac{Tr\{\gamma_{1^-}(\not{k}+\not{Q}_1+m)\gamma_5\gamma_1\ (\not{k}+\not{k}_3+m)\gamma_{3^-}(\not{k}+m)\}}{(k-m^2)([k+Q_1]^2-m^2)([k+k_3]^2-m^2)}\qquad+\ \ \cdots
\end{aligned}\tag{4.8}$$

where $k_{33^-}=0$ and k_{33^+} is determined from the δ-function used in (4.7), and that part of the amplitude not written explicitly now contains either a vector coupling or a non-local coupling in place of the $\gamma_5\gamma_1$ coupling. If we again remove the $k_{ii\perp}$ integrations, the gluon propagators, and the p_{ii^+} dependence that are all associated with the three two-reggeon states, (4.8) gives a six-reggeon interaction containing the triangle diagram of Fig. 4.7, i.e.

$$\Gamma^a(Q_1,Q_3,k_{33\perp})\ =\ \int d^4k\frac{Tr\{\gamma_{1^-}(\not{k}+\not{Q}_1+m)\gamma_5\gamma_1\ (\not{k}+\not{k}_3+m)\gamma_{3^-}(\not{k}+m)\}}{(k-m^2)([k+Q_1]^2-m^2)([k+k_3]^2-m^2)}\ \ +\ \cdots\tag{4.9}$$

where we still have $k_{33^-}=0$ and k_{33^+} is determined by the mass-shell constraint of (4.7) - giving the Q_3-dependence of (4.9).

Since $\Gamma^a(Q_1,Q_3,k_{33\perp})$ contains a γ_5 coupling, it is straightforward to identify it with a component of the triangle diagram tensor for an axial current and two vector currents. However, the maximal singularity associated with the anomaly requires

specific momenta and tensor components to be present. We must have two tensor components that can project on to the same light-cone component - this would have to be γ_{1^-} and $\gamma_5\gamma_1$. The third vertex must then carry spacelike momentum of $O(q) \to 0$, implying that we should take $k_3 \sim q \to 0$. Finally a finite light-like momentum parallel to $\underline{n}_{1^-}$ must enter at the γ_5 vertex. But the light-cone component of Q_1 is orthogonal to $\underline{n}_{1^-}$. This conflict implies that a kinematical configuration producing the maximal anomaly divergence is not present.

4.3 Alternative Light-Cone Co-ordinates and Absence of the Anomaly

We can give a direct argument that there is no anomaly in the full reggeon interaction produced by Fig. 4.6(a). This argument will be important for the general analysis of discontinuities in Section 6.

In Appendix B we have shown that light-cone co-ordinates and associated γ-matrices can be introduced using any two light-like momenta whose space components are orthogonal. The regge limit calculations of Appendix C demonstrate that equivalent results are obtained using such co-ordinates and we use various co-ordinates of this form elsewhere in the paper (including the discussion of helicity-pole limits in the previous Section.) In particular let us repeat our evaluation of Fig. 4.6(a), with k_3 routed as shown, but for the k_3 longitudinal integration use co-ordinates in which $\underline{n}_{2^+}$ and $\underline{n}_{3^+}$ are the basic light-like momenta. Our k_3 co-ordinates are now

$$k_{33^-} = k_{30} - k_{33} \ , \quad k_{32^-} = k_{30} - k_{32} \ , \quad k_{31} \ , \quad \tilde{k}_{23} = k_{32} + k_{33} - k_{30} \tag{4.10}$$

The k_{33^-} integration can again be performed using the evaluation of Fig. 4.3. However, instead of (4.7), the k_{32^-} integration of the upper dotted propagator of Fig. 4.6(a) gives

$$\begin{aligned}
&\int dk_{32^-}\ \delta\Big((k_3+k+Q_3)^2 - m^2\Big)\ \gamma_{2^-}\ \Big((k_3+k+Q_3)\cdot\gamma + m\Big)\ \gamma_{3^-} \\
&\quad = \int dk_{32^-}\ \delta\Big((k_{3^-} + Q_{33^-})k_{32^-} + \cdots\Big) \\
&\qquad\qquad \times \gamma_{2^-}\ \Big((k_{3^-} + Q_{33^-})\cdot\gamma_{2^-} + \cdots\Big)\ \gamma_{3^-} \\
&\quad = \gamma_{2^-}\gamma_{2^-}\gamma_{3^-} \ + \ \cdots \\
&\quad = 0 \ + \ \cdots
\end{aligned} \tag{4.11}$$

Now no local terms appear. Only omitted "non-local" terms are generated. Evaluation of the contribution from the lower dotted propagator in Fig. 4.6(a) will similarly give no local terms. While a distinction between the contributions of local and non-local couplings may be difficult to maintain in general (after integration), if we assume that the anomaly can appear only when an appropriate local γ_5 coupling is present. then we have demonstrated it's absence in the diagram of Fig. 4.6.

4.4 A Maximally Non-Planar Diagram

Finally we study the third diagram of Fig. 2.3. In this case there are clear anomaly contributions which, when general external couplings are present, cancel only after all diagrams of this kind are summed. As illustrated in Fig. 2.4, this diagram has a "maximally non-planar" property - which produce a "maximal complexity" in terms of evaluating the longitudinal gluon momentum integrations.

The first point we note is that there is no natural choice for routing the gluon loop momenta through the internal quark loop. Each momentum flows through three quark propagators no matter in which direction we send it. As to which combinations of propagators can be simultaneously close to mass-shell, we note that if we draw the scattering as in Fig. 4.8(a) then

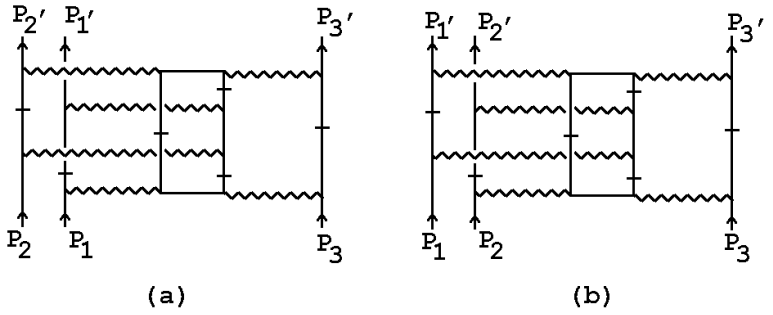

Fig. 4.8 Two Scattering Processes Described by the Diagram of Fig. 2.4

the hatched propagators can obviously be simultaneously close to mass-shell. However, if we redraw the diagram as in Fig. 4.8(b), an alternative set of hatched lines is naturally chosen. It is easy to check that the second set corresponds to the three loop propagators not hatched in Fig. 4.8(a). (These two contributions were already recognized Section 2.) Note that the hatched lines in Fig. 4.8(a) correspond to taking a double discontinuity in s_{13} and $s_{2'3'}$ while the hatched lines in Fig. 4.8(a) correspond to taking a double discontinuity in s_{23} and $s_{1'3'}$. This will be an important distinction in the following.

There are further scattering processes described by the diagram we are discussing that involve interchanging ingoing and outgoing particles. For example, the processes of Fig. 4.9.

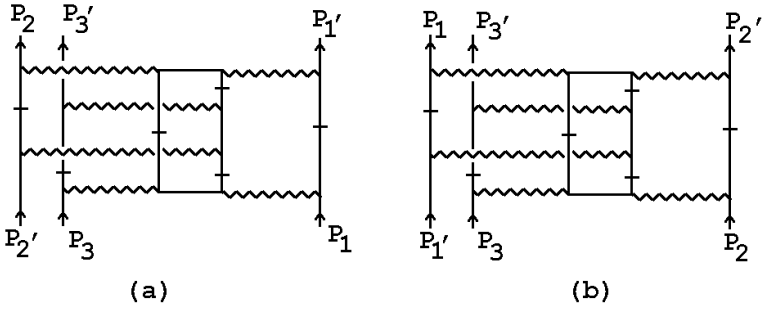

Fig. 4.9 Further Scattering Processes Described by the Diagram of Fig. 2.4

Such contributions will be included separately in the multiple discontinuity formalism of the next two Sections. (In the language of the next Section, one maximally non-planar Feynman diagram contains discontinuities associated with several different hexagraphs.) In this sub-section we will discuss only the contribution of Fig. 4.8(a) in detail. After we have discussed Fig. 4.8(a), it will be obvious that the discussion immediately extends to Fig. 4.8(b) and that it also generalises to the corresponding contributions from the diagrams of Fig. 4.9.

For reasons that will become apparent, it will be desirable to keep us much symmetry as possible in our kinematic analysis, even at the cost of using a more complicated labeling for momenta flowing along the quark loop lines. Therefore, we label the momentum flow into the internal quark loop of Fig. 4.8(a) as in Fig. 4.10, where the γ matrices that contribute in the triple-regge limit are also shown.

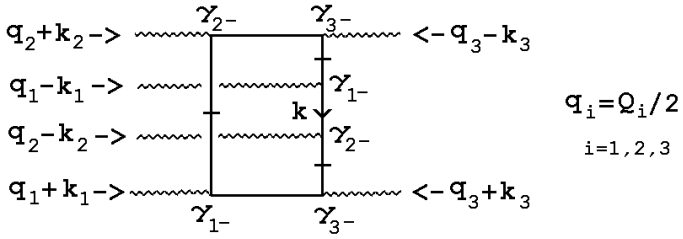

Fig. 4.10 The Quark Loop in Fig. 4.8(a).

This time we use the light-cone co-ordinates $(k_{i1^-}, k_{i2^-}, \underline{\tilde{k}}_{i\perp})$ to perform the k_1 and k_2 integrations and to evaluate the γ-matrix trace associated with the quark loop. For the k_3 integration we use conventional light-cone co-ordinates. The evaluation of the integral I_i of Fig. 4.3 can be used to perform the k_{11^-}, k_{22^-} and k_{3^-} integrations. The remaining longitudinal integrations have to be carried out using δ-functions for propagators belonging to the internal quark loop, A-priori there are six different options for choosing the longitudinal k_i to be used to put the hatched lines in Fig. 4.10 on-shell. These possibilities are indicated schematically in Fig. 4.11

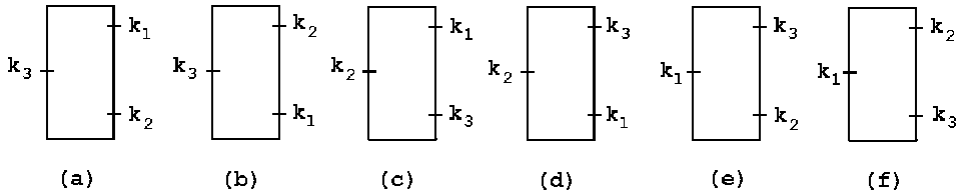

Fig. 4.11 Possible Choices of δ-function Integrations for Fig. 4.10.

For the δ-function assignment of Fig. 4.11(b), we note that both the k_{12^-} and the k_{21^-} integrations will be analagous to (4.11) in that the potential point-coupling, involving the γ-matrix (within the numerator of the on-shell quark) that is multiplied by the momentum scaling the δ-function momentum, is eliminated by one of the adjacent γ-matrices. Hence no local coupling is produced. For Fig. 4.11(c) the k_{21^-} integration similarly produces no local coupling. For Fig. 4.11(d) it is the k_{12^-} and the k_{21^-} integrations, for Fig. 4.11(e) the k_{12^-} integration, and for Fig. 4.11(f) both the k_{12^-} and k_{21^-} integrations, that produce no local coupling. Consequently, with the light-cone co-ordinates we have chosen, only the δ-function assignment of Fig. 4.11(a) gives a contribution with local couplings from all three integrations.

For the δ-function assignment of Fig. 4.11(a) we route momenta through the quark loop of Fig. 4.10 as illustrated in Fig. 4.12

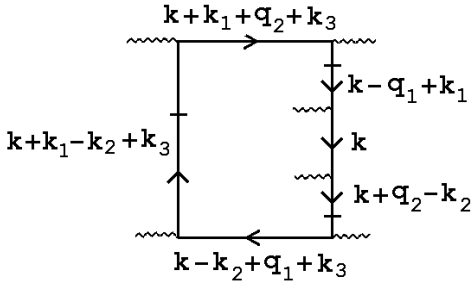

Fig. 4.12 Momentum Flow for the δ-function Assignment of Fig. 4.11(a).

We calculate the local couplings generated as follows.

$$\begin{aligned}
&\int dk_{12^-}\ \delta\Big((k_1+k-q_1)^2-m^2\Big)\ \gamma_{3^-}\ \Big((k_1+k-q_1)\cdot\gamma+m\Big)\ \gamma_{1^-} \\
&\quad = \int dk_{12^-}\ \delta\Big(k_{1^-}\ k_{12^-}+\cdots\Big) \\
&\qquad\quad \times \gamma_{3^-}\ \Big(k_{1^-}\cdot\gamma_{2^-}+\cdots\Big)\ \gamma_{1^-} \\
&\quad = \gamma_{3^-}\gamma_{2^-}\gamma_{1^-}\ +\ \cdots
\end{aligned} \tag{4.12}$$

$$
\begin{aligned}
&\int dk_{21^-}\delta\Big((k_2-k-q_2)^2-m^2\Big)\ \gamma_{2^-}\ \Big((k_2-k-q_2)\cdot\gamma+m\Big)\ \gamma_{3^-}\\
&\quad=\ \int dk_{21^-}\ \delta\Big(k_{2^-}k_{21^-}+\cdots\Big)\\
&\qquad\qquad\times\gamma_{2^-}\ \Big(k_{2^-}\cdot\gamma_{1^-}+\cdots\Big)\ \gamma_{3^-}\\
&\quad=\ \gamma_{2^-}\gamma_{1^-}\gamma_{3^-}\ \ +\ \ \cdots
\end{aligned}
\tag{4.13}
$$

$$
\begin{aligned}
&\int dk_{33^+}\ \delta\Big((k_3+k+k_1-k_2)^2-m^2\Big)\ \gamma_{1^-}\ \Big((k_3+k+k_1-k_2)\cdot\gamma+m\Big)\ \gamma_{2^-}\\
&\quad=\ \int dk_{33^+}\ \delta\Big((k_{3^-}+k_{13^-}-k_{23^-})k_{33^+}+\cdots\Big)\\
&\qquad\qquad\times\gamma_{1^-}\ \Big((k_{3^-}+k_{13^-}-k_{23^-})\cdot\gamma_{3^+}+\cdots\Big)\ \gamma_{2^-}\\
&\quad=\ \gamma_{1^-}\gamma_{3^+}\gamma_{2^-}\ \ +\ \ \cdots
\end{aligned}
\tag{4.14}
$$

In each case the dots indicate the contribution of additional non-local couplings. We defer the evaluation of the δ-functions for the moment. The triangle diagram structure of the local couplings is illustrated in Fig. 4.13,

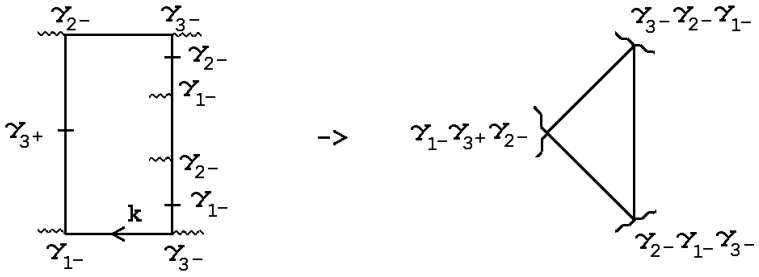

Fig. 4.13 Local couplings generated by the δ-function Assignment of Fig. 4.11(a).

With all longitudinal integrations performed, the asymptotic amplitude obtained from Fig. 4.8(a) can be written as

$$
\begin{aligned}
&g^{12}\ \ \frac{p_{11^+}\ p_{22^+}\ p_{3^+}}{m^3}\quad\times\\
&\int\frac{d^2\underline{k}_{112+}}{(q_1+\underline{k}_{112+})^2(q_1-\underline{k}_{112+})^2}\ \int\frac{d^2\underline{k}_{212}}{(q_2+\underline{k}_{212+})^2(q_2-\underline{k}_{212+})^2}\ \int\frac{d^2\underline{k}_{33\perp}}{(q_3+\underline{k}_{33\perp})^2(q_3-\underline{k}_{33\perp})^2}\\
&\int d^4k\ \frac{Tr\{\hat{\gamma}_{12}(\not{k}+\not{k}_1+\not{q}_2+\not{k}_3+m)\hat{\gamma}_{31}(\not{k}+m)\hat{\gamma}_{23}(\not{k}-\not{k}_2+\not{q}_1+\not{k}_3+m)\}}{([k+k_1+q_2+k_3]^2-m^2)(k^2-m^2)([k-k_2+q_1+k_3]^2-m^2)}\ +\ \cdots
\end{aligned}
\tag{4.15}
$$

where

$$
\hat{\gamma}_{31}=\gamma_{3^-}\gamma_{2^-}\gamma_{1^-}\ ,\quad \hat{\gamma}_{23}=\gamma_{2^-}\gamma_{1^-}\gamma_{3^-}\ ,\quad \hat{\gamma}_{12}=\gamma_{1^-}\gamma_{3^+}\gamma_{2^-}
\tag{4.16}
$$

and $k_{11^-} = k_{22^-} = k_{33^-} = 0$, with k_{12^-}, k_{21^-} and k_{33^+} still to be determined by δ-function constraints. That part of the amplitude not shown explicitly in (4.15) contains non-local couplings at one, or more, vertices of the triangle diagram.

Before extracting a reggeon interaction from (4.15) we first separate out a potential anomaly generating part. Using, again, the identity (C.21), we can write

$$\hat{\gamma}_{31} \;=\; \gamma^{-,+,-} \;+\; i\,\gamma^{-,-,-}\,\gamma_5 \tag{4.17}$$

$$\hat{\gamma}_{23} \;=\; \gamma^{+,-,-} \;+\; i\,\gamma^{-,-,-}\,\gamma_5 \tag{4.18}$$

$$\hat{\gamma}_{12} \;=\; \gamma^{-,-,-} \;-\; i\,\gamma^{-,-,+}\,\gamma_5 \tag{4.19}$$

where

$$\gamma^{\pm,\pm,\pm} \;=\; \gamma^\mu \cdot n_\mu^{\pm,\pm,\pm}\,, \qquad n^{\pm,\pm,\pm\mu} \;=\; (1,\pm 1,\pm 1,\pm 1) \tag{4.20}$$

It will also be helpful to project the $n^{\pm,\pm,\pm\mu}$ on the basis vectors that we are using for our light-cone co-ordinate system.

$$\begin{aligned}
n^{-,-,-\mu} \;&=\; n_{2^-}^{-,-,-\mu}\,\underline{n}_{1^+} \;+\; n_{1^-}^{-,-,-\mu}\,\underline{n}_{2^+} \;+\; \tilde{n}_{12^+}^{-,-,-\mu}\,\underline{n}_{12^+} \;+\; n_3^{-,-,-\mu}\,\underline{n}_3 \\
&=\; 2\,\underline{n}_{1^+} \;+\; 2\,\underline{n}_{2^+} \;-\; 3\,\underline{n}_{12^+} \;-\; \underline{n}_3 \\
n^{-,-,+\mu} \;&=\; 2\,\underline{n}_{1^+} \;+\; 2\,\underline{n}_{2^+} \;-\; 3\,\underline{n}_{12^+} \;+\; \underline{n}_3 \\
n^{+,-,-\mu} \;&=\; 2\,\underline{n}_{1^+} \;-\; \underline{n}_{12^+} \;-\; \underline{n}_3 \\
n^{-,+,-\mu} \;&=\; 2\,\underline{n}_{2^+} \;-\; \underline{n}_{12^+} \;-\; \underline{n}_3
\end{aligned} \tag{4.21}$$

As we noted in Appendix B, the ϵ-tensor has the usual form in this co-ordinate system.

To obtain the divergence (A.6) when $m = 0$, we must have a component of the axial-vector triangle diagram tensor $\Gamma^{\mu\nu\lambda}$ with $\mu = \nu$ having a lightlike projection and λ an orthogonal index having a spacelike projection. Since $\hat{\gamma}_{31}$ and $\hat{\gamma}_{23}$ have the same γ_5 component, this requirement is met if we choose the γ_5 component from all three of the $\hat{\gamma}_{ij}$. The finite light-like momentum (k^μ) can have a projection on either $\underline{n}_{1^+}$ (i.e. $k_{2^-}^\mu \neq 0,\ k_{1^-}^\mu = 0$) or $\underline{n}_{2^+}$ (i.e. $k_{1^-}^\mu \neq 0,\ k_{2^-}^\mu = 0$). $n^{-,-,+\mu}$ has the necessary spacelike component orthogonal to $n^{-,-,-\mu}$. As we discussed in Appendix A, the anomaly infra-red divergence (like the ultra-violet anomaly) is also present in the corresponding tensor component of the triangle diagram for one axial and two vector currents. Since the vector part of $\hat{\gamma}_{12}$ is identical to the γ_5 component of $\hat{\gamma}_{31}$ and $\hat{\gamma}_{23}$, the requirements for this case are met when we take the γ_5 part of either $\hat{\gamma}_{31}$ or $\hat{\gamma}_{23}$ together with the vector parts of the remaining two $\hat{\gamma}_{ij}$.

We will consider in detail the contribution to (4.15) from the three γ_5 couplings. As we will discuss, the single γ_5 contributions are better discussed in terms of different

light-cone co-ordinates. The three γ_5 couplings give the $(m = 0)$ reggeon interaction

$$\Gamma_6(q_1, q_2, q_3, \underline{\tilde{k}}_1, \underline{\tilde{k}}_2, \underline{k}_{3\perp}, 0) \;=$$
$$\int d^4k \frac{Tr\{\gamma_5\gamma_{-,-,+}(\not{k} + \not{k}_1 + \not{q}_2 + \not{k}_3)\gamma_5\gamma_{-,-,-}\; \not{k}\; \gamma_5\gamma_{-,-,-}(\not{k} - \not{k}_2 + \not{q}_1 + \not{k}_3)}{(k + k_1 + q_2 + k_3)^2\; k^2\; (k - k_2 + q_1 + k_3)^2} \;+\; \cdots \tag{4.22}$$

where, again, we note that $k_{11^-} = k_{22^-} = k_{33^-} = 0$ and that k_{12^-}, k_{21^-} and k_{33^+} remain to be determined by the δ-functions of (4.12) - (4.14). (4.22) corresponds to the triangle diagram illustrated in Fig. 4.14.

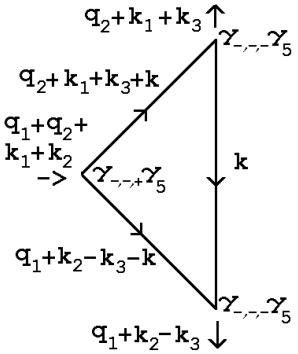

Fig. 4.14 The Triangle Diagram Corresponding to (4.22)

To see the anomaly divergence we must take the limit

$$(k_1 + q_2 + k_3)^2 \sim (q_1 + q_2 + k_1 + k_2)^2 \sim (k_2 + q_1 - k_3)^2 \sim \mathbf{q}^2 \to 0 \tag{4.23}$$

of (4.22) with a finite light-like momentum flowing through the diagram parallel to $\underline{n}_{1^-}$ (or, as we discuss shortly, $\underline{n}_{2^-}$). Such a momentum configuration must also be consistent with the three mass-shell constraints determining k_{12^-}, k_{21^-} and k_{33^+} respectively, i.e.

$$(k - q_1 + k_1)^2 \;=\; 0 \tag{4.24}$$
$$(k + q_2 - k_2)^2 \;=\; 0 \tag{4.25}$$
$$(k + k_1 - k_2 + k_3)^2 \;=\; 0 \tag{4.26}$$

To show that momenta exist satisfying all of the required constraints, we consider the limiting configuration in which $\mathbf{q} = 0$ and show that this can be realized with the loop momentum $k \sim \mathbf{q} = 0$ (as discussed in Appendix A). It is then straightforward to add momenta that are $O(\mathbf{q})$. We identify Fig. 4.14 with Fig. A2 by identifying

$q_1 + k_2 - k_3$ with $\mathbf{q}_1$ and $q_1 + q_2 + k_1 + k_2$ with $\mathbf{q}_2$. This requires that (in the limit $\mathbf{q} \to 0$)

$$q_1 + q_2 + k_1 + k_2 \;=\; 0 \tag{4.27}$$

and that (for the tensor component we have identified)

$$q_1 + k_2 - k_3 \;\sim\; (1, -1, 0, 0) \tag{4.28}$$

To satisfy (4.24) and (4.25) we take $q_1 - k_1$ and $q_2 - k_2$ lightlike, i.e. (using again the co-ordinates of Appendix B)

$$\begin{aligned} q_1 - k_1 \;&=\; (2l_{2^-}, 2l_{2^-}, 0, 0)\;, \quad q_2 - k_2 \;=\; (2l_{1^-}, 0, 2l_{1^-}, 0) \\ &=> \underline{q}_{112^+} \;=\; \underline{k}_{112^+}\;, \quad \underline{q}_{212^+} \;=\; \underline{k}_{212^+} \end{aligned} \tag{4.29}$$

Since the light-cone components of $q_1 + k_1$ and $q_2 + k_2$ can not cancel, satisfying (4.27) then requires that

$$q_{12^-} \;=\; -\; k_{12^-} \;=\; l_{2^-}\;, \quad q_{21^-} \;=\; -\; k_{21^-} \;=\; l_{1^-} \quad \underline{q}_{112^+} \;=\; -\,\underline{q}_{212^+} \tag{4.30}$$

We then have

$$q_3 \;=\; -\,(q_1 + q_2) \;=\; -\,(l_{2^-} + l_{1^-}, l_{2^-}, l_{1^-}, 0) \tag{4.31}$$

and so for q_3 to have the form (3.1), we must have

$$l_{2^-} \;=\; -\; l_{1^-} \;=\; l \quad => \quad Q_3^2 \;=\; 4\; q_3^2 \;=\; 2\; l^2 \tag{4.32}$$

We could choose either sign for l in the following, the value of invariants is unchanged.

To satisfy (4.28) we now require

$$\begin{aligned} q_1 + k_2 - k_3 \;&=\; (l, l, 0, 0) \;+\; \underline{q}_{112^+} \;+\; (l, 0, l, 0) \;+\; \underline{k}_{212^+} \;-\; (k_{33^+}, k_{31}, k_{32}, k_{33^+}) \\ &=\; (l, l, 0, 0) \;+\; (l, 0, l, 0) \;-\; (k_{33^+}, k_{31}, k_{32}, k_{33^+}) \\ \sim\; (1, -1, 0, 0) => \quad & k_{33^+} = 0\;, \quad k_{32} = l\;, \quad k_{31} \;=\; 3\; l \end{aligned} \tag{4.33}$$

which fixes

$$(q_3 - k_3)^2 \;=\; 2(q_3 + k_3)^2 \;=\; 2\; Q_3^2 \;=\; 16\; l^2 \tag{4.34}$$

Finally, we must satisfy the last mass-shell condition (4.26). Writing

$$-k_1 + k_2 - k_3 \;=\; q_1 + k_2 - k_3 \;-\; 2\; \underline{q}_{112^+} \tag{4.35}$$

and using (4.28) together with (4.33), (4.26) becomes

$$8\; l\; q_{112^-} \;=\; q_1^2 \;=\; \underline{q}_{112^+}^2 \;=\; q_{112^-}^2 + q_{13}^2 \tag{4.36}$$

So that, finally, we have

$$(q_1+k_1)^2 \;=\; 4\,q_1^2 \;=\; Q_1^2 \;=\; (q_2+k_2)^2 \;=\; 4q_2^2 \;=\; Q_2^2 \;=\; 32\;l\;q_{112-} \tag{4.37}$$

Therefore, as $Q_3^2 \;\sim\; l^2 \;\to\; 0$ then also $(q_1+k_1)^2 \;\sim\; (q_2+k_2)^2 \;\to\; 0$

If we now add momenta of $O(\mathbf{q})$ parallel to $\underline{n}_{12-}$ and let $\mathbf{q}\to 0$, with l fixed, we obtain

$$(q_1-k_1)^2 \;\sim\; (q_2-k_2)^2 \;\sim\; \mathbf{q}^2 \;\to 0 \tag{4.38}$$

$$(q_1+k_1)^2 \;\to\; (q_2+k_2)^2 \not\to 0\;, \quad (q_3-k_3)^2 \;\to\; 2(q_3+k_3)^2 \not\to 0 \tag{4.39}$$

together with

$$\Gamma_6 \quad\sim\quad \epsilon_{\underline{n}_{1+},\underline{n}_3,\underline{n}_{2+},\underline{n}_{12+}} \quad \frac{l^2}{\mathbf{q}} \quad\sim\quad \frac{Q_3^2}{q} \tag{4.40}$$

Note that the singular behavior (4.40) occurs when not only $Q_3^2\neq 0$ but also $Q_1^2 = Q_2^2\neq 0$. However, (4.37) allows $Q_1^2=Q_2^2\to 0$ with $q_{12^-}\sim q_{21^-}\sim \sqrt{Q_3^2}\neq 0$. That the anomaly divergence persists when $Q_1^2=Q_2^2\to 0$ is important for identifying its occurrence when the helicity-flip limit is taken, in addition to the triple-regge limit, as in (3.9).

If, in the previous discussion, we instead impose

$$q_2+k_1+k_3 \;\sim\; \underline{n}_{2^-} \;\sim\; (1,0,-1,0) \tag{4.41}$$

the role of 1 and 2 will be interchanged. In this case we obtain

$$\Gamma_6 \quad\sim\quad \epsilon_{\underline{n}_{2+},\underline{n}_3,\underline{n}_{1+},\underline{n}_{12+}} \quad \frac{Q_3^2}{q} \tag{4.42}$$

In the full diagram of Fig. 4.8(a), both (4.40) and (4.42) will contribute. Since the momenta that are $O(q)$ will be the same and the singularity occurs at the symmetric point $q_1^2=q_2^2$, the antisymmetry of the ϵ-tensor could provide a simple cancelation of the two contributions. (This antisymmetry is, of course, the same as that discussed in Appendix A. In the co-ordinates we are using 2^- and 1^- are the analogue of the $+$ and $-$ co-ordinates discussed there.) However, the singular configuration for (4.42) differs from that for (4.40) by $k_3\leftrightarrow -k_3$, in addition to $1\leftrightarrow 2$. Nevertheless, if the integration over k_3 is symmetric, as it is obviously is in the lowest-order contribution (4.15), then there will be a cancelation of the anomaly within the single contribution of Fig. 4.8(a).

In higher-orders the external reggeon coupling $G_h(q_3, k_3)$, which is simply a constant in lowest-order, aquires non-trivial momentum dependence. For fixed helicity h the coupling appearing in a contribution from an individual diagram need not be symmetric under $q_3 + k_3 \leftrightarrow q_3 - k_3$. In this case the anomaly will not cancel in the single contribution corresponding to Fig. 4.8(a). There remains, however, a further possibility for cancelation. It is straightforward to repeat the above analysis of Fig. 4.8(a) for Fig. 4.8(b). In Fig. 4.8(b) the roles of P_1 and P_2 are interchanged compared to Fig. 4.8(a), except that $k_1 \leftrightarrow -k_1$ and $k_2 \leftrightarrow -k_2$. If the k_1 and k_2 integrations are symmetric (as again they are at lowest-order in (4.15)), then summing over the contributions of Figs. 4.8(a) and (b) will introduce sufficient symmetry with respect to q_1, k_1, q_2, k_2 that there will be a cancelation, even when the k_3 integration is not symmetric. In higher-orders, however, external couplings $G_h(q_2, k_2)$, $G_h(q_2, k_2)$ also appear which again need not be symmetric. To discuss cancelations in this case it is necessary to add the contributions from the twisted diagrams of Fig. 2.6 and also to discuss the signature properties of the reggeon states. We will reserve a more extensive discussion of this for Section 7. Here we simply remark that, for elementary quark scattering, both the color factors and all three of the k_i-integrations are symmetric also in higher-orders when we sum over all diagrams of the form of Figs. 2.4 and 2.6. Therefore the anomaly cancelation continues to hold. The deeper question, is whether, in more complicated diagrams, there are circumstances in which the color quantum numbers can be such that anomaly interactions can appear without cancelation. This is also discussed in Section 7.

For the configurations involving only the γ_5 components of either $\hat{\gamma}_{23}$ or $\hat{\gamma}_{31}$ the lightlike momentum flows in at the corresponding vertex and out at the $\hat{\gamma}_{12}$ vertex and the $1 \leftrightarrow 2$ symmetry is not mainifested so simply, although the antisymmetry of the ϵ-tensor will again provide potentially canceling contributions. In fact these configurations are most simply discussed in terms of light-cone co-ordinates that treat either 2 and 3 or 3 and 1 symmetrically. As we noted above, the Feynman diagram of Fig. 2.4 that we are discussing also contributes to the scattering processes illustrated in Fig. 4.9. The on-shell lines of Fig. 4.9(a) are the same as those of Fig. 4.8(a) and the on-shell lines of Fig. 4.9(b) are the same as those of Fig. 4.8(b). However, the role of 3 is switched with either 1 or 2 and correspondingly either $P_{2'} \leftrightarrow P_2$ or $P_{1'} \leftrightarrow P_1$. The role of the three anomaly contributions is correspondingly interchanged. (This is only possible because we don't have a full Lorentz structure for the triangle diagram reggeon interactions we discuss. As a result there is no real distinction between the anomaly due to three "axial" couplings from that due to one "axial" and two "vector" coupings). In discussing the possible cancelation of the anomaly in the sum of all diagrams we will concentrate on the anomaly that we have discussed as originating from three γ_5 couplings. However, the full symmetry of the problem implies that the same arguments immediately apply to the other anomaly contributions if we start from scattering processes such as those of Fig. 4.9 rather than those of Fig. 4.8.

5. Multi-Regge Theory

In this Section we describe the asymptotic dispersion relation formalism, together with the multi-regge theory based on it, that is needed to systematically study the contribution of quark loops to triple-regge vertices in QCD. There will be some overlap with Section 4 of [3]. However, the treatment we gave in [3] is missing several crucial elements that we discuss here. As a result, we have made the following essentially self-contained and independent of [3].

5.1 Angular Variables: s- and t-channel Physical Regions

We begin with the introduction of the angular variables that provide the link between asymptotic limits taken in an "s-channel" and partial-wave analysis in various "cross-channels" or "t-channels". We use the variables $z_1, z_2, z_3, u_{12}, u_{23}$ and u_{31} corresponding to the "Toller Diagram" of Fig. 5.1 .

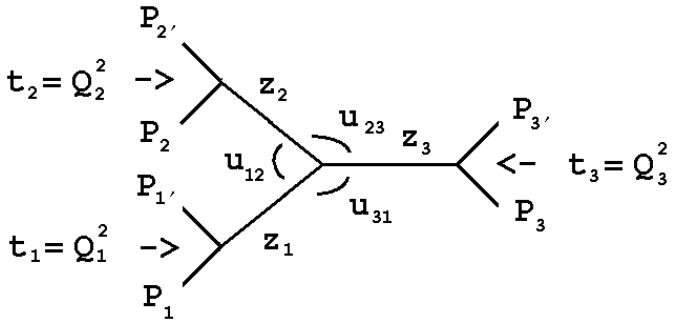

Fig. 5.1 A Toller Diagram for the Six-Particle Amplitude

The definition of these variables via "standard Lorentz frames" as well as complete expressions for invariant variables in terms of them, is given in Appendix D. We discuss their definition in three t-channel physical regions where the t_i are positive and in four s-channel physical regions where the t_i are negative. The variables introduced in the different regions are related by analytic continuation. The z_i (and the t_i) are independent variables but the u_{ij} satisfy

$$u_{12}u_{23}u_{31} = 1 \tag{5.1}$$

Choosing any two of the u_{ij}, together with the t_i and the z_i, gives the appropriate eight independent variables. In the following we will take u_{31} and $u_{32} = u_{23}^{-1}$ as our independent variables and, for simplicity, relabel them as $u_1 = u_{31}$ and $u_2 = u_{32}$. (5.1) then gives

$$u_{12} \;=\; \frac{u_2}{u_1} \tag{5.2}$$

In principle, since we will be considering the scattering of particles with spin (i.e. quarks) we should add additional azimuthal angles to describe the rotation of helicities. However, as we already saw in the last Section, for the lowest-order quark-gluon couplings there is (s-channel) helicity-conservation. It is trivial to carry out helicity projections and show that the lowest-order couplings are also helicity-independent. In discussing anomaly cancelations at the end of the last Section we saw that the higher-order helicity dependence of these couplings is important. However, we will discuss the consequences of this only qualitatively in Section 7. To keep our discussion in this Section as simple as possible we will treat the scattering quarks kinematically as if they were scalar particles. Also, since this Section will be concerned with abstract kinematics and analyticity properties, we will continue to ignore color (and any other) quantum numbers. In Section 7, both color quantum numbers and the existence of two helicities will be important when we discuss discrete C, P and T transformations on amplitudes. In this Section we will refer only to the CPT combination. Nevertheless the presence of both helicity and color should be kept in mind.

As we show in Appendix D, all invariants are polynomial functions of the $z_i = cos\ \theta_i$, the $sin\ \theta_i$ and the $cos\ \omega_{ij}$ ($u_{ij} = e^{i\ \omega_{ij}}$). The following approximations give the leading behavior when all the z_i are large and are easily derived from (D.17) and (D.18). These approximations will be sufficient for us to describe the behavior of invariants in the limits we discuss.

$$\begin{aligned} s_{122'} \sim s_{1'3'3} \sim -s_{1'22'} \sim -s_{13'3} \quad &\to \quad 2\Big(\frac{t_1-4m^2}{t_1}\Big)^{\frac{1}{2}}\lambda^{\frac{1}{2}}(t_1,t_2,t_3)\ z_1 \\ &\sim \quad z_1 \end{aligned} \tag{5.3}$$

$$\begin{aligned} s_{233'} \sim s_{2'1'1} \sim -s_{2'33'} \sim -s_{21'1} \quad &\to \quad 2\Big(\frac{t_2-4m^2}{t_2}\Big)^{\frac{1}{2}}\lambda^{\frac{1}{2}}(t_1,t_2,t_3)\ z_2 \\ &\sim \quad z_2 \end{aligned} \tag{5.4}$$

$$\begin{aligned} s_{311'} \sim s_{3'2'2} \sim -s_{3'11'} \sim -s_{32'2} \quad &\to \quad 2\Big(\frac{t_3-4m^2}{t_3}\Big)^{\frac{1}{2}}\lambda^{\frac{1}{2}}(t_1,t_2,t_3)\ z_3 \\ &\sim \quad z_3 \end{aligned} \tag{5.5}$$

$$\begin{aligned} &s_{13} \sim s_{1'3'} \sim -s_{13'} \sim -s_{1'3} \to \\ &\quad -4(t_1-4m^2)^{\frac{1}{2}}(t_3-4m^2)^{\frac{1}{2}}\Big[(1-z_1^2)^{\frac{1}{2}}(1-z_3^2)^{\frac{1}{2}}\Big(u_1+\frac{1}{u_1}\Big)+\frac{t_3+t_1-t_2}{\sqrt{t_1}\sqrt{t_3}}z_1z_3\Big] \\ &\sim \quad z_1\ z_3\ u_1\ [1+O(\frac{1}{u_1})] \end{aligned} \tag{5.6}$$

$$
\begin{aligned}
s_{23} \quad &\sim \; s_{2'3'} \;\sim \; -\,s_{23'} \;\sim \; -\,s_{2'3} \quad \rightarrow \\
&-\,4(t_2-4m^2)^{\frac{1}{2}}(t_3-4m^2)^{\frac{1}{2}}\Big[(1-z_2^2)^{\frac{1}{2}}(1-z_3^2)^{\frac{1}{2}}\Big(u_2+\frac{1}{u_2}\Big)+\frac{t_3+t_2-t_1}{\sqrt{t_2}\sqrt{t_3}}z_2z_3\Big] \\
\sim \quad & z_2\; z_3\; u_2^{-1}\;[1+O(u_2)]
\end{aligned}
\tag{5.7}
$$

$$
\begin{aligned}
s_{12} \quad &\sim \; s_{1'2'} \;\sim \; -\,s_{12'} \;\sim \; -\,s_{1'2} \quad \rightarrow \\
&-\,4(t_1-4m^2)^{\frac{1}{2}}(t_2-4m^2)^{\frac{1}{2}}\Big[(1-z_1^2)^{\frac{1}{2}}(1-z_2^2)^{\frac{1}{2}}\Big(\frac{u_1}{u_2}+\frac{u_2}{u_1}\Big)+\frac{t_3-t_1-t_2}{\sqrt{t_1}\sqrt{t_2}}z_1z_2\Big] \\
\sim \quad & z_1\; z_2\; (u_1/u_2)\;[1+O(u_2/u_1)]
\end{aligned}
\tag{5.8}
$$

$\lambda(t_1,t_2,t_3)$ is the familiar triangle function defined explicitly in (D.7). The branch-points at $\lambda(t_1,t_2,t_3)=0$ in (5.3) - (5.5) play an important role when analytic continuation between the different physical regions is discussed. Note that all invariants are unchanged when $u_1 \rightarrow 1/u_1, u_2 \rightarrow 1/u_2$.

In each of the three t-channels $t_i = Q_i^2 > 4m^2$ and $\lambda(t_1,t_2,t_3) > 0$. Also, in each t_i channel

$$
|Q_i| > |Q_j| + |Q_k| \tag{5.9}
$$

The choice of signs in (5.3)-(5.5) is a convention which is irrelevant in the t-channels since

$$
-1 \;\leq\; z_i \;\leq\; 1, \quad |u_i| \;=\; 1 \tag{5.10}
$$

i.e. the z_i take both positive and negative values. Note, however, that the sign convention can be reversed by, for example, interchanging the role of Q_1 and Q_2 when introducing the variables via standard frames defined in the t_3-channel. This is discussed in Appendix D. We also distinguish two sub-regions of an s-channel physical region - the "$s-t$" and "$s-s$" regions[2]. In an $s-t$ region $\lambda(t_1,t_2,t_3) > 0$ and the physical range of the z_i is along the real axis with $z_i \geq 1$ or $z_i \leq -1$, while $|u_{ij}| = 1$. As we also discuss in Appendix D, the antisymmetry of the signs in (5.3)-(5.5) is removed because each of the four s-channel physical regions has two distinct parts, in one of which the z_i each have a certain sign and the other in which they all have the opposite sign.

In summary, when the t_i satisfy the $s-t$ sub-region constraint, the four s-

channel physical regions are,

$$
\begin{aligned}
&i) \quad z_1,\ z_2,\ z_3 \ \geq\ 1\ , \qquad z_1,\ z_2,\ z_3 \ \leq\ -1\ , \quad |u_i| \ =\ 1 \\
&\quad \text{the initial particles carry momenta } P_1, P_2 \text{ and } P_3 \\
&ii) \quad -z_1,\ z_2,\ z_3 \ \geq\ 1\ , \qquad -z_1,\ z_2,\ z_3 \ \leq\ -1\ , \quad |u_i| \ =\ 1 \\
&\quad \text{the initial particles carry momenta } P_{1'}, P_2 \text{ and } P_3 \\
&iii) \quad z_1,\ -z_2,\ z_3 \ \geq\ 1\ , \qquad z_1,\ -z_2,\ z_3 \ \leq\ -1\ , \quad |u_i| \ =\ 1 \\
&\quad \text{the initial particles carry momenta } P_1, P_{2'} \text{ and } P_3 \\
&iv) \quad z_1,\ z_2,\ -z_3 \ \geq\ 1\ , \qquad z_1,\ z_2,\ -z_3 \ \leq\ -1\ , \quad |u_i| \ =\ 1 \\
&\quad \text{the initial particles carry momenta } P_1, P_2 \text{ and } P_{3'}
\end{aligned}
\tag{5.11}
$$

We will encounter subtleties associated with the doubling of the range of the z_i in individual physical regions at several points in the following.

When the t_i satisfy the $s-s$ sub-region constraint $\lambda(t_1,t_2,t_3)<0$, the physical range of the z_i and u_i in the above physical regions is

$$
\begin{aligned}
&i) \quad -\infty \ <\ iz_i \ <\infty\ , \quad 0 \ \leq\ u_1,\ u_2 \ <\ \infty \\
&ii) \quad -\infty \ <\ iz_i \ <\infty\ , \quad 0 \ \leq\ -u_1,\ u_2 \ <\ \infty \\
&iii) \quad -\infty \ <\ iz_i \ <\infty\ , \quad 0 \ \leq\ u_1,\ -u_2 \ <\ \infty \\
&iv) \quad -\infty \ <\ iz_i \ <\infty\ , \quad 0 \ \leq\ -u_1,\ -u_2 \ <\ \infty
\end{aligned}
\tag{5.12}
$$

The relationship between the three t-channels and the sub-regions of one s-channel is illustrated topographically in Fig. D2. For our analysis of anomaly cancelations it is important that a change of sign of all the z_i is equivalent to a change of sign of $\lambda^{\frac{1}{2}}(t_1,t_2,t_3)$. This is apparent from (5.3) - (5.8).

5.2 Definition of Limits via Angular Variables

The full triple-regge limit is defined to be

$$
z_1,\ z_2,\ z_3 \ \rightarrow\ \infty\ , \qquad t_1,t_2,t_3,u_{31},u_{23} \ \ fixed \tag{5.13}
$$

Helicity-pole limits are those in which one or two of the u_{ij} are taken either large or small. This can be, but need not be, combined with taking one or more of the z_i large.

It will be useful to distinguish two distinct helicity-pole limits involving u_1 and u_2. The first is

$$
z_3,\ u_1,\ u_2 \ \rightarrow\ \infty \ \ (\text{or } u_1,u_2 \rightarrow 0) \quad t_1,t_2,t_3,z_1,z_2 \ \ fixed \tag{5.14}
$$

When applied to the relevant discontinuity (with P_1 and P_2, and P_1' and P_2', respectively identified) this limit coincides with the familiar (incorrectly named) "triple-regge" limit of the one-particle inclusive cross-section. The second helicity-pole limit is

$$z_3,\ u_1,\ u_2^{-1}\ \rightarrow\ \infty\ \ (\text{or } u_1, u_2^{-1} \rightarrow 0) \qquad t_1, t_2, t_3, z_1, z_2\ \ fixed \tag{5.15}$$

For reasons that will soon become apparent, we refer to the limit (5.14) as the "non-flip limit" and the limit (5.15) as the "helicity-flip limit".

As we elaborated in [5] and [3], and will discuss further below, helicity-pole limits are controled by singularities in complex helicity planes directly related to angular momentum plane Regge singularitites. In an $s-t$ part of an s-channel physical region the triple-regge limit is a physical limit but the helicity-pole limits are not. In the $s-s$ region both the triple-regge limit and the helicity-pole limits are physical.

With the approximations (5.3) - (5.8) the inter-relation between the helicity-pole limits (5.14) and (5.15) and the triple-Regge limit (5.13) is apparent. It is also straightforward, using (3.4), to identify the triple-Regge limit (5.13) with the light-cone formulated limit (3.1), with

$$P_1\ \sim\ z_1\ , \qquad P_2\ \sim\ z_2\ , \qquad P_3\ \sim\ z_3\ . \tag{5.16}$$

For the helicity non-flip limit (5.14) we have, from (5.3) - (5.8),

$$s_{12}\ \ \sim\ \ s_{1'2'}\ \sim\ -\,s_{12'}\ \sim\ -\,s_{1'2}\ \not\rightarrow\ \infty \tag{5.17}$$

$$s_{23}\ \ \sim\ \ -\,s_{2'3}\ \sim\ z_3\ u_2\ , \quad s_{31}\ \sim\ s_{3'1}\ \sim\ z_3\ u_1 \tag{5.18}$$

$$s_{122'}\ ,\ s_{133'}\ ,\ s_{233'}\ \not\rightarrow\ \infty\ . \qquad s_{311'}\ \sim s_{3'22'}\ \sim\ z_3 \tag{5.19}$$

Because $s_{12}\ \not\rightarrow\ \infty$ we can not reproduce the non-flip limit (5.14) with the light-cone variables of (3.1). However, for the helicity limit (5.15), the behavior (5.17) is replaced by

$$s_{12}\ \sim\ s_{1'2'}\ \sim\ -\,s_{12'}\ \sim\ -\,s_{1'2}\ \sim\ u_1\ u_2^{-1} \tag{5.20}$$

Therefore, we can formulate the helicity-flip limit in terms of the variables of (3.1) as

$$P_1\ \sim\ u_1\ , \qquad P_2\ \sim\ u_2^{-1}\ , \qquad P_3\ \sim\ z_3\ . \tag{5.21}$$

together with

$$\begin{aligned} q_{12^-} = \hat{q}_1 - q_{12}\ = q_{32} - \hat{q}_3\ = 0\ , \quad & q_{21^-} = \hat{q}_2 - q_{21}\ = q_{31} - \hat{q}_3\ = 0 \\ \hat{q}_1 - q_{13}\ \neq\ 0\ , \quad & \hat{q}_2 - q_{23}\ \neq\ 0 \end{aligned} \tag{5.22}$$

We can also take the helicity-flip limit (5.15) in conjunction with the triple-regge limit so that

$$z_1,\ z_2,\ z_3,\ u_1\ u_2^{-1}\ \rightarrow\ \infty\ ,\qquad t_1, t_2, t_3,\quad fixed \tag{5.23}$$

It will be important in discussing the anomaly in later Sections to keep account of the t_1 and t_2 dependance in (5.3)-(5.8) when the limit (5.23) is taken with $t_1, t_2 \sim 0$. Therefore, using (3.5) and (3.6) we can write (for small q_{21^-}, q_{12^-})

$$u_1\ \sqrt{t_1}\ +\ O(1)\ \sim\ \frac{s_{13}}{s_{133'}\ s_{311'}}\quad =>\quad u_1\ \sim\ \frac{1}{\sqrt{t_1}\ \ q_{21^-}} \tag{5.24}$$

$$u_2^{-1}\ \sqrt{t_2}\ +\ O(1)\ \sim\ \frac{s_{23}}{s_{233'}\ s_{322'}}\quad =>\quad u_2^{-1}\ \sim\ \frac{1}{\sqrt{t_2}\ \ q_{12^-}} \tag{5.25}$$

As we will see below, the helicity-flip limit selects leading (flipped) helicities from the full triple-Regge vertex. (The non-flip limit similarly selects non-flipped leading helicities). (5.24) and (5.25) imply that while the helicity-flip is directly expressed as

$$q_{12^-}\ ,\ q_{21^-}\ \rightarrow\ 0\ ,\qquad t_1 = q_1^2,\ t_2 = q_2^2,\ fixed \tag{5.26}$$

this limit is also reached if

$$q_1^2\ ,\ q_2^2\ \rightarrow\ 0\ ,\qquad q_{12^-},\ q_{21^-},\ t_3\ \ fixed \tag{5.27}$$

This important because our discussion, in the last Section, of kinematical configurations in which the anomaly occurs, showed that it occurs in the limit (5.27). This will imply that it occurs at $t_1 = t_2 = 0$ in the leading helicity-flip amplitude that we extract below.

5.3 Dispersion Theory and Asymptotic Cut Structure

A fundamental ingredient for our multi-regge analysis is the existence[5, 6] of an "asymptotic dispersion relation" that breaks the full triple-regge asymptotic amplitude up into components that each have a distinct set of asymptotic cuts. The dispersion relation is written in z_1, z_2 and z_3 with t_1, t_2, t_3, u_1 and u_2 kept fixed. It is initially written with all the $t_i < 0$ and with $\lambda(t_1, t_2, t_3) > 0$ so that contributions are obtained from an $s - t$ region of each of the four s-channels. However, we expect the form of the dispersion relation to remain unchanged as we continue between s-channel sub-regions and also to the t_i-channels.

The most important point[5, 6] is that the asymptotic cut structure (including multiple discontinuities) can be treated as if there were only normal threshold cuts satisfying the Steinmann relations. i.e. no double discontinuities in overlapping

channels. (Technically this is possible because the "bad boundary-values", in which a variety of complications due to higher-order singularities appear, are hidden in multi-regge limits.) As a result, the dispersion relation breaks the amplitude up into the leading triple-regge behavior given by a sum over triple discontinuity contributions allowed by the Steinmann relations, plus non-leading behavior. As we discussed in Section 2, the physical region triple discontinuities are of two kinds corresponding to Figs. 2.8(a) and (b). Since there are 6 possible combinations of initial and final subenergies, there are 12 triple discontinuities in each physical region. The 4 physical regions provide a total of 48 triple discontinuities contributing to the dispersion relation.

We write the dispersion relation in the form

$$M(P_1,P_2,P_3,Q_1,Q_2,Q_3) \;=\; \sum_{\mathcal{C}} M^{\mathcal{C}}(P_1,P_2,P_3,Q_1,Q_2,Q_3) \;+\; M^0 \;, \qquad (5.28)$$

where M^0 contains all non-leading triple-regge behavior, double-regge behavior, etc. and the sum is over all triplets $\mathcal{C}$ of three non-overlapping, asymptotically distinct, cuts. For each triplet $\mathcal{C}$ of cuts in invariants, say $\mathcal{C} = (s_1, s_2, s_3)$, we write

$$M^{\mathcal{C}}(P_1,P_2,P_3,Q_1,Q_2,Q_3) \;=\; \frac{1}{(2\pi i)^3} \int_{\{s_i > s_{i0}, \forall i\}} ds_1' ds_2' ds_3' \; \frac{\Delta^{\mathcal{C}}(\underset{\sim}{t}, \underset{\sim}{u}, s_1', s_2', s_3')}{(s_1'-s_1)(s_2'-s_2)(s_3'-s_3)} \qquad (5.29)$$

where $\Delta^{\mathcal{C}}$ is the triple discontinuity

$$\Delta^{\mathcal{C}}(\underset{\sim}{t}, \underset{\sim}{u}, s_1, s_2, s_{n-3}) \;=\; \sum_{\epsilon} (-1)^{\epsilon} M(\underset{\sim}{t}, \underset{\sim}{w}, s_1 \pm i0, s_2 \pm i0, s_3 \pm i0), \qquad (5.30)$$

The sum over ϵ is over all combinations of $+$ and $-$ signs in (5.30) and $(-1)^{\epsilon}$ is positive when the number of $+$ signs is even. The integration region in (5.29) is bounded by finite, but arbitrary, values s_{i0} of the s_i and the asymptotic relation between the z_i, and s_i has to be used to change variables from the z_i back to the s_i. Because of the validity of the Steinmann relations, $\Delta^{\mathcal{C}}$ can be expressed in terms of normal phase-space integrals. The simplicity of the discontinuity formulae implies that we can take multiple discontinuities simply by putting appropriate lines on mass-shell. (For the low-order Feynman diagrams we discuss the subtlety of the boundary values for the amplitudes in the discontinuity formulae[6] will not appear.)

5.4 Hexagraph Notation for Triple Discontinuities

To develop our multi-regge analysis we introduce a "hexagraph" notation[5, 6] for classifying triple discontnuities. The hexagraphs link each triple discontinuity to

a particular t-channel and determine it's contribution to asymptotic behavior via a Sommerfeld-Watson representation. The full sum over triple discontinuities in (5.28) is broken up into partial sums forming a hexagraph amplitude. Each hexagraph amplitude M^H contains a sum of triple discontinuity integrals, i.e.

$$M^H = \sum_{\mathcal{C}\epsilon H} M^{\mathcal{C}}(P_1, P_2, P_3, Q_1, Q_2, Q_3), \tag{5.31}$$

where the sum is over all triplets $\mathcal{C}$ of asymptotic cuts in which each cut is an "allowable discontinuity" of the hexagraph H.

The hexagraphs associated with a particular Toller diagram are obtained by redrawing the tree diagram in all possible ways (in a plane) with the internal lines drawn as horizontal lines and the internal vertices drawn separately, with relative angles of 120^o, and joined to the horizontal lines. The multiple discontinuities associated with a particular hexagraph all appear in the same s-channel physical region, which we therefore associate directly with the graph. This physical region is obtained by regarding the external scattering particles as entering from the bottom of the hexagraph and exiting at the top.

For the Toller diagram of Fig. 5.1 we draw an intial hexagraph, say the first graph of Fig. 5.2, and then form the set of graphs, illustrated in Fig. 5.2, that are all associated with the same s-channel and are related by cyclical rotation of the t_i-channels .

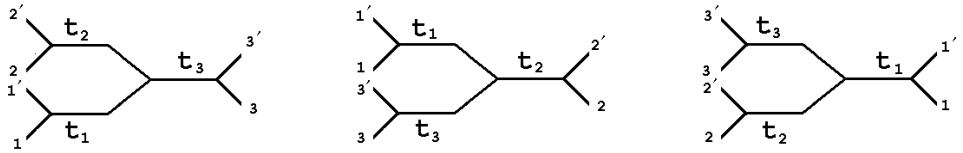

Fig. 5.2 Hexagraphs Related by Cyclical Rotation of the t_i-channels

We form a further set of hexagraphs from each of those shown in Fig. 5.2 by making twists (of one half of the graph relative to the other) about each of the horizontal lines of the graph. A twist introduces a new s-channel and, generalizing simpler multi-regge applications of the hexagraph formalism, we would expect it to be associated with signature and a change of sign of the z_i associated with the chosen line. In Fig. 5.3 we have shown again the first hexagraph of Fig. 5.2 together with the seven hexagraphs related to it by twisting.

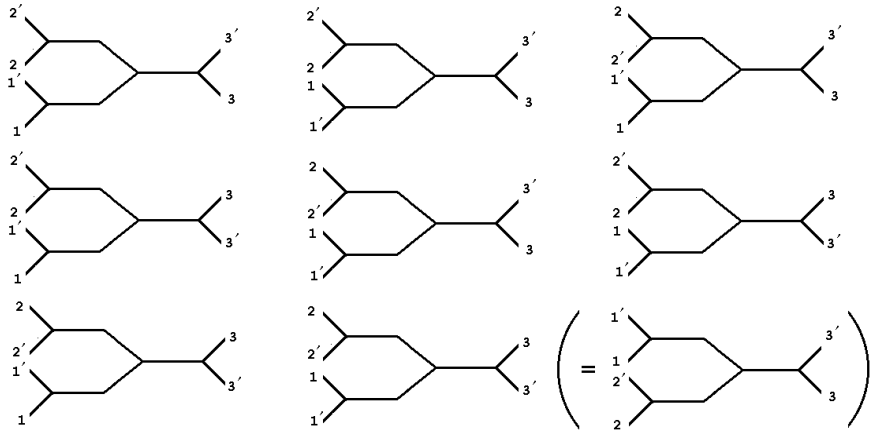

Fig. 5.3 Eight Hexagraphs Related by Twisting

Twisting also the other two hexagraphs in Fig. 5.4 gives a total of $(2\times2\times2=8)\times3=24$ hexagraphs.

Each hexagraph is also associated with a particular t-channel. This channel is obtained by interpreting the graph as representing a scattering in which external particles enter from the left of the hexagraph and exit to the right. While each twist of a hexagraph produces a change of s-channel, it leaves the t-channel unchanged. Therefore, as is immediately obvious, all the hexagraphs in Fig. 5.3 are associated with the same t-channel. The partial-wave analysis that follows this sub-section, introducing complex angular momenta and helicities, is carried out in the t-channel. We do not distinguish scattering processes related by a CPT transformation which interchanges all incoming particles with all outgoing particles. We could equally well regard the s-channel scattering particles as entering from the top of the diagram and the t-channel scattering particles as entering from the right of the diagram. (Although, as we noted at the beginning of this Section, it is important to note that there are helicities and color quantum numbers that distinguish the amplitudes related by a CPT transformation.)

Since we have 48 triple discontinuities and 24 hexagraphs, we initially expect each hexagraph to be associated with two triple discontinuities - one of each of the forms depicted in Fig. 2.8. There is a subtlety, however. In Fig. 5.3 we have also shown the CPT reversed version of the last hexagraph to emphasize that the associated s-channel is the same as that of the first hexagraph, but with the 1 and 2 t-channels interchanged. As a result, although our choice of an initial hexagraph appears to treat the 1 and 2 channels differently, this distinction is removed once we have formed the complete set of graphs.

That the combination of twists in all three channels does not result in a new s-channel is directly related to the association of two z_i-plane regions with one s-channel in (5.11). The combination of three twists can indeed be associated with a

change of sign of the three z_i, but, as we already noted this is equivalent to remaining in the same physical region and changing the sign of $\lambda^{\frac{1}{2}}(t_1, t_2, t_3)$. (As discussed in Appendix D, the same kinematic effect is also achieved by the interchange of 1 and 2 in the t_3-channel associated with this set of hexagraphs.) Clearly, rather than associating two hexagraphs (related by three twists) with the same complete physical region, we should instead associate each graph separately with one half of the region. In the multi-regge theory that follows this will be esssential in allowing us to identify signature with the twisting of hexagraphs. It is also essential that all the triple discontinuities associated with each hexagraph lie in the same half of the physical region.

A cut in an invariant channel is an "allowable discontinuity" of a hexagraph if the minimal path (cut) drawn through the graph (along internal lines), connecting all the particles (in the channel) enters and exits only between non-horizontal lines. The allowable discontinuities of the first hexagraph of Fig. 5.2 are shown in Fig. 5.4, together with the corresponding paths.

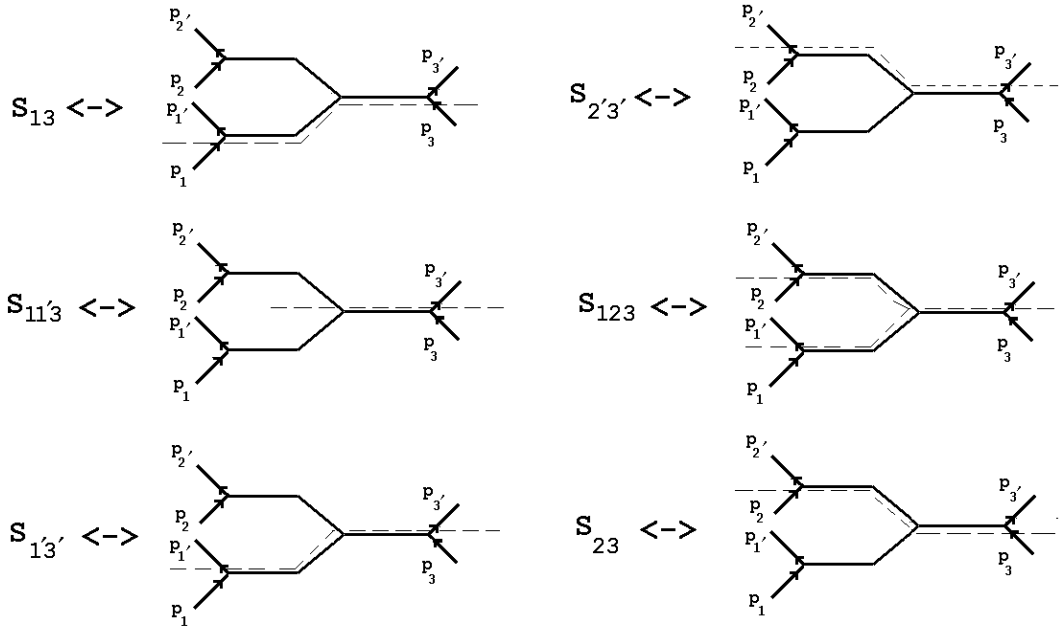

Fig. 5.4 Allowable Cuts for the First Hexagraph of Fig. 5.2.

To form a triplet $\mathcal{C}$ the three cuts must also be "asymptotically distinct" from each other when all the z_j variables are large. A first triplet formed from the cuts of Fig. 5.4 is

$$\mathcal{C}_a \;=\; (s_{13}, s_{2'3'}, s_{11'3}) \tag{5.32}$$

This triplet has the form of Fig. 2.7(a). A second triplet having the form of Fig. 2.7(b)

is

$$\mathcal{C}_b \;=\; (s_{13}, s_{2'3'}, s_{123}) \tag{5.33}$$

Note that since

$$s_{123} \;=\; s_{31} \;+\; s_{12} \;+\; s_{23} \;-\; 3m^2 \tag{5.34}$$

(where m is the mass of the scattering particles) the cut in s_{123} will be distinguished from the asymptotic cuts in s_{31} and s_{23} only when s_{12} is large. Consequently, the contribution of the s_{123} cut, as a distinct asymptotic cut, is effectively as a cut in s_{12}. In the following, therefore, we will use (5.8) also as an approximation for s_{123}.

If we simply associated the triplets $\mathcal{C}_a$ and $\mathcal{C}_b$ with the hexagraph we are discussing, and similarly associated analagous pairs with all other hexagraphs we would have the unique association of triplet pairs with each hexagraph as we said we initially expected. However, there is obviously a third triplet that can be formed from the cuts of Fig. 5.4, i.e.

$$\mathcal{C}_c \;=\; (s_{1'3'}, s_{23}, s_{123}) \tag{5.35}$$

The presence of this additional triplet is very important for our anomaly analysis. As is clear from our discussion of the scattering processes of Fig. 4.8, the subenergy discontinuities that distinguish $\mathcal{C}_b$ and $\mathcal{C}_c$ also distinguish the two contributions from the diagram of Fig. 2.3 that we anticipate will be involved in a cancelation. Referring to (5.6) - (5.8) we notice that these distinguishing cuts are also asymptotically equivalent. This implies that kinematically the two triplets give identical asymptotic behavior and so could be involved in a cancelation. However, the asymptotic equivalence identifies final state and initial state discontinuities and so, a-priori, the two contributions could have different quantum number dependence and different dependence on the the non-asymptotic variables.

The presence of both $\mathcal{C}_b$ and $\mathcal{C}_c$ in the same hexagraph is another consequence of the occurrence of two distinct z_i-plane regions in a single s-channel. As is easily checked from (5.6)-(5.8), both triplets are present in both $z_i \geq 1,\ i = 1, 2, 3$ and $z_i \leq -1,\ i = 1, 2, 3$. This clearly produces a conflict with the need to have all the multiple discontinuities associated with a particular hexagraph located on a unique product of (positive or negative) real z_i axes. For the set of cuts $\mathcal{C}_a$ there is no conflict. From (5.5) it follows that the sign of $s_{11'3}$ determines that of z_3 while (for u_1 and u_2 fixed, z_1 and z_2 large) the sign of z_1 and z_2 is then directly determined by the sign of s_{13} and $s_{2'3'}$ respectively. The set of cuts $\mathcal{C}_a$ therefore determines the product of z_i axes to be associated with the hexagraph. The same is true for the analogue of $\mathcal{C}_a$ in each of the 24 hexagraphs.

In contrast, the analogues of the triple discontinuities $\mathcal{C}_b$ and $\mathcal{C}_c$ in each of the 24 hexagraphs, appear on two products of half-axes on which the z_i have opposite signs. Note that the triplet $\mathcal{C}_b$ for the first hexagraph of Fig. 5.3 is the analogue

of $\mathcal{C}_c$ for the last hexagraph. If (as a choice of sign convention) the first graph is associated with $z_i \geq 1, \forall\ i$, then the last graph (related to the first by three twists) should be associated with $z_i \leq -1, \forall\ i$. To achieve this we associate with the first hexagraph of Fig. 5.3 the triple discontinuity $\mathcal{C}_b$ that occurs when all the z_i are positive, and associate the same triple discontinuity, with all the z_i negative, with the last hexagraph. Similarly, in all hexagraphs, we keep only the triple discontinuities associated with the analogues of the $\mathcal{C}_b$ and $\mathcal{C}_c$ cuts that are on products of half-axes on which the z_i have the appropriate signs.

In summary, there are three sets of cuts associated with each hexagraph. Of the three, two appear also in a second hexagraph. Therefore, the corresponding triple discontinuity appears twice in the sum over hexagraphs. From the total of 24 hexagraphs there are, of course, only 48 distinct triple discontinuities contributing to the dispersion relation (5.28). That $\mathcal{C}_b$ and $\mathcal{C}_c$ appear in the same hexagraphs is fundamental for the purpose of this paper. An important cancelation of anomaly contributions from maximally non-planar Feynman graphs is, in the language of discontinuities, a cancelation between triplets of cuts of the form $\mathcal{C}_b$ and $\mathcal{C}_c$.

For $M^{\mathcal{C}_a}$ we can write straightforwardly

$$M^{\mathcal{C}_a} \;=\; \frac{1}{(2\pi i)^3}\int_{\{s_{13}>s_{130},\ s_{2'3'}>s_{2'3'0},\ s_{11'3}>s_{11'30}\}} \frac{ds'_{13}ds'_{2'3'}ds'_{11'3}\Delta^{\mathcal{C}_a}(\underset{\sim}{t},\underset{\sim}{u},s'_{13},s'_{2'3'},s'_{11'3})}{(s'_{13}-s_{13})(s'_{2'3'}-s_{2'3'})(s'_{11'3}-s_{11'3})} \tag{5.36}$$

where the integration region maps directly onto $\{z_1z_3 > z_{130},\ z_2z_3 > z_{230},\ z_3 > z_{30}\}$. It follows from the representation (5.36) that for small $s_{13}, s_{2',3'}$ and $s_{11'3}$, $M^{\mathcal{C}_a}$ can be expanded as

$$M^{\mathcal{C}_a} \;=\; \sum_{m,n,r=0}^{\infty} c^a_{mnr}\ s^m_{13}\ s^n_{2'3'}\ s^r_{123} \tag{5.37}$$

where the c^a_{mnr} are functions of the u_i and t_i only. The analogues of $M^{\mathcal{C}_a}$ for each of the hexagraphs have analagous representations and expansions. The expansion (5.37) places an important constraint on our partial-wave analysis in the next sub-section.

The analogue of (5.29) for $M^{\mathcal{C}_b}$ is

$$M^{\mathcal{C}_b} = \frac{1}{(2\pi i)^3}\int \frac{ds'_{13}ds'_{2'3'}ds'_{123}\Delta^{\mathcal{C}_b}(\underset{\sim}{t},\underset{\sim}{u},s'_{13},s'_{2'3'},s'_{123})}{(s'_{13}-s_{13})(s'_{2'3'}-s_{2'3'})(s'_{123}-s_{123})} \tag{5.38}$$

As we discussed above, in order to introduce signatured amplitudes in the following, we will separate $M^{\mathcal{C}_b}$ into two terms, with one written as an integral over $z_i \geq 1\ i = 1,2,3$ and the other written as an integral over $z_i \leq -1\ i = 1,2,3$. However, it follows

from the asymptotic forms (5.3)-(5.8) that up to non-leading powers, and therefore in the full asymptotic dispersion relation, the two multiple discontinuities must be identical. Consequently, for the purpose of writing the dispersion relation, it suffices to write the single term (5.38). For small $s_{13}, s_{2'3'}, s_{123}$, (5.38) gives the expansion

$$M^{\mathcal{C}_b} \;=\; \sum_{m,n,r=0}^{\infty} c^b_{mnr}\; s_{13}^m\; s_{2'3'}^n\; s_{11'3}^r \tag{5.39}$$

We can give a parallel discussion for $\mathcal{C}_c$ and also for the analagous sets of cuts in all other hexagraphs. The expansion (5.39) has strong implications for the partial-wave expansions that we discuss next.

The association of one set of cuts, such as $\mathcal{C}_b$, with two distinct hexagraphs will facilitate our discussions of signature. That the same triple discontinuity appears on the (product of the) positive and negative z_i axes will lead to important signature properties. Note that $\mathcal{C}_a$ and $\mathcal{C}_b$ share a common double discontinuity, in s_{13} and $s_{2'3'}$. For the purpose of counting all triple discontinuities we can clearly ignore the $\mathcal{C}_c$ set for each hexagraph, since it is counted as a $\mathcal{C}_b$ in another graph. The double discontinuity shared by $\mathcal{C}_a$ and $\mathcal{C}_b$ is uniquely associated with that hexagraph. We will exploit this defining property of hexagraph amplitudes further in the next Section.

5.5 Partial-Wave Expansions

The next step in developing the multi-regge theory associated with the Toller diagram of Fig. 5.1 is to write a partial-wave expansion for each set of hexagraph amplitudes that are related by twisting and, therefore, have the same t-channel. For the set of amplitudes corresponding to the hexagraphs of Fig. 5.3 we write

$$\sum_H M^H(z_1,z_2,z_3,u_1,u_2) = \sum_{\substack{J_1,J_2,J_3=0 \\ |n_1|\le J_1, |n_2|\le J_2 \\ |n_1+n_2|\le J_3}}^{\infty} d^{J_1}_{0,n_1}(z_1)\, d^{J_2}_{0,n_2}(z_2)\, d^{J_3}_{-n_1-n_2,0}(z_3)\, u_1^{n_1} u_2^{n_2} a_{\underset{\sim}{J},\underset{\sim}{n}} \tag{5.40}$$

Our analysis will be focussed on the sub-series in (5.40) with $n_1, -n_2 > 0$ and $n_2, -n_1 > 0$. In our notation n_1 and $-n_2$ are t_3-channel center-of-mass helicities. If n_1 and n_2 have opposite signs, this corresponds to same sign "t-channel" helicities and therefore (at "zero mass" $\equiv t_1$ or $t_2 \;= 0$)) to opposite sign "s-channel" helicities. For this reason, we will refer to amplitudes with opposite signs for n_1 and n_2 as "helicity-flip" amplitudes.

Writing (5.40) for $M^{\mathcal{C}_a}$ we can compare the expansion obtained directly with the expansion (5.37). In the same leading-power approximation that gives (5.3) -

(5.8), we can write

$$\begin{aligned} d^{J_1}_{0,n_1}(z_1)\, d^{J_2}_{0,n_2}(z_2)\, d^{J_3}_{-n_1-n_2,0}(z_3)\, u_1^{n_1} u_2^{n_2} \quad &\sim \quad z_1^{J_1} z_2^{J_2} z_3^{J_3} u_1^{n_1} u_2^{n_2} \\ &= \; (z_1 z_3 u_1)^{J_1} (z_2 z_3 u_2^{-1})^{J_2} z_3^{J_3-J_1-J_2}\; u_1^{n_1-J_1}\; u_2^{J_2-n_2} \end{aligned} \tag{5.41}$$

Using (5.3) - (5.7) we can therefore write

$$\begin{aligned} d^{J_1}_{0,n_1}(z_1)\, d^{J_2}_{0,n_2}(z_2)\, d^{J_3}_{-n_1-n_2,0}(z_3)\, u_1^{n_1} u_2^{n_2} \quad &\sim \quad (s_{13})^{J_1} (s_{2'3'})^{J_2} (s_{11'3})^{J_3-J_1-J_2} \\ &\qquad \times c_a(u_1, u_2) \end{aligned} \tag{5.42}$$

Since we must have a non-negative power of $s_{11'3}$ to obtain a term in the expansion (5.37), we see that we must have

$$J_3 \;\geq\; J_1 + J_2 \tag{5.43}$$

We can repeat this last discussion for $M^{\mathcal{C}_b}$ by rewriting (5.41) as

$$\begin{aligned} & d^{J_1}_{0,n_1}(z_1)\, d^{J_2}_{0,n_2}(z_2)\, d^{J_3}_{-n_1-n_2,0}(z_3)\, u_1^{n_1} u_2^{n_2} \\ & \quad \sim \quad (z_1 z_3 u_1)^{(J_3+J_1-J_2)/2} (z_2 z_3 u_2^{-1})^{(J_3+J_2-J_1)/2} (z_1 z_2 u_1 u_2^{-1})^{(J_1+J_2-J_3)/2} u_1^{n_1-J_1} u_2^{J_2-n_2} \\ & \quad \sim \quad (s_{13})^{(J_3+J_1-J_2)/2} (s_{2'3'})^{(J_3+J_2-J_1)/2} (s_{123})^{(J_1+J_2-J_3)/2} \quad \times \; c_b(u_1, u_2) \end{aligned} \tag{5.44}$$

where we have used (5.8) for s_{123} ($\sim s_{12}$) instead of (5.5). Now the requirement of a non-negative power for s_{123} implies that terms in (5.39) can contribute only to those terms in (5.40) with

$$J_3 \;\leq\; J_1 \;+\; J_2 \tag{5.45}$$

Thus we see that the asymptotic contributions of the triple discontinuities $M^{\mathcal{C}_a}$ and $M^{\mathcal{C}_b}$ appear in two distinct parts of the partial-wave expansion (5.40). As a result, the Sommerfeld-Watson representation discussed in the next sub-section is very different in the two cases. This important point was not brought out in [3]. An identical analysis to that made for $M^{\mathcal{C}_b}$ can obviously be made for $M^{\mathcal{C}_c}$.

An additional requirement for (5.44) to correspond to a term in (5.37) is that the powers of the invariants in (5.44) must be integer. This places a further restriction on the partial-waves that $M^{\mathcal{C}_b}$ can contribute to. In fact, if we constrain $J_1 + J_2 - J_3$ to be an even integer, then no further constraint on the J_i is required (other than that they be positive integers). This is equivalent to the signature constraint

$$\tau_1 \tau_2 \tau_3 \;=\; 1 \tag{5.46}$$

where at this stage $\tau_i = \pm 1$ when J_i is *even/odd*. As we discuss below, this constraint on signatured amplitudes for $M^{\mathcal{C}_b}$ is closesly related to the doubling of triple discontinuities discussed above.

Note that if we consider leading helicity physical amplitudes (i.e. with $|n_i| = J_i,\ i = 1, 2$) then if $n_1, n_2 > 0$, necessarily

$$J_3 \ \geq \ n_1 \ + \ n_2 \ = \ J_1 \ + \ J_2 \tag{5.47}$$

Consequently $J_3 < J_1 + J_2$ is only possible for (leading) helicity-flip amplitudes. It was observed by Detar and Weis[17], in their study many years ago of the dual-model triple-Regge vertex, that the term in the vertex with (essentially) the set of cuts $M^{\mathcal{C}_b}$ contributes to partial-wave amplitudes satisfying inequalities of the form (5.45). The S-W formalism that we will be using was not developed at the time of the Detar and Weis paper.

5.6 Signature and the Sommerfeld-Watson Representations

As in elementary Regge theory, it is necessary to introduce signature before making Froissart-Gribov (F-G) continuations of partial-wave amplitudes and introducing Sommerfeld-Watson (S-W) representations. We define signatured hexagraph amplitudes

$$\begin{aligned} M^{H,\underset{\sim}{\tau}} \ &= \ M^{H,(\tau_1,\tau_2,\tau_3)} \\ &= \ \frac{1}{8}\Big[\ M^H \ + \ \tau_1 M^{\mathcal{T}_1 H} \ + \ \tau_2 M^{\mathcal{T}_2 H} \ + \ \tau_3 M^{\mathcal{T}_3 H} \ + \ \tau_1\tau_2 M^{\mathcal{T}_1\mathcal{T}_2 H} \\ &\qquad + \ \tau_2\tau_3 M^{\mathcal{T}_2\mathcal{T}_3 H} \ + \ \tau_3\tau_1 M^{\mathcal{T}_3\mathcal{T}_1 H} \ + \ \tau_1\tau_2\tau_3 M^{\mathcal{T}_1\mathcal{T}_2\mathcal{T}_3 H}\ \Big] \end{aligned} \tag{5.48}$$

where $\tau_i = \pm 1$, and $\mathcal{T}_i H$ is the hexagaph obtained from the hexagraph H by a twist about the ith horizontal line. The full amplitude, or rather the sum over hexagraph amplitudes, is recoverd as a sum over signatured amplitudes, i.e.

$$\sum_{\underset{\sim}{\tau}} M^{H,\ \underset{\sim}{\tau}} = M^H + M^{\mathcal{T}_1 H} + M^{\mathcal{T}_2 H} + M^{\mathcal{T}_3 H} + M^{\mathcal{T}_1\mathcal{T}_2 H} + M^{\mathcal{T}_2\mathcal{T}_3 H} + M^{\mathcal{T}_3\mathcal{T}_1 H} + M^{\mathcal{T}_1\mathcal{T}_2\mathcal{T}_3 H} \tag{5.49}$$

Provided we make the separation into separate hexagraphs of the two triple discontinuities of $M^{\mathcal{C}_b}$ etc., (5.48) is a simple generalisation of the analytic definition of signature for elastic scattering amplitudes, where combinations of amplitudes with right and left-hand cuts are formed.

In writing the initial dispersion relation (5.28) we are, of course, assuming a generalization of the usual crossing relation that there is a single analytic function

that connects all the physical region amplitudes. When quark quantum numbers and helicities are involved, there are additional subtleties in the crossing relation. These subtleties are resolved if we assume that our analytic definition of signatured amplitudes in (5.48) is equivalent to the following alternative "group-theoretic" definition of signature. Beginning with an N-point amplitude in a particular s-channel, we form the positive (or negative) signatured amplitude, with respect to a particular internal line of a Toller diagram, by adding (or subtracting) the amplitude obtained by making a complete CPT transformation on all external particles connected (through the diagram) to one end of the internal line. The fully signatured amplitude is formed by carrying out this procedure for all internal lines of the Toller diagram. In this way, signature is introduced at the amplitude level without introducing spectral components. It is an operation defined directly on the external states and so is often easier to implement. Although the equivalence of the two definitions has only been proven in the simplest cases, we have no reason to doubt that the equivalence is true in general. To understand the implications of signature for phases etc. it is, of course, essential to utilise the analytic formulation.

In a t-channel the twisting process does not involve interchanging incoming and outgoing particles. Therefore, a signature twist becomes a CP rather than a CPT transformation. The charge conjugation part of the transformation is very important for our discussion of the anomaly. However, if we ignore quantum numbers then a signature twist is effectively a t-channel parity transformation of the final state relative to the initial state. In order to have three independent parity transformations, we must have a dependence on invariants that involve directly the momenta at the central vertex, i.e. the Q_i. In Fig. 5.4, only $s_{11'3}$ has this property. This is why only triplets of the $\mathcal{C}_a$ kind produce three independent signatures.

The S-W transform of (5.40) is obtained by converting the sums over n_1, n_2, and J_3 to integrals. Initially this process is carried out with z_1 and z_2 small, although we will then use the representation to discuss large z_1 and z_2. The conversion of sums over n_1, n_2, to integrals represents many of the asymptotic cuts as cuts in the u_1 and u_2 planes and therefore should be carried out in the $s - s$ region where large u_1 and u_2 are physical regions.

The treatment of that part of the expansion satisfying (5.43) is straightforward. This contains $M^{\mathcal{C}_a}$ together with the corresponding contribution from all the hexagraphs of Fig. 5.3. To illustrate the structure of the S-W transform we first omit the complications due to signature and (effectively) assume a F-G continuation can be made for $M^{\mathcal{C}_a}$ alone. Because the definition of $d^J_{n,0}$ changes non-analytically at $n = 0$ we must make separate continuations for $n_1, n_2, n_1 + n_2 \gtrless 0$. For $n_1, -n_2, n_1 + n_2 \geq 0$,

we can write

$$M^{\mathcal{C}_a} = \frac{1}{(2\pi)^3} \int_> \frac{dn_1\ (u_1)^{n_1}}{\sin \pi n_1} \int_< \frac{dn_2\ (u_2)^{n_2}}{\sin \pi n_2}$$
$$\times \sum_{\substack{N_1=J_1-|n_1|=0 \\ N_2=J_2-|n_2|=0}}^{\infty} \int_{C_{N_1+N_2}} \frac{dJ_3\ \ d^{J_3}_{n_1+n_2,0}(z_3)}{\sin \pi(J_3 - n_1 + n_2)} d^{J_1}_{0,n_1}(z_1) d^{J_2}_{0,n_2}(z_2)\ \ a_{\mathcal{C}_b,\underset{\sim}{J},\underset{\sim}{n},\underset{\sim}{>}} \tag{5.50}$$

where each integration contour is asymptotically parallel to the imaginary axis and chosen to reproduce the partial-wave sum when closed in the appropriate half-plane (because of the symmetry under $u_1 \to u_1^{-1}, u_2 \to u_2^{-1}$, $n_1 \leq 0, n_2 \geq 0$ gives an identical contribution). The contour $C_{N_1+N_2}$ imposes (5.43) i.e.

$$J_1 + J_2 \ = \ N_1 + n_1 + N_2 - n_2 \leq J_3 \tag{5.51}$$

and so has the form shown in Fig. 5.5

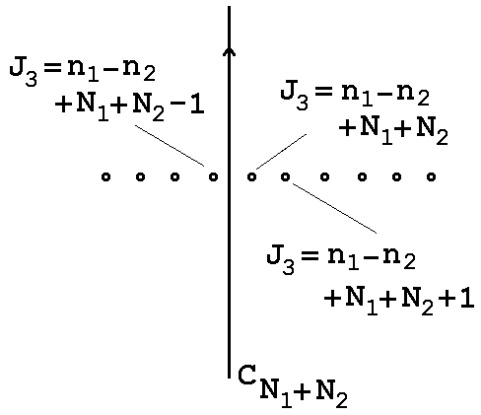

Fig. 5.5 The Contour in the J_3 Plane.

The $>$ and $<$ labels for the n_i integrals indicate that they reproduce the associated positive/negative helicity sums.

For small $z_i,\ i = 1, 2$, a twist in the ith channel corresponds to $u_i \to \ -u_i$ and $z_i \to \ -z_i$. For small z_i, and integer $j_i - |n_i| = N_i$,

$$d^{J_i}_{0,n_i}(-z_i) \ = \ (-1)^{J_i - n_i} d^{J_i}_{0,n_i}(z_i) \tag{5.52}$$

Consequently for $M^{\mathcal{C}_a}$ we can adapt (5.50) to represent the sum over amplitudes involving twists in the 1 and 2 channels by making the replacement

$$(u_i)^{n_i} d^{J_i}_{0,n_i}(z_i) \ \ \to \ \ (u_i)^{n_i} d^{J_1}_{0,n_i}(z_i) \ + \ \tau_i\ (-u_i)^{n_i} d^{J_i}_{0,n_i}(-z_i) \qquad i = 1, 2 \tag{5.53}$$

A twist in the 3 channel is more complicated since $d^{J_3}_{n_1+n_2,0}(z_3)$ depends on n_1 and n_2 as well as J_3. For amplitudes that already have specific τ_1 and τ_2 signatures, we can introduce signature for $z_3 \to -z_3$ by writing

$$d^{J_3}_{n_1+n_2,0}(z_3) \;\; \to \;\; d^{J_3}_{n_1+n_2,0}(z_3) \;+\; \tau_3\tau_1\tau_2(-1)^{N_1+N_2} d^{J_3}_{n_1+n_2,0}(-z_3) \tag{5.54}$$

Of course, we also write

$$a_{\mathcal{C}_b,\underset{\sim}{J},\underset{\sim}{n},\underset{\sim}{\geq}} \;\; \to \;\; a_{\mathcal{C}_b,\underset{\sim}{J},\underset{\sim}{n},\underset{\sim}{\geq},\underset{\sim}{\tau}} \tag{5.55}$$

The construction of signatured F-G continuations $a_{\mathcal{C}_b,\underset{\sim}{J},\underset{\sim}{n},\underset{\sim}{\geq},\underset{\sim}{\tau}}$ that are equal to the physical partial-waves at "right-signature" points (i.e. J_i = even/odd for $\tau_i = +/-,\ i = 1,2,3$) is described in detail in [5].

The S-W transform of that part of the expansion (5.40) that satisfies (5.45), and so contains $M^{\mathcal{C}_b}$ and $M^{\mathcal{C}_c}$, requires extra discussion. When (5.45) is satisfied at physical points, n_1 and n_2 will generally have opposite signs. (For leading helicities this must be the case, as we noted above.) Consider that part of (5.40) with $n_1, -n_2, n_1+n_2 \geq 0$. (5.45) becomes

$$N_1 + n_1 + N_2 - n_2 - J_3 \;=\; even\ integer \;\geq\; 0 \tag{5.56}$$

Temporarily ignoring the full signature problem, we can write

$$\begin{aligned} M^{\mathcal{C}_b} =& \frac{1}{(2\pi)^3}\int dn_1 dn_2 (u_1)^{n_1}(u_2)^{n_2} \sum_{\substack{N_1,N_2=0 \\ N_1+N_2\ even}}^{\infty} d^{N_1+n_1}_{0,n_1}(z_1)\; d^{N_2-n_2}_{0,n_2}(z_2) \\ & \int_{C_{J_3}} \frac{dJ_3 \qquad d^{J_3}_{n_1+n_2,0}(z_3)}{\sin\pi(n_1+n_2)\sin\frac{\pi}{2}(J_3-n_1-n_2\sin\frac{\pi}{2}(n_1-n_2-J_3)} \quad a_{\mathcal{C}_b,\underset{\sim}{J},\underset{\sim}{n},\underset{\sim}{\geq}} \end{aligned} \tag{5.57}$$

(The symmetry under $u_1 \to u_1^{-1}, u_2 \to u_2^{-1}$ implies that $n_1 \leq 0, n_2 \geq 0$ gives an identical contribution.) The integration contours are again asymptotically parallel to the imaginary axis. The contour C_{J_3} is as shown in Fig. 5.6.

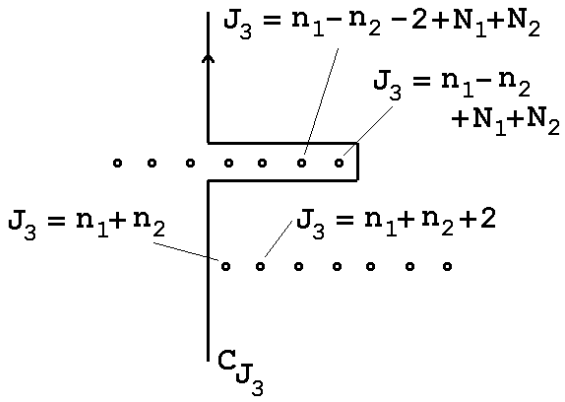

Fig. 5.6 Another Contour in the J_3 Plane.

Poles at negative integer n_2 are produced when the poles at $J_3 - n_1 + n_2 - N_1 - N_2$ a negative even integer collide with the series at $J_3 - n_1 - n_2$ a positive even integer. As always the $\gtrsim$ labels on ${}^{a}_{\mathcal{C}_b,\underset{\sim}{J},\underset{\sim}{n},\underset{\sim}{\gtrsim},\underset{\sim}{\tau}}$ refer to distinct F-G continuations made for distinct combinations of helicity signs.

(5.57) gives both even and odd values of n_1 and n_2. Consequently (5.53) can again be used to introduce signature in the 1 and 2 channels. Since we must impose (5.46), we need not add any further signature effects. However, we note that the arguments of two of the denominator sine factors in (5.57) are already restricted to even integer physical values. Therefore, each term in the signatured form of (5.57) could be modified by phase factors of the form $(-1)^E$ where E is either of these sine function arguments. In principle the uniquenes of the F-G continuation resolves such anbiguities. We will resolve them by determining the appropriate asymptotic phases of signatured Regge pole amplitudes. Finally we make the obvious remark that we can directly apply all of our discussion of $M^{\mathcal{C}_b}$ to $M^{\mathcal{C}_c}$.

5.7 Regge Behavior

The Steinmann relations imply that for each hexagraph amplitude the asymptotic cuts are completely represented by the S-W integrals of (5.50) and (5.57). (We again, temporarily, ignore signature.) Consequently the sums over $N_1 = J_1 - n_1$ and $N_2 = J_2 - |n_2|$ should be uniformly convergent also in the Regge asymptotic region. We will assume, therefore, that we can liberally interchange limits and sums in the S-W representations. For fixed N_1 and N_2, the integrals over n_1 and n_2 can be treated as integrals over either n_1 and n_2 or J_1 and J_2. Consequently asymptotic expansions can be obtained as either $z_1, z_2 \to \infty$ or as u_1 $(u_1^{-1}), u_2$ $(u_2^{-1}) \to \infty$ by pulling contours to the left (right) in the complex plane in the conventional manner. In this way, each of the triple-regge and helicity-pole limits defined above can be studied. The replacement of the $d^J_{n,0}$ by second-type representation functions proceeds in direct

parallel with elementary Regge theory. This is a technical necessity to ensure that a genuine asymptotic expansion is obtained but we will not describe it here. For our purposes it is sufficient to assume that we simply pick up the leading power behavior of the $d^J_{n,0}(z)$ of the form z^J, as contours are pulled back in (5.50) and (5.57).

The most important point for studying limits via the S-W transform is that (by analytically continuing t-channel unitarity equations in all complex angular momentum and helicity planes) it can be shown that the Regge singularities of $a_{\mathcal{C},\underset{\sim}{J},\underset{\sim}{n},\underset{\sim}{>}} = a_{\mathcal{C},\underset{\sim}{>}}(J_3, n_1, n_2, N_1, N_2, t_1.t_2, t_3)$ occur at fixed values of the J_i. In particular, Regge poles at $J_i = \alpha_i = \alpha(t_i)$ occur in $a_{\mathcal{C},>,>}(J_3, n_1, n_2, N_1, N_2, t_1.t_2, t_3)$ (the F-G continuation made from $n_1, n_2 > 0$) at

$$n_1 = \alpha_1 - N_1 \ , \quad n_2 = \alpha_2 - N_2 \ , \quad J_3 = \alpha_3 \tag{5.58}$$

In $a_{\mathcal{C},>,<}(J_3, n_1, n_2, N_1, N_2, t_1.t_2, t_3)$ (the continuation from $n_1, -n_2 > 0$), the Regge poles occur at

$$n_1 = \alpha_1 - N_1 \ , \quad -n_2 = \alpha_2 - N_2 \ , \quad J_3 = \alpha_3 \tag{5.59}$$

etc.

In the triple-regge limit, Regge poles give contributions to each of the terms in the double sums in (5.50) and (5.57). We initially omit the denominator sine factors since they are modified by the introduction of signature. We can then write the triple Regge pole contribution to $M^{\mathcal{C}_a}$ via (5.50) as

$$\begin{aligned} M^{\mathcal{C}_a} \underset{\substack{z_1, z_2, \\ z_3, \to \infty}}{\sim} & z_1^{\alpha_1} z_2^{\alpha_2} z_3^{\alpha_3} \sum_{N_1,N_2=0}^{\infty} \Big[u_1^{\alpha_1 - N_1} u_2^{\alpha_2 - N_2} \beta^a_{\alpha_1,\alpha_2,\alpha_3,N_1,N_2} + \\ & u_1^{-\alpha_1+N_1} u_2^{\alpha_2-N_2} \beta^a_{-\alpha_1,\alpha_2,\alpha_3,N_1,N_2} + u_1^{\alpha_1-N_1} u_2^{-\alpha_2+N_2} \beta^a_{\alpha_1,-\alpha_2,\alpha_3,N_1,N_2} \\ & + u_1^{-\alpha_1+N_1} u_2^{-\alpha_2+N_2} \beta^a_{-\alpha_1,-\alpha_2,\alpha_3,N_1,N_2} \Big] \end{aligned} \tag{5.60}$$

where $\beta^a_{\alpha_1,\alpha_2,\alpha_3,N_1,N_2}$ is the Regge-pole residue of the "non-flip" F-G amplitude $a_{\mathcal{C},>,>}(J_3, n_1, n_2, N_1, N_2, t_1.t_2, t_3)$ at $J_i = \alpha_i,\ i = 1, 2, 3$ and $n_i = J_i - N_i,\ i = 1, 2$ and $\beta^a_{-\alpha_1,\alpha_2,\alpha_3,N_1,N_2}$ is the corresponding residue of the "helicity-flip" F-G amplitude $a_{\mathcal{C},<,>}(J_3, n_1, n_2, N_1, N_2, t_1.t_2, t_3)$. Because of the symmetry under $u_1 \to 1/u_1, u_2 \to 1/u_2$, the first and last sums in (5.60) can be identified, as can the second and third. When the hexagraph containing $M^{\mathcal{C}_a}$ is part of a larger hexagraph this symmetry is, in general, not present.

The contribution of Regge poles to $M^{\mathcal{C}_b}$, in the triple-Regge limit, has less

structure than (5.60). From (5.57) we obtain

$$M^{\mathcal{C}_b} \underset{\substack{z_1, z_2, \\ z_3, \to \infty}}{\sim} z_1^{\alpha_1} z_2^{\alpha_2} z_3^{\alpha_3} \sum_{N_1+N_2 even} \Big[u_1^{-\alpha_1+N_1} u_2^{\alpha_2-N_2} \beta^b_{-\alpha_1,\alpha_2,\alpha_3,N_1,N_2} + u_1^{\alpha_1-N_1} u_2^{-\alpha_2+N_2} \beta^a_{\alpha_1,-\alpha_2,\alpha_3,N_1,N_2} \Big] \tag{5.61}$$

Again the symmetry under $u_1 \to 1/u_1, u_2 \to 1/u_2$ implies that (in this case) the two terms in (5.61) can be identified. $M^{\mathcal{C}_c}$ has an identical contribution but with, of course, $\beta^b_{\pm\alpha_1,\pm\alpha_2,\alpha_3,N_1,N_2} \to \beta^c_{\pm\alpha_1,\pm\alpha_2,\alpha_3,N_1,N_2}$

To obtain the behavior of the full amplitude in the triple-regge limit we must not only add $M^{\mathcal{C}_a}$, $M^{\mathcal{C}_b}$, and $M^{\mathcal{C}_c}$, but we must also add all the contributions corresponding to the additional hexagraphs illustrated in Fig. 5.2. These contributions will have the same form as (5.60) and (5.61) but with the indices $1, 2$ and 3 cyclically rotated. Twisted graphs also have to be added by incorporating signature factors. Before discussing signature in detail, it will be useful to first discuss the contribution of Regge poles in helicity-pole limits.

The non-flip helicity-pole limit (5.14) picks out only the first term of the first (and identical third) sum in (5.60) i.e.

$$M^{\mathcal{C}_a} \underset{\substack{u_1, u_2, \\ z_3, \to \infty}}{\sim} (z_1 u_1)^{\alpha_1} (z_2 u_2)^{\alpha_2} z_3^{\alpha_3} \beta^a_{\alpha_1,\alpha_2,\alpha_3,0,0} \tag{5.62}$$

There is no triple-Regge contribution from $M^{\mathcal{C}_b}$ and $M^{\mathcal{C}_c}$ in this limit. In the helicity-flip limit each of $M^{\mathcal{C}_a}$, $M^{\mathcal{C}_b}$, and $M^{\mathcal{C}_c}$ give contributions, i.e.

$$M^{\mathcal{C}_{a,b,c}} \underset{\substack{u_1, 1/u_2, \\ z_3, \to \infty}}{\sim} (z_1 u_1)^{\alpha_1} (z_2 u_2^{-1})^{\alpha_2} z_1^{\alpha_3} \beta^{a,b,c}_{\alpha_1,-\alpha_2,\alpha_3,0,0} \tag{5.63}$$

In summary, distinct leading helicity amplitudes, i.e. non-flip and flip, contribute in the distinct helicity-pole limits while the complete series of both amplitudes contribute in the full triple-regge limit. This explains why we refer to (5.14) and (5.15) respectively as non-flip and helicity-flip limits. Note that in both limits the dependence on both z_1 and z_2 is determined by the u_1 and u_2 dependence. This is necessary for the amplitudes to be directly expressible in terms of invariants, as we see in the next sub-section.

5.8 Asymptotic Analytic Structure

We can now discuss how the cuts of $M^{\mathcal{C}_a}$, $M^{\mathcal{C}_b}$, and $M^{\mathcal{C}_c}$ are represented

asymptotically in the triple-Regge formulae. Similarly to the rewriting of (5.41) in the form (5.42), we can use (5.3) - (5.7) to write

$$\begin{aligned}\beta^a_{\alpha_1,\alpha_2,\alpha_3,0,0}\ (z_1u_1)^{\alpha_1}(z_2u_2)^{\alpha_2}z_3^{\alpha_3} &= \beta^a_{\alpha_1,\alpha_2,\alpha_3,0,0}\ (z_1z_3u_1)^{\alpha_1}(z_1z_3u_2)^{\alpha_2}\ (z_3)^{\alpha_3-\alpha_1-\alpha_2}\\ &\sim \beta^a_{\alpha_1,\alpha_2,\alpha_3,0,0}\ (s_{13})^{\alpha_1}(s_{2'3'})^{\alpha_2}(s_{11'3})^{\alpha_3-\alpha_1-\alpha_2}\end{aligned} \tag{5.64}$$

showing how (5.62) represents the cuts of $M^{\mathcal{C}_a}$ in both the non-flip helicity-pole limit and the full triple-Regge limit. Similarly we can write

$$\begin{aligned}\beta^a_{\alpha_1,-\alpha_2,\alpha_3,0,0}\ (z_1u_1)^{\alpha_1}(z_2u_2^{-1})^{\alpha_2}z_3^{\alpha_3} &= \beta^a_{\alpha_1,-\alpha_2,\alpha_3,0,0}\ (z_1z_3u_1)^{\alpha_1}\left(\frac{z_2z_3}{u_2}\right)^{\alpha_2}\ (z_3)^{(\alpha_3-\alpha_1-\alpha_2)}\\ &\sim \beta^a_{\alpha_1,-\alpha_2,\alpha_3,0,0}\ (s_{13})^{\alpha_1}(s_{2'3'})^{\alpha_2}(s_{11'3})^{\alpha_3-\alpha_1-\alpha_2}\end{aligned} \tag{5.65}$$

to see the cuts of $M^{\mathcal{C}_a}$ also represented in the helicity-flip limit and in helicity-flip contributions to the triple-Regge limit.

For the helicity-flip contribution from $M^{\mathcal{C}_b}$ we utilise (5.8) and write

$$\begin{aligned}&\beta^b_{\alpha_1,-\alpha_2,\alpha_3,0,0}\ (z_1u_1)^{\alpha_1}(z_2u_2^{-1})^{\alpha_2}z_3^{\alpha_3}\\ &\quad= \beta^b_{\alpha_1,-\alpha_2,\alpha_3,0,0}\ (z_1z_3u_1)^{(\alpha_1+\alpha_3-\alpha_2)/2}\left(\frac{z_2z_3}{u_2}\right)^{(\alpha_2+\alpha_3-\alpha_1)/2}\left(\frac{z_1z_2u_1}{u_2}\right)^{(\alpha_1+\alpha_2-\alpha_3)/2}\\ &\quad\sim\ \beta^b_{\alpha_1,-\alpha_2,\alpha_3,0,0}\ (s_{13})^{(\alpha_1+\alpha_3-\alpha_2)/2}(s_{2'3'})^{(\alpha_2+\alpha_3-\alpha_1)/2}(s_{123})^{(\alpha_1+\alpha_2-\alpha_3)/2}\end{aligned} \tag{5.66}$$

showing how the cuts of $M^{\mathcal{C}_b}$ are represented in the helicity-flip limit and in helicity-flip contributions to the triple-Regge limit. $M^{\mathcal{C}_b}$ is represented in an identical fashion.

To add signature factors to (5.64) note that for $J_i - |n_i| = N_i = 0$

$$\frac{(u_i)^{n_i}d^{J_1}_{0,n_i}(z_i)\ +\ \tau_i\ (-u_i)^{n_i}d^{J_i}_{0,n_i}(-z_i)}{sin\pi n_i} \underset{u_i,\,z_i\,\to\,\infty}{\sim} |u_iz_i|^{J_i}\Big[\frac{1+\tau_ie^{i\pi J_i}}{sin\pi J_i}\Big] \tag{5.67}$$

and

$$\frac{d^{J_3}_{n_1+n_2,0}(z_3)+\tau_3\tau_1\tau_2d^{J_3}_{n_1+n_2,0}(-z_3)}{sin\pi(J_3-J_1-J_2)} \underset{z_3\,\to\,\infty}{\longrightarrow} |z_3|^{J_3}\Big[\frac{1+\tau_1\tau_2\tau_3e^{i\pi(J_3-J_1-J_2)}}{sin\pi(J_3-J_1-J_2)}\Big] \tag{5.68}$$

Therefore the signatured form of the S-W representation (5.57) will give (5.64) multiplied by a factor

$$\Big[\frac{1+\tau_1e^{i\pi\alpha_1}}{sin\pi\alpha_1}\Big]\Big[\frac{1+\tau_2e^{i\pi\alpha_2}}{sin\pi\alpha_2}\Big]\Big[\frac{1+\tau_1\tau_2\tau_3e^{i\pi(\alpha_3-\alpha_1-\alpha_2)}}{sin\pi(\alpha_3-\alpha_1-\alpha_2)}\Big] \tag{5.69}$$

giving

$$\beta^a_{\alpha_1,\alpha_2,\alpha_3,0,0}\left[\frac{(s_{13})^{\alpha_1}+\tau_1(-s_{13})^{\alpha_1}}{sin\pi\alpha_1}\right]\left[\frac{(s_{2'3'})^{\alpha_2}+\tau_2(-s_{2'3'})^{\alpha_2}}{sin\pi\alpha_2}\right] \times \left[\frac{(s_{11'3})^{\alpha_3-\alpha_1-\alpha_2}+\tau_1\tau_2\tau_3(-s_{11'3})^{\alpha_3-\alpha_1-\alpha_2}}{sin\pi(\alpha_3-\alpha_1-\alpha_2)}\right] \tag{5.70}$$

This expression now represents the leading helicity (non-flip) triple-regge contribution of the sum of amplitudes corresponding to the eight hexagraphs appearing in Fig. 5.3.

It is straightforward to take discontinuities in (5.70) and to recover the single hexagraph amplitude (5.64).

$$[Disc]_{s_{13}} = 2\,\beta^a_{\alpha_1,\alpha_2,\alpha_3,0,0}\,(s_{13})^{\alpha_1}\left[\frac{(s_{2'3'})^{\alpha_2}+\tau_2(-s_{2'3'})^{\alpha_2}}{sin\pi\alpha_2}\right] \times \left[\frac{(s_{11'3})^{\alpha_3-\alpha_1-\alpha_2}+\tau_1\tau_2\tau_3(-s_{11'3})^{\alpha_3-\alpha_1-\alpha_2}}{sin\pi(\alpha_3-\alpha_1-\alpha_2)}\right] \tag{5.71}$$

$$[Disc]_{s_{13}}\,[Disc]_{s_{2'3'}} = 4\,\beta^a_{\alpha_1,\alpha_2,\alpha_3,0,0}\,(s_{13})^{\alpha_1}(s_{2'3'})^{\alpha_2} \times \left[\frac{(s_{11'3})^{\alpha_3-\alpha_1-\alpha_2}+\tau_1\tau_2\tau_3(-s_{11'3})^{\alpha_3-\alpha_1-\alpha_2}}{sin\pi(\alpha_3-\alpha_1-\alpha_2)}\right] \tag{5.72}$$

$$[Disc]_{s_{13}}\,[Disc]_{s_{2'3'}}[Disc]_{s_{11'3}} = 8\,\beta^a_{\alpha_1,\alpha_2,\alpha_3,0,0}\,(s_{13})^{\alpha_1}(s_{2'3'})^{\alpha_2}(s_{11'3})^{\alpha_3-\alpha_1-\alpha_2} \tag{5.73}$$

Note that if $\alpha_i = 1 + O(g^2)$, as is the case for a reggeized gluon, then since

$$sin\pi\alpha_2 \;\sim\; sin\pi(\alpha_3-\alpha_1-\alpha_2) \;\sim\; O(g^2) \tag{5.74}$$

each discontinuity that is taken reduces the amplitude by $O(g^2)$.

Moving on to the contributions to $M^{\mathcal{C}_b}$ obtained from the signatured form of (5.57). Since we only have two signature factors to add, the factor (5.69) is replaced by

$$\frac{[1+\tau_1 e^{i\pi\alpha_1}+\tau_2 e^{i\pi\alpha_2}+\tau_1\tau_2 e^{i\pi(\alpha_1+\alpha_2)}]}{[sin\pi(\alpha_1-\alpha_2)sin\frac{\pi}{2}(\alpha_2+\alpha_3-\alpha_1)sin\frac{\pi}{2}(\alpha_1+\alpha_2-\alpha_3)]} \tag{5.75}$$

After adding the term corresponding to (5.57) from $n_1+n_2<0$, we obtain the factor

$$\frac{[1+\tau_1 e^{i\pi\alpha_1}+\tau_2 e^{i\pi\alpha_2}+\tau_1\tau_2 e^{i\pi(\alpha_1+\alpha_2)}]}{[sin\frac{\pi}{2}(\alpha_1+\alpha_3-\alpha_2)sin\frac{\pi}{2}(\alpha_2+\alpha_3-\alpha_1)sin\frac{\pi}{2}(\alpha_1+\alpha_2-\alpha_3)]} \tag{5.76}$$

The interpretation of the phases in terms of cut structure is now more subtle. The τ_1 twist of the hexagraph containing $M^{\mathcal{C}_b}$ sends $s_{123} \to -s_{123}$ in addition to $s_{13} \to -s_{13}$. The corresponding triple-regge behavior should therefore be

$$\begin{aligned}(-s_{13})^{(\alpha_1+\alpha_3-\alpha_2)/2}(s_{2'3'})^{(\alpha_2+\alpha_3-\alpha_1)/2}(-s_{123})^{(\alpha_1+\alpha_2-\alpha_3)/2} \\ = \; e^{i\pi\alpha_1}(s_{13})^{(\alpha_1+\alpha_3-\alpha_2)/2}(s_{2'3'})^{(\alpha_2+\alpha_3-\alpha_1)/2}(s_{123})^{(\alpha_1+\alpha_2-\alpha_3)/2}\end{aligned} \tag{5.77}$$

which is the phase-factor corresponding to the τ_1 term in (5.76). This phase is due, however, to the contribution of two cuts and not a single cut, as is conventionally the case, and was the case for $M^{\mathcal{C}_a}$. Clearly the τ_2 twist gives the analagous result and explains the τ_2 term in (5.76). Because of the signature constraint (5.46) we have $\tau_1\tau_2 \equiv \tau_3$. We can obtain the corresponding phase for the $\tau_1\tau_2$ term if we multiply by $e^{i\pi(\alpha_3-\alpha_1-\alpha_2)}$. The presence or absence of phases of this kind is the ambiguity in (5.57) that we discussed at the end of sub-section 5.5. Invoking this phase, we can write the analogue of (5.70) as

$$\begin{aligned}\beta^b_{\alpha_1,-\alpha_2,\alpha_3,0,0}\Big[&(s_{13})^{(\alpha_1+\alpha_3-\alpha_2)/2}(s_{2'3'})^{(\alpha_2+\alpha_3-\alpha_1)/2}(s_{123})^{(\alpha_1+\alpha_2-\alpha_3)/2} \\ &+ \tau_1(-s_{13})^{(\alpha_1+\alpha_3-\alpha_2)/2}(s_{2'3'})^{(\alpha_2+\alpha_3-\alpha_1)/2}(-s_{123})^{(\alpha_1+\alpha_2-\alpha_3)/2} \\ &+ \tau_2(s_{13})^{(\alpha_1+\alpha_3-\alpha_2)/2}(-s_{2'3'})^{(\alpha_2+\alpha_3-\alpha_1)/2}(-s_{123})^{(\alpha_1+\alpha_2-\alpha_3)/2} \\ &+ \tau_3(-s_{13})^{(\alpha_1+\alpha_3-\alpha_2)/2}(-s_{2'3'})^{(\alpha_2+\alpha_3-\alpha_1)/2}(s_{123})^{(\alpha_1+\alpha_2-\alpha_3)/2}\Big]\end{aligned} \tag{5.78}$$

which is now the leading helicity-flip triple-regge contributions of cuts of the form of $M^{\mathcal{C}_b}$ in the first four hexagraphs of Fig. 5.3. Again $M^{\mathcal{C}_c}$ will contribute almost identically.

The process of taking discontinuities is analagous to that of (5.71)-(5.73). We give only the double and triple discontinuities that will be needed in the next Section and are trivially related.

$$\begin{aligned}[Disc]_{s_{13}}\,[Disc]_{s_{2'3'}} \;&=\; 4\;\beta^a_{\alpha_1,-\alpha_2,\alpha_3,0,0}\;(s_{13})^{(\alpha_1+\alpha_3-\alpha_2)/2}(s_{2'3'})^{(\alpha_2+\alpha_3-\alpha_1)/2} \\ &\times\; \frac{(s_{123})^{(\alpha_1+\alpha_2-\alpha_3)/2}}{sin\frac{\pi}{2}(\alpha_1+\alpha_1-\alpha_3)}\end{aligned} \tag{5.79}$$

$$\begin{aligned}[Disc]_{s_{13}}\,[Disc]_{s_{2'3'}}[Disc]_{s_{123}} \;&=\; 8\;\beta^a_{\alpha_1,-\alpha_2,\alpha_3,0,0}\;(s_{13})^{(\alpha_1+\alpha_3-\alpha_2)/2}(s_{2'3'})^{(\alpha_2+\alpha_3-\alpha_1)/2} \\ &\times\; (s_{123})^{(\alpha_1+\alpha_2-\alpha_3)/2}\end{aligned} \tag{5.80}$$

Note that in this case, for reggeized gluon states with $\alpha_i = 1 + O(g^2)$,

$$\begin{aligned} (s_{ij})^{(\alpha_i+\alpha_j-\alpha_k)/2} &= (s_{ij})^{\frac{1}{2}} + O(g^2) \\ &= i\ |s_{ij}|^{\frac{1}{2}} \end{aligned} \tag{5.81}$$

which is pure imaginary. Therefore if $\beta^a_{\alpha_1,-\alpha_2,\alpha_3,0,0}$ is real, both (5.79) and (5.80) are both pure imaginary. Because of this and because also

$$sin\frac{\pi}{2}(\alpha_i + \alpha_j - \alpha_k) = sin\frac{\pi}{2}(1 + O(g^2)) = 1 + O(g^4) \tag{5.82}$$

taking the third discontinuity does not reduce the amplitude by $O(g^2)$ and, in lowest-order, the double discontinuity (5.79) and the triple discontinuity (5.80) differ only by the factor of 2 obtained by writing

$$(s_{123})^{\frac{1}{2}} - (-s_{123})^{\frac{1}{2}} = 2\ (s_{123})^{\frac{1}{2}} \tag{5.83}$$

Strictly, the simplicity in taking the s_{123} discontinuity holds only for the leading helicity amplitude that we have isolated. However, since we expect the azimuthal angle sums to be convergent, we also expect the simplicity to apply to the full triple-regge amplitude.

5.9 Regge Cuts

(5.70) and (5.78) contain the contribution of Regge poles only. To replace a Regge pole by the Regge cut corresponding to a two-reggeon state is straightforward in principle but in practise can be quite complicated. However, for odd-signature reggeized gluons with $\alpha \sim 1$ it is relatively simple to describe the first-order approximation. For example, replacing the Regge pole in the 1 channel in (5.70) by an even signature two-reggeon state gives,

$$\begin{aligned} \left[\frac{(s_{13})^{\alpha_1} + (-s_{13})^{\alpha_1}}{sin\pi\alpha_1}\right] \longrightarrow & \int \frac{d^2k}{sin\pi\alpha(k^2)sin\pi\alpha((Q_1-k)^2)} \\ & \times \left[\frac{(s_{13})^{(\alpha(k^2)+\alpha(Q_1-k)^2-1)} + (-s_{13})^{(\alpha(k^2)+\alpha(Q_1-k)^2-1)}}{sin\pi(\alpha(k^2)+\alpha(Q_1-k)^2-1)}\right] \\ \sim & \int \frac{d^2k}{(k^2)(Q_1-k)^2}\ [\ s_{13}\ ]\left[1 + O(g^2)\right] \\ \sim & J_1(Q_1^2)\ [\ s_{13}\ ]\left[1 + O(g^2)\right] \end{aligned} \tag{5.84}$$

Similarly

$$\begin{aligned}[Disc]_{s_{13}} \;&\longrightarrow\; \int \frac{d^2k}{sin\pi\alpha(k^2)sin\pi\alpha((Q_1-k)^2)}(s_{13})^{(\alpha(k^2)+\alpha(Q_1-k)^2-1)} \\ &\sim\; J_1(Q_1^2)\;\;[\;s_{13}\;]\;\Big[1+O(g^2)\Big]\end{aligned} \tag{5.85}$$

Analagous changes occur if we replace any of the other Regge pole contributions in the foregoing by Regge cuts. In particular our discussion of the simple relation between the double discontinuity (5.79) and the triple discontinuity (5.80) goes through if regge poles are replaced by regge cuts.

5.10 Dimensions of Reggeon Interactions

Finally we note a crucial difference between (5.65) and (5.66) that is vital for the appearance of the triangle anomaly as we discuss in the next Section. First we set

$$\alpha_1 \;=\; \alpha_2 \;=\; \alpha_3 \;=\; 1 \tag{5.86}$$

corresponding to the contribution of (multi-)gluon reggeon states. We then compare the momentum dimension of (5.65) and (5.66). For (5.65) we obtain

$$(s_{13})^{\alpha_1}(s_{2'3'})^{\alpha_2}(s_{11'3})^{\alpha_3-\alpha_1-\alpha_2} \;\equiv\; [s]^{1+1-1} \;=\; [s] \tag{5.87}$$

while for (5.66) we obtain

$$(s_{31})^{(\alpha_1+\alpha_3-\alpha_2)/2}(s_{23})^{(\alpha_2+\alpha_3-\alpha_1)/2}(s_{12})^{(\alpha_1+\alpha_2-\alpha_3)/2} \;\equiv\; [s]^{\frac{1}{2}+\frac{1}{2}+\frac{1}{2}} \;=\; [s]^{\frac{3}{2}} \tag{5.88}$$

The difference in dimensions of (5.87) and (5.88) has to be compensated by a difference in the transverse momentum dimension of the accompanying reggeon vertex. If we anticipate that (as is the case) the dimension of the vertex accompanying (5.87) is the normal $[Q]^2$ for a reggeon vertex in QCD, then the vertex accompanying (5.88) will have the "anomalous dimension" of $[Q]$. The anomalous dimension is what allows the reggeon interaction vertices generated by $M^{\mathcal{C}_b}$ to contain the anomaly of the four-dimensional triangle diagram - which is linear in it's momentum dimension and is independent of any other scale.

6. Multiple Discontinuities

In this Section we evaluate multiple discontinuities and look for the anomaly in reggeon interactions via the multi-regge formalism of the last Section. We should emphasize that the writing of an asymptotic dispersion relation, without subtractions, depends[5, 6] on the feature that all asymptotic behavior originates from multi-regge singularities. Therefore we can anticipate that if we proceed via multiple discontinuities, we will only discover those reggeon interactions that persist as higher-order reggeization effects are added.

6.1 The Simplest Diagrams

As we noted in subsection 5.4, to count all triple discontinuities, and the diagrams that contribute to them, we first consider the initial and final state double discontinuities that are uniquely associated with each hexagraph. We then separate diagrams according to which additional discontinuity they contain. To obtain a double discontinuity requires a minimum of two gluons exchanged in each t-channel. For the $s_{13}, s_{2'3'}$ double discontinuity (associated with the first hexagraph of Fig. 5.2) we consider the diagrams of Fig. 6.1. The desired double discontinuity is obtained by putting the hatched quark lines on-shell. If we ignore gluon self-interactions, we can argue that these diagrams are a complete set as follows.

The initial scattering process producing the s_{13} intermediate state is necessarily the production of a quark-antiquark pair and without loss of generality we can draw this process as in the bottom part of Fig. 6.1(a), provided we don't distinguish a quark direction on the exchanged quark line. Similarly the $s_{2'3'}$ intermediate state is associated with the reverse of this production process. The quark loop obtained by joining the amplitudes for these initial and final scatterings is either planar, as in the first six diagrams of Fig. 6.1, or it has a twist in it, as in the second six diagrams. The six diagrams of each kind are obtained by attaching the two gluons that do not participate in either the initial or final scattering process, in all possible ways.

Apart from the need to sum over the direction of the quark line around the loop, the diagrams of Fig. 6.1 are all of the lowest-order diagrams with both an s_{13} and an $s_{2'3'}$ discontinuity. In addition to the double discontinuity, some diagrams have an additional $s_{11'3}$ discontinuity, some have an additional s_{123} discontinuity, and some have both. From the discussion of the previous Section we understand that the distinct additional discontinuities are associated with distinct partial-wave amplitudes and therefore distinct reggeon interactions. Nevertheless, since the double discontinuity provides a sufficient number of δ-functions to perform all longitudinal integrations in each diagram, it will be useful to initially discuss the behavior of the double discontinuity in the limits we are interested in and then discuss the effect

of taking the additional discontinuity. Following our discussion at the end of the previous Section, we anticipate that the triangle anomaly occurs only in diagrams with an s_{123} discontinuity. In particular, from the discussion at the end of sub-section 5.8 we expect to find reggeon amplitudes containing the s_{123} discontinuity for which the double and triple discontinuities are essentially identical in lowest-order.

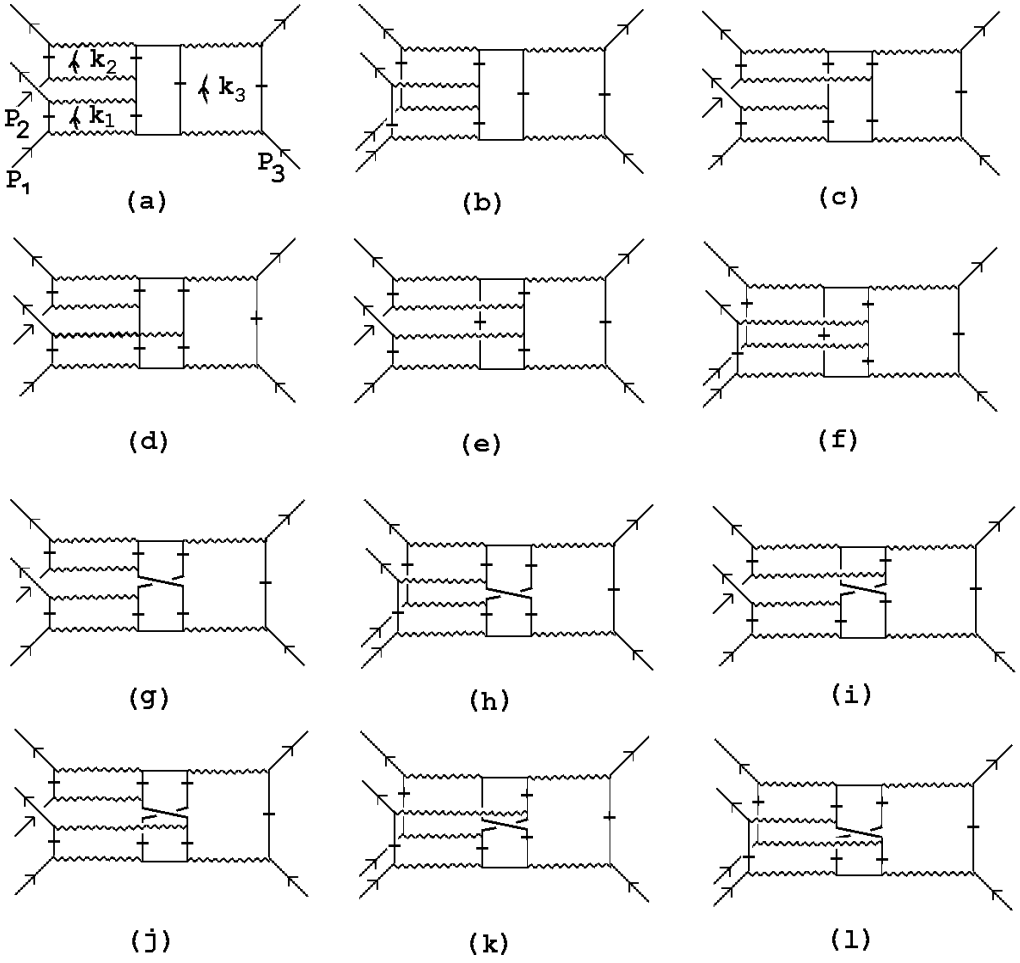

Fig. 6.1 Diagrams with Two Gluons in each t-channel.

We begin by evaluating diagrams in the full triple Regge limit (3.1) in which the P_i become lightlike in distinct directions and the Q_i have the general form given in (3.1).

6.2 The Diagram of Fig. 6.1(a).

We have already discussed this diagram at length in sub-section 4.1. Indeed the hatched lines of Fig. 6.1(a), that are placed on-shell to obtain the double discontinuity, are the same as those of Fig. 4.2. There is only an additional $s_{11'3}$ discontinuity

which, to take, we must put the only unhatched vertical line on shell. However, now we encounter an important point. We can repeat our evaluation of Fig. 4.2 but use co-ordinates for the k_1 and k_2 integrations in which $\underline{n}_{1^+}$ and $\underline{n}_{2^+}$ are the basic light-like momenta. In this case, the longitudinal k_1 and k_2 integrations will lead to the γ-matrix couplings shown in Fig. 6.2

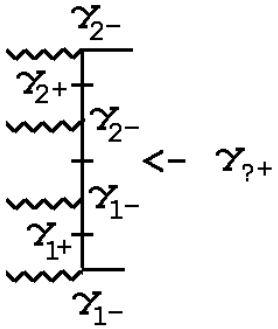

Fig. 6.2 γ-Matrix Couplings for Fig. 6.1(a)

If the middle quark line is to put be put on-shell, then it must be helicity-conserving with respect to both the upper and lower on-shell states. However, this is clearly not possible. As a result we conclude that there is no leading triple-regge contribution from the triple discontinuity of Fig. 6.1(b). This is consistent with the argument, following our analysis of Fig. 4.2, that higher-order reggeization effects cancel the reggeon interaction obtained from this diagram.

6.3 Isolating the Anomaly

In all of the remaining diagrams of Fig. 6.1, one or more of the k_i loop momenta flow through more than one line of the internal quark loop. Consequently, as we already saw in Section 4, the reduction of the k_i integrations to two dimensions is not as straightforward as it was for Fig. 6.1(a). The internal quark loop and the remaining two-dimensional k_i integrations are not, in general, coupled only by an effective point-coupling and the reggeon vertices generated are very complicated. As we made clear in the Introduction, we will not attempt to obtain complete expressions for the vertices generated by the remaining diagrams in Fig. 6.1. Rather we will concentrate on isolating contributions that might contain the anomaly.

Our search for the anomaly will, as in Section 4, be based on the discussion of Appendix A. We will look for effective vector-like point-couplings for the three vertices of a quark triangle diagram with an odd number of axial couplings. We will also look for the appropriate flow of a light-like momentum through the the diagram. We will assume that the anomaly, if present in a diagram, can be found using any of the possible sets of light-cone variables discussed in Appendix B, provided we consider all choices for assigning particular quark propagators to particular longitudinal k_i

integrations. As will become clear, the appropriate choice of variables will often enable us to see immediately whether a local coupling occurs or whether only non-local couplings arise.

6.4 The Diagram of Fig. 6.1(b).

This diagram is potentially interesting since it has an s_{123} discontinuity and does not have an $s_{11'3}$ discontinuity. There is a general point concerning the s_{123} discontinuity that we discuss first. This discontinuity can again be taken by cutting the remaining uncut vertical line in Fig. 6.1(b). Again, as illustrated in Fig. 6.3,

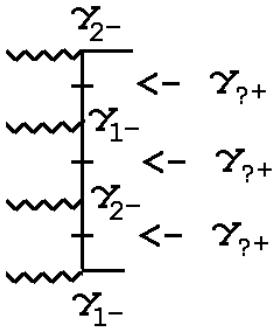

Fig. 6.3 γ-Matrix Couplings for Fig. 6.1(b)

there are two on-shell scatterings for which it is impossible to choose helicities such that both give the leading behavior. We conclude that there is no triple-regge leading behavior obtained by taking the s_{123} discontinuity through the uncut vertical quark line. This is fortunate because if such a triple discontinuity contributed it would be significantly different from the double discontinuity, in contrast to what we are expecting from a triple-regge amplitude containing only multi-reggeon singularities.

To see that there is a reggeon triple discontinuity contribution having the same form as the double discontinuity, we note that we can also introduce an s_{123} discontinuity by adding an extra gluon, as illustrated in Fig. 6.4.

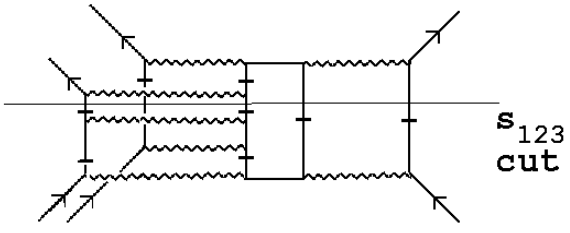

Fig. 6.4 Adding a Gluon to Fig. 6.1(b) to Give an s_{123} Discontinuity.

In effect we replace a single real gluon in the original diagram by the one-loop contribution to the reggeization of this gluon. This implies that the reggeon vertex obtained

from the original diagram of Fig. 6.1(b), with the s_{123} discontinuity not taken, will be obtained from the higher-order diagram of Fig. 6.4 when the s_{123} discontinuity is taken. The sum total of such higher-order triple discontinuity contributions to the asymptotic dispersion relation determine that the lower-order diagram is obtained as a "real part". Equivalently, in the lowest-order diagram it is correct to interpret the large momentum factors as in (2.2) and so take the s_{123} discontinuity by adding a factor of 2, as in (5.83). For our purposes, therefore, we need not take the third discontinuity through a diagram if a contribution to this discontinuity is obtained by simply "cutting through a gluon line". We must, of course, remember that this gluon has necessarily to be considered as reggeized when we extract reggeon interactions. (Note that cutting through a gluon line does not, however, allow a consistent triple discontinuity to be obtained from Fig. 6.1(a).)

The momentum flow through the internal quark loop of Fig. 6.1(b) and the γ matrices involved are shown in Fig. 6.5.

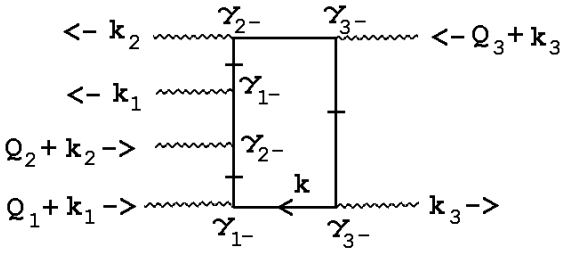

Fig. 6.5 The Quark Loop in Fig. 6.1(b).

As in our discussion of diagrams in Section 4, we use the light-cone co-ordinates $(k_{i1^-}, k_{i2^-}, \underline{\tilde{k}}_{i\perp})$ introduced in Appendix B to perform the k_1 and k_2 integrations and to evaluate the γ-matrix trace associated with the quark loop. For the k_3 integration, the choice of co-ordinates is not critical. For simplicity, we choose conventional light-cone co-ordinates $(k_{3^+}, k_{3^-}, k_{3\perp})$. Our evaluation of the integral I_i of Fig. 4.3 can be repeated to perform the k_{11^-}, k_{22^-} and k_{3^-} integrations using the δ-function associated with the correponding external quark line.

To perform the remaining longitudinal integrations we first route the k_i momenta along the shortest path through the quark loop. This matches a unique on-shell (hatched-line) propagator in the loop with each k_i. As before, to look for a potential γ-matrix point-coupling, we look for that momentum factor within the numerator of the on-shell quark that is multiplied by the same momentum that is scaling the longitudinal momentum integrated over via the δ-function. In particular the k_{12^-}

integration has the form

$$\begin{aligned}
&\int dk_{12^-}\ \delta\Big((k_1+k+Q_1)^2-m^2\Big)\ \gamma_{1^-}\ \Big((k_1+k+Q_1)\cdot\gamma-m\Big)\ \gamma_{2^-}\times\quad\cdots\\
&\quad=\ \int dk_{12^-}\ \delta\Big((k_{11^-}+k_{1^-}+Q_{11^-})k_{12^-}+\cdots\Big)\\
&\qquad\qquad\times\gamma_{1^-}\ \Big((k_{11^-}+k_{1^-}+Q_{11^-})\cdot\gamma_{2^-}+\cdots\Big)\ \gamma_{2^-}\ \times\ \cdots\\
&\quad=\ \gamma_{1^-}\gamma_{2^-}^2\quad+\quad\cdots\\
&\quad=\ 0\quad+\quad\cdots
\end{aligned}\tag{6.1}$$

In this case the potential point-coupling from the $(k_{11^-}+k_{1^-}+Q_{11^-})\gamma_{2^-}$ term in the quark numerator is eliminated by one of the adjacent γ-matrices (c.f. our evaluation of Fig. 4.8(a) in sub-section 4.3). Since the k_{21^-} integration has the same structure as the k_{12^-} integration, performing each of these integrations will produce couplings of the form (C.19) rather than the point couplings necessary to produce the anomaly. In any alternative momentum flow and assignment of δ-functions, it is straightforward to show that either the k_{12^-} or the k_{21^-} integration gives an analagous result to (6.1), i.e. only non-local couplings remain. (Note that our choice of light-cone co-ordinates has enabled us to reach this conclusion rather simply).

6.5 The Diagrams of Fig. 6.1(c) and (d).

Because of the number of lines put on-shell by taking the s_{13} and $s_{2'3'}$ discontinuities, there are not three quark lines off-shell in either of these diagrams. As a result neither has a remaining discontinuity and so can not contribute directly to a triple discontinuity. We could obtain an s_{123} discontinuity by taking a cut through a gluon as discussed in the previous sub-section, but because only two quark lines are off-shell there is no possibility to generate the anomaly divergence.

6.6 The Diagram of Fig. 6.1(e).

Since this diagram has only an additional $s_{11'3}$ discontinuity, our prejudice is that it will not contain the anomaly and in fact this is the case. The $s_{11'3}$ discontinuity can not be taken by cutting only a gluon line. Consequently to take this discontinuity we must cut the remaining uncut vertical quark linel leading again to the problem that there is no consistent helicity assignment. Therefore, this diagram does not contribute a leading order triple discontinuity.

6.7 The Diagram of Fig. 6.1(f).

This is the third diagram appearing in Fig. 2.2 and it has already been extensively discussed in Section 4. We showed that with the hatched lines in Fig. 6.1(f) put

on-shell, the anomaly is present. An s_{123} discontinuity is obtained both by cutting through a gluon, leaving the anomaly unaffected, and directly by putting the remaining uncut vertical line on-shell. However, cutting the vertical line once again has a helicity problem and does not contribute a leading-order triple-regge amplitude.

We consider now the twisted diagrams of Fig. 6.1. We will find that two of these diagrams contain the appropriate local couplings, but can not satisfy all the constraints on the momentum flow. As we will comment on further, the two diagrams are those related to Fig. 6.1(f) via reggeon Ward identities.

6.8 The Diagrams of Fig. 6.1(g) - (j).

The diagrams of Fig. 6.1(g) and (h) also appear in Fig. 4.6, except that an extra line is now on-shell. In Section 4 we argued that such diagrams do not contain the anomaly. With the extra line on-shell we again have only two quark lines off-shell and so clearly there is no triangle anomaly.

The diagrams of Fig. 6.1(i) and (j) have only an $s_{11'3}$ discontinuity, they do not have the s_{123} discontinuity that is associated with the anomaly. However, the $s_{11'3}$ discontinuity again has a helicity-matching problem that implies there is no leading-order amplitude.

6.9 The Diagrams of Fig. 6.1(k) and (l).

The diagrams of Fig. 6.1(k) and (l) both have an s_{123} discontinuity, which can be taken through a gluon line. Fig. 6.1(l) is simply obtained from Fig. 6.1(k) by time reversal of the scattering process and so has analagous properties. Therefore our discussion below of Fig. 6.1(k) will immediately extend to Fig. 6.1(l).

We can repeat much of the discussion of Fig. 6.1(f) for Fig. 6.1(k). We do this briefly as follows. Again writing $q_i = Q_i,\ i = 1, 2, 3$, the internal quark loop gives the contribution shown in Fig. 6.6

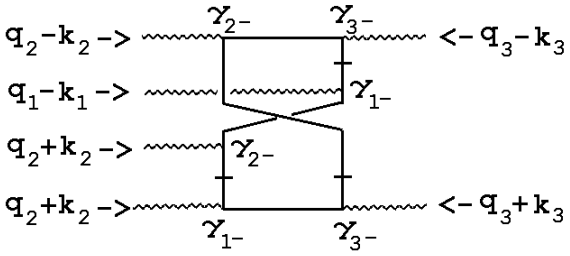

Fig. 6.6 The Quark Loop in Fig. 6.1(k).

If we take the shortest routes for each of the k_i momenta then we obtain the δ-function assignment and internal momentum flow shown in Fig. 6.7

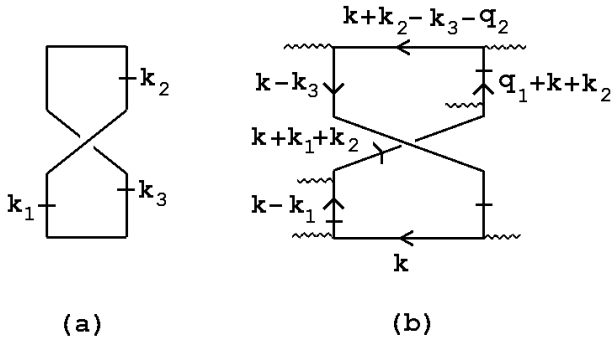

Fig. 6.7 The "Shortest Route" (a) δ-function Assignment and (b) Momentum Flow for Fig. 6.6.

However, for this assignment we immediately discover that, in parallel with our discussion of Fig. 6.1(b), neither the k_{12-} nor the k_{21-} integrations give local couplings.

The only δ-function assignment giving local couplings at all vertices is that shown in Fig. 6.8(a), with the corresponding momentum flow shown in Fig. 6.8(b).

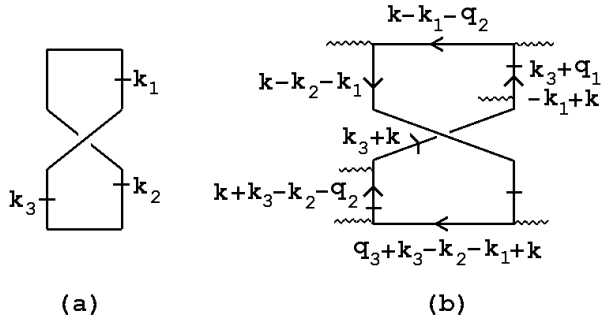

Fig. 6.8 Another (a) δ-function Assignment and (b) Momentum Flow for Fig. 6.6.

In this case each of the k_i passes through two δ-function lines (ultimately this is what causes a conflict with the conditions needed to produce the anomaly). The calculation of local couplings proceeds in close parallel to (4.12) - (4.14). The result is as illustrated in Fig. 6.9

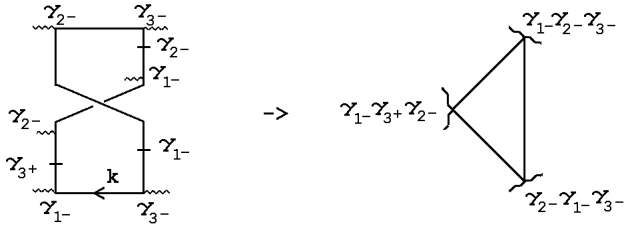

Fig. 6.9 Local couplings generated by Fig. 6.8.

The couplings generated in Fig. 6.9 differ from those of Fig. 4.13 only in that

$$\hat{\gamma}_{31} \;=\; \gamma_3 \gamma_2 \gamma_1 \;\rightarrow\; \hat{\gamma}_{13} \;=\; \gamma_1 \gamma_2 \gamma_3 \;=\; \gamma_{-,+,-} \;-\; i\,\gamma_{-,-,-}\,\gamma_5 \tag{6.2}$$

Therefore the three γ_5 couplings potentially giving the anomaly are again present. The momentum flow and couplings in the corresponding triangle diagram are shown in Fig. 6.10.

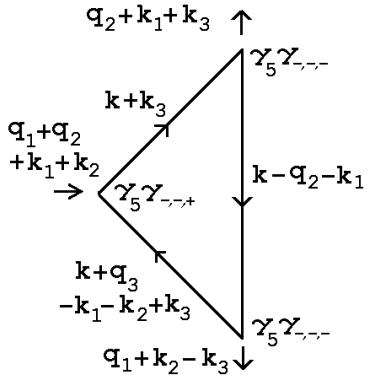

Fig. 6.10 The Triangle Diagram Generated by Fig. 6.1(k).

At this point we note that Fig. 6.9 is identical to Fig. 4.14, apart from a shift of the internal momentum

$$k \;\;\rightarrow\;\; k - q_2 - k_1 \tag{6.3}$$

This implies that the anomaly should appear in the limit (4.23), with $(q_1+q_2+k_1+k_2)$ spacelike and $(q_2 + k_1 + k_3)$ having a light-like component. However, the mass-shell δ-constraints (4.24)-(4.26) determining k_{12^-}, k_{21^-} and k_{33^+}, are replaced by

$$(k_3 + q_1 + k - k_1)^2 \;\;=\;\; 0 \tag{6.4}$$

$$(k + k_1 + k_2)^2 \;\;=\;\; 0 \tag{6.5}$$

$$(k + k_3 - q_2 - k_2)^2 \;\;=\;\; 0 \tag{6.6}$$

If the shift (6.3) is made, k_1 is routed along a different path and the δ-function assignment of Fig. 6.8(a) can no longer be made. As we already noted, with any other δ-function assignment besides that of Fig. 6.8(a), no local couplings are generated.

To have any possibility of generating the anomaly we must stay with the triangle diagram of Fig. 6.10 and the constraints (6.4)-(6.6). We therefore identify Fig. 6.10 with Fig. A2 by identifying $q_1 + k_2 - k_3$ with $\mathbf{q}_1$ and $q_1 + q_2 + k_1 + k_2$ with $\mathbf{q}_2$. We again take the limit $\mathbf{q} \rightarrow 0$ so that

$$q_1 + q_2 + k_1 + k_2 \;=\; 0 \tag{6.7}$$

and

$$q_1 + k_2 - k_3 \ \sim \ (1, -1, 0, 0) \tag{6.8}$$

and look for a finite momentum configuration that satisfies both (6.7) and (6.8) and the constraints (6.4)-(6.6). We again set the loop momentum $k \sim \mathbf{q} = 0$.

The internal lines of the diagram will be on-shell in the limit we are discussing only if the shift (6.3) is a light-like momentum of the kind flowing in externally, i.e.

$$q_2 \ + \ k_1 \ \sim \ (1, -1, 0, 0) \tag{6.9}$$

Combining this with (6.7) and (6.8), we must also have

$$q_1 \ + \ k_2 \ = \ -\, q_2 \ - \ k_1 \ \sim \ k_3 \ \sim \ (1, -1, 0, 0) \tag{6.10}$$

However, since $k_{33^-} = 0$, this implies that k_3 is identically zero. It is then not difficult to show that, in this case, the only solution for the mass-shell constraints (6.4)-(6.6) is that all the momenta involved are identically zero. We conclude that Fig. 6.10, and therefore Fig. 6.1(k) can give an anomaly contribution only at the point where all the transverse momentum invariants vanish. However, at this point the singular behavior (4.40) is lost because the numerator also vanishes.

Note that the diagram of Fig. 6.1(k) has to contain the same γ-matrix structure as that of Fig. 6.1(f), and contribute equally and with opposite sign at the zero momentum point. If we consider the amplitudes forming the s_{13} discontinuities as in Fig. 6.11,

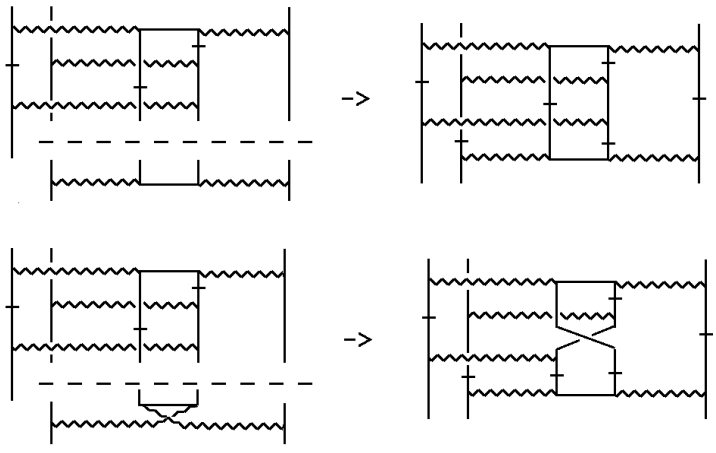

Fig. 6.11 Forming s_{13} Discontinuities

we see that the two diagrams are formed by two of the production amplitudes appearing in Fig. C6 that are related by a reggeon Ward identity. Therefore, even

though Fig. 6.1(k) does not contain the anomaly divergence, at the zero momentum point, it must provide a cancelation with Fig. 6.1(f). Fig. 6.1(l) is similarly related to Fig. 6.1(f) via final state amplitudes satisfying a reggeon Ward identity.

Finally we are left with Fig. 6.1(f) as the only diagram in Fig. 6.1 containing the anomaly. To discuss whether the anomaly cancels, therefore, we have to consider only the sum of the double discontinuities of the form of Fig. 6.1(f), each of which is associated with a separate hexagraph. In Section 4, we have already discussed the kinematical symmetries that will produce a cancelation. We enlarge this with a discussion of color factors in the next Section.

7. Color Factors, Cancelations and Divergences

We have narrowed down the occurrence of the anomaly, at lowest-order, to contributions from double (or triple) discontinuities occurring in Feynman diagrams of the maximally non-planar type. In Section 4 we already discussed the kinematical symmetries that can produce a cancelation. As a result we can give only a minimal discussion of the role played by color quantum numbers. First we recall what we have established in terms of kinematic properties.

[A] The anomaly occurs only in reggeon interactions appearing in triple discontinuities that contribute to signatured amplitudes satisfying the signature rule $\tau_1\tau_2\tau_3 = 1$. In particular, if we consider identical quantum numbers for the reggeon states in the 1 and 2 channels, then the reggeon state in the 3 channel must be even signature. (We believe this property produces an even signature pomeron in the hadron S-matrix, as we discuss below.)

[B] The anomaly occurs only in reggeon interactions generated by Feynman graphs having a maximal planarity property, at lowest-order this includes the third diagram in Fig. 2.3. This diagram gives, amongst others, two double discontinuities corresponding to Figs. 2.4 and 2.6 which can also be drawn as Fig. 4.8(a) and (b).

[C] The contributions of Fig. 4.8(a) and (b) are respectively associated, in an identical manner, with the first and last hexagraphs in Fig. 5.3. and so in the triple-regge limit give identical dependence on the large momentum variables. After addition of these contributions the antisymmetric kinematic dependence of the anomaly is such that there is a cancelation when either the remaining k_3-integration is symmetric or both the k_1 and k_2 remaining integrations are symmetric.

The above properties have a generality that we anticipate will allow them to continue to hold for higher-order diagrams.

When signatured amplitudes are formed the two-reggeon state appears only when the corresponding channel has even signature. The reggeon interactions containing the anomaly that we have discussed couple two reggeized gluons in each t_i-channel and so all three channels have $\tau_i = 1$. Therefore property $[A]$ is immediately satisfied. As discussed in Section 5, to obtain an amplitude for which all signatures are positive we add the contributions from all eight of the hexagraphs in Fig. 5.3. This requires that we add the contributions of the twisted diagrams of the form of Fig. 2.6 to the untwisted contributions of Figs. 4.8(a) and (b).

To begin our discussion of color factors we first consider the external coupling of two gluons (or reggeons) to a scattering quark. The color factor that appears can be written as shown diagrammatically in Fig. 7.1.

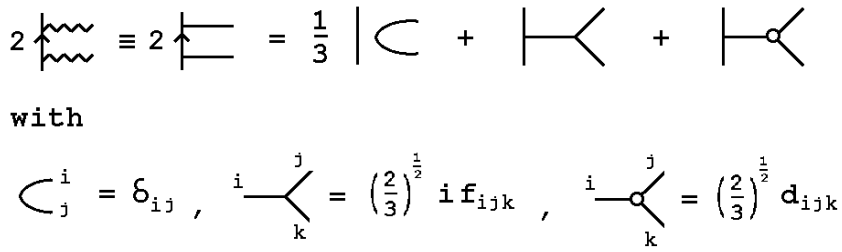

Fig. 7.1 Color Factors for Two Gluons Coupling to Two Quarks

f_{ijk} and d_{ijk} are the usual antisymmetric and symmetric tensors for SU(3) color. In lowest order, the G_h have no momentum dependence and so, in the even signature amplitude, only the symmetric δ_{ij} and d_{ijk} couplings survive. Therefore, the (two-gluon) two-reggeon state has to be in either a color zero state, or a "symmetric octet" (8_s) state. At this order it is obvious that a single scattering quark does not couple to an "anti-symmetric octet" (8_a) two-reggeon state.

It will be important to discuss the color parity of reggeon states. Color charge conjugation on gluon fields is defined by the transformation of gluon color matrices

$$A^i_{ab} \;\rightarrow\; -\; A^i_{ba} \tag{7.1}$$

For SU(3) we can choose $A^i \sim \lambda^i$ so that

$$A^i \;\rightarrow\; -A^i \quad i = 1,3,4,6,8\;, \qquad A^i \;\rightarrow\; A^i \quad i = 2,5,7\;, \tag{7.2}$$

For a trace of gluon matrices the color parity transformation reverses the trace order. In particular, in a space-time path-ordered integral of gluon fields it reverses the direction of the path integration. For gauge-invariant states involving such integrals there may be an inter-relation between color parity and space-time symmetry properties.

We consider the minus sign in (7.1) as defining the negative color parity of the gluon. The odd-signature reggeized gluon then has a color parity equal to it's signature. Color-zero combinations of color matrices also have a definite color parity, e.g.

$$\begin{gathered} \delta_{ij}\; A^iA^j \;\rightarrow\; \delta_{ij}\; A^iA^j\;, \qquad f_{ijk}\; A^iA^jA^k \;\rightarrow\; f_{ijk}\; A^iA^jA^k\;, \\ d_{ijk}\; A^iA^jA^k \;\rightarrow\; -\; d_{ijk}\; A^iA^jA^k \end{gathered} \tag{7.3}$$

i.e. the d-tensor provides a "color parity violating" coupling for gluon fields. Ultimately our main interest is in color zero multi-reggeon states and these can immediately be assigned a color parity. Also since

$$\begin{aligned} f_{ijk}\ A^j A^k\ /\ A^i\ &\rightarrow\ f_{ijk}\ A^j A^k\ /\ A^i\ , \\ d_{ijk}\ A^j A^k\ /\ A^i\ &\rightarrow\ -\ d_{ijk}\ A^j A^k\ /\ A^i \end{aligned} \tag{7.4}$$

we can assign negative and positive color parities, respectively, to the 8_a and 8_s states discussed above. We can also assign color parities to multi-reggeon states with color factors containing combinations of f- and d- tensors. Any reggeon state, and in particular an even-signature 8_a two-reggeon state, has "anomalous color parity" if it has a color parity not equal to it's signature. We will argue below that, in general, anomalous color parity reggeon states do not couple to a scattering quark.

Color charge conjugation invariance implies color charge parity conservation and so, after summing over quark directions, the quark loop color factor must contain an even number of d-tensors. Given the color structure of the external couplings, the possible color couplings for the Γ_6 reggeon interaction extracted from the lowest-order diagrams are those shown in Fig. 7.2

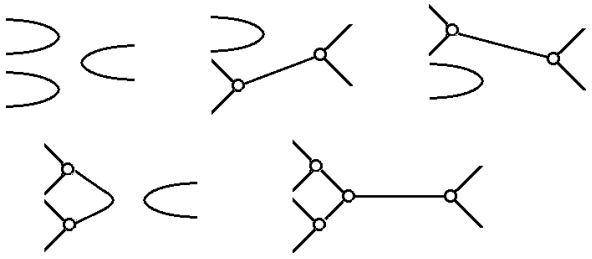

Fig. 7.2 Color Factors for the Lowest-Order Reggeon Interaction

In lowest-order, therefore, both the color factors and the remaining k_i-integrations are symmetric with respect to the two reggeons in each of the t_i channels. From [C] above we know that this implies the anomaly is canceled.

In higher-orders, helicity conserving couplings $G_h(q_i, k_i)$ that appear within multiple discontinuities, need not be symmetric under $k_i \leftrightarrow -k_i$. Therefore, the 8_a two-reggeon state could appear in such discontinuities. However, as explained in Section 5, a positive signatured amplitude can be obtained either by adding hexagraph amplitudes or by adding full amplitudes related by a CPT transformation applied selectively to external states. For an external (left-handed) scattering quark q_L, the second procedure gives directly that the full signatured coupling is as shown in Fig. 7.3. Because of helicity conservation, the two vertices in Fig. 7.3 are also related by a CP transformation. Therefore, since CP is conserved, their equality

in lowest-order must extend to all orders. Consequently, the two-reggeon coupling remains symmetric to all orders and the 8_a state does not couple.

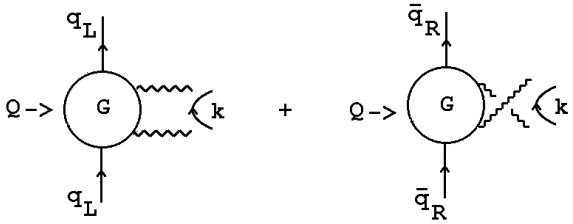

Fig. 7.3 The Signatured Two-Reggeon Coupling to a Quark

More generally, even signature implies that the external "state" formed by the initial and final scattering particles is even under CPT. Therefore, the internal two-reggeon state must similarly be even. However, the reggeon state lies entirely in the transverse plane and so is independent of the T transformation. Instead, therefore, it must be even under CP. (The same conclusion could be reached by working in the t-channel.) The antisymmetry in the k_i integrations required for the anomaly is equivalent to requiring $P = -1$ for the two-reggeon state. Therefore $C = -1$, i.e. the two-reggeon state must carry anomalous color parity. Equivalently, to produce a coupling there must be a component of the external scattering state that is antisymmetric with repect to parity.

A-priori, the necessary parity antisymmetry could appear if there is helicity non-conservation. If we consider scattering gluons then helicity-flip vertices coupling a reggeized gluon do appear in next-to-leading order[11]. However, parity conservation, applied when the reggeized gluon goes on-shell, implies there is a change of sign when the gluon helicity is reversed. This determines that the "anomalous color parity" 8_a two-reggeon state again decouples in all orders. More generally, we anticipate that no reggeon states with anomalous color parity couple to scattering quarks (or gluons).

The parity asymmetry needed to couple the anomalous color parity two-reggeon state can be obtained if we add an extra particle (or particles) to the initial or final state as in Fig. 7.4.

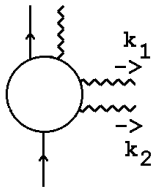

Fig. 7.4 A Two-Reggeon Coupling with an Additional Final State Gluon.

This coupling can be directly studied in the two-to-four amplitude[6] where the novel

signature properties produced by an imbalance between discontinuities is well-known. Nevertheless, even if all three external couplings have the required asymmetry between initial and final states, a triple-regge amplitude containing the anomaly still can not exist, because of the conservation of color parity. An equivalent way of stating this is to say that for the anomaly to appear in the coupling of three 8_a two-reggeon states, a d-tensor coupling is required and this is forbidden by color parity conservation.

We can outline how we anticipate the anomaly does appear in amplitudes as follows, although more explicit verification is clearly required. In a ditriple regge limit reggeon diagrams, of the form illustrated in Fig. 7.5, containing two anomaly vertices can appear. A single d-coupling can be present for each anomaly vertex while the full amplitude is not color parity violating.

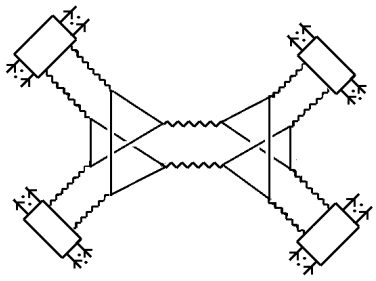

Fig. 7.5 A Ditriple-Regge Limit Amplitude.

It is then important to note that the external coupling will have reggeon Ward identity zeroes[3] (which follow from gauge invariance). For example, the coupling of Fig. 7.4 has a zero when either k_1 or $k_2 \to 0$. The anomaly divergence occurs at just such points. If the corresponding zeroes are present in all four of the external couplings of Fig. 7.5, the linear divergence of the anomaly will always be compensated by at least two Ward identity (linear) zeroes and this will be sufficient to prevent a divergence of the full amplitude. (There are also logarithmic divergences present due to zero mass gluon propagators. These are not relevant - until we discuss the anomaly divergences associated with a reggeon condensate.)

In general we anticipate that all reggeon states coupling to anomaly vertices will have anomalous color parity to compensate for the antisymmetric parity properties of the anomaly. As a generalisation of the foregoing discussion reggeon interactions containing the anomaly will appear in any amplitude of the form of Fig. 7.6

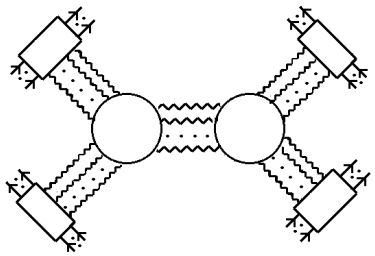

Fig. 7.6 A General Ditriple-Regge Reggeon Amplitude

provided that there is sufficient imbalance between the initial and final states that anomalous color parity reggeon states appear. We also expect a generalization of the dimensional argument at the end of Section 5 to imply that the anomaly appears only in amplitudes that satisfy the signature conservation rule. The anomalous color parity of each reggeon state implies that, correspondingly, color parity will not be conserved. However, reggeon Ward identity zeroes will continue to prevent the occurrence of divergences in full amplitudes.

In additionally complicated multi-regge limits reggeon diagrams containing any number of anomalous vertices will similarly appear[3]. The presence of compensating Ward identity zeroes will continue to prevent the divergent reggeon interactions from producing divergent amplitudes. Even if infra-red divergences do not appear in full amplitudes, the ulltraviolet presence of the anomaly, that must accompany it's infra-red appearance in reggeon interactions, most likely still causes problems. As discussed in [3], and briefly referred to in Section 2, we anticipate that the ultra-violet anomaly produces powerlike enhancement of reggeon diagrams and a consequent conflict with unitarity. We can avoid this conflict at finite, but small, physical quark mass by introducing large (but finite) mass fermion Pauli-Villars regulators. If the "physical" reggeon S-Matrix is obtained, as we anticipate, by taking the quark mass to zero and extracting infra-red divergent contributions from anomaly amplitudes, the regulator fermions will not appear. To produce infra-red divergent amplitudes, however, we have to remove the Ward identity zeroes in some of the external reggeon couplings. This brings us to the program, mentioned in the Introduction, that is outlined at length in [3] and can be briefly described as follows.

Starting in a color superconducting phase in which the gauge symmetry is broken from SU(3) to SU(2) (perhaps due to a diquark condensate[18]), a "reggeon condensate" can be consistently introduced as follows. The logarithmic infra-red divergences, due to the zero gluon mass, exponentiate to zero all reggeon diagrams except those carrying SU(2) color zero in each t-channel. We then consider initial reggeon scattering states (produced by appropriate external couplings) that each contain an SU(2) color zero, anomalous color parity reggeon component with $k_\perp = 0$ (i.e there is no Ward identity zero for this $k_\perp = 0$ component). The presence of this reggeon condensate in two (or more) initial reggeon states will be just sufficient for

the anomaly divergences to overcome the Ward identity zeroes. The anomalous color parity introduced by the condensate also allows reggeon states to interact via vertices containing the anomaly. We anticipate that, as in our analysis in [3], there will be an overall logarithmic divergence (as the quark mass goes to zero) in amplitudes that contain the initial reggeon states and also contain some number of anomaly vertices. If these amplitudes are extracted and the divergence absorbed into the condensate, the "physical S-Matrix amplitudes" obtained should then contain the same $k_\perp = 0$ condensate in each produced reggeon state that was present in the initial states. That is to say. an S-Matrix "completeness" property holds, in the sense that if two, or more, states containing the condensate scatter via QCD interactions, the final states contain only arbitrary numbers of the same kind of states. "Confinement" will be present if, as we believe will be the case, all reggeon states carry color-zero and there are no massless multigluon states. As we indicated in [3] it appears that chiral symmetry breaking will also be produced by the reggeon condensate.

Essentially the correct phenomenon is outlined in [3]. However, there are some differences. In particular, because of the signature conservation for anomalous amplitudes, there is no triple anomalous odderon vertex, as was assumed in [3]. Instead, the anomaly divergence occurs within the primary momentum carrying interactions of a reggeon diagram and not just in accompanying vertices as was suggested in [3]. This is possible because, as we now understand, the anomaly divergence occurs when only some of the interacting reggeized gluons carry zero transverse momentum. As we noted above, a very important consequence of the signature rule is that it promises to explain the even signature of the pomeron - a property that previously we had not clearly seen the origin of. We will not describe the infra-red divergence phenomenon any further in this paper, but will simply give Fig. 7.7 as an example

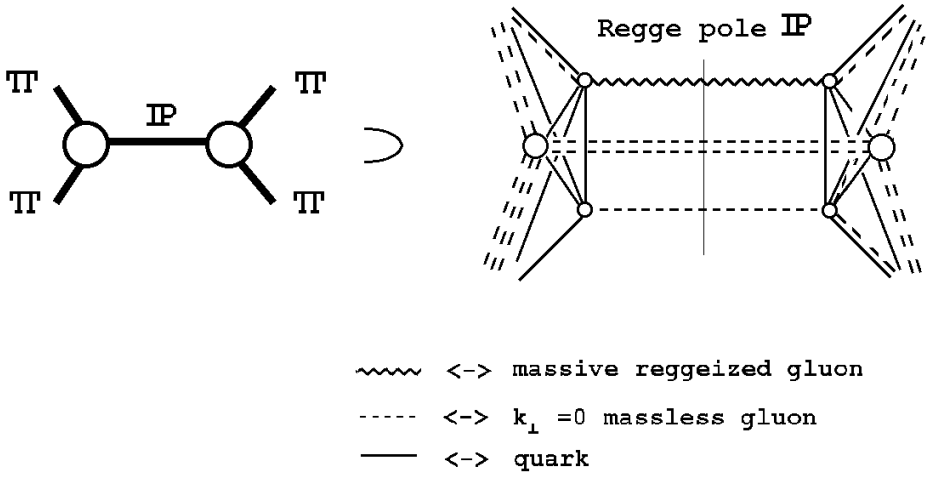

Fig. 7.7 Pion-Pion Scattering via Pomeron Exchange

of a reggeon diagram that we anticipate contributes to pion reggeons scattering via pomeron exchange in the color superconducting phase. Our expectation is that the full set of reggeon diagrams corresponds to those of a supercritical phase of RFT. If such a correspondence is established, SU(3) gauge symmetry will be reached via RFT critical pomeron behavior[15] in which both the condensate and the color superconductivity disappears.

8. The Physics ?

In general, the dynamical role of the U(1) anomaly in QCD is not well-understood. For supersymmetric gauge theories many results have been obtained on the effective action and other dynamical properties of instanton interactions[19]. In sharp contrast, for QCD very little is established on how topological gauge fields and the anomaly contribute to the dynamical solution of the theory. 't Hooft's argument[20] that instanton interactions explain the non-appearance of a light η' meson in the spectrum is widely accepted. Beyond this, however, the conventional wisdom is that such interactions are not mainly responsible for confinement or chiral symmetry breaking. These last properties are generally thought to be a consequence of strong-coupling dynamics that produces a confinement scale having little, or nothing, to do with the U(1) anomaly. In fact the confinement scale is believed to produce the infra-red cut-off for instanton interactions that is essential for 't Hooft's argument that such interactions produce the η' mass.

If strong coupling dynamics is absent because, for example, the presence of a sufficient number of massless quark flavors prevents the infra-red growth of the gauge coupling, the general expectation is that the theory will be close to perturbation theory, with (off-shell) quark and gluon Green's functions existing in a "non-abelian Coulomb phase". However, in this circumstance the U(1) anomaly has the greatest potential to play the dynamical role that we envisage. A fundamental non-perturbative property of the anomaly is that when quarks are massless, instanton interactions (and, perhaps, interactions due to other topological configurations) produce a "spectral flow" of the Fermi-Dirac sea. When there is no infra-red cut-off for such interactions (nor any supersymmetry limiting their effect), the consequence of this flow could be a major rearrangement of the sea. This rearrangement could be equivalent to the presence of gauge fields with non-integer topology in random SU(2) subgroups (in addition to quark condensates) in the "true vacuum" of the theory. (We should emphasize that we study only the S-Matrix and so can not see the vacuum. We see only the "wee parton" component of physical states - which should reflect properties of the vacuum, to the extent such a state can be defined.) In such a vacuum it could be that the only gauge-invariant physical states are those allowed by confinement and chiral symmetry breaking, with the S-Matrix as the only gauge-invariant operator. A situation of this kind is what, in effect, we suspect the dynamics of the regge-limit divergences associated with the anomaly is equivalent to. In the color superconductivity phase the reggeon "winding-number condensate", produced by the quark sea, is naturally oriented in SU(3) color space by the symmetry-breaking color superconductivity. The SU(3) critical behavior is associated with a transition to random orientation of such effects.

If the construction we hope to complete would be the only way to obtain a finite, unitary, regge limit S-Matrix within a gauge theory then it will clearly only exist in very special circumstances[††].

Acknowledgements

I am grateful to both Jochen Bartels and Lev Lipatov very useful discussions on the contents of this paper.

[††]This is not the current wisdom. "We now know that there are an infinite number of consistent S-Matrices that satisfy all the sacred principles. One can take any non-abelian gauge theory, with any gauge group, and many sets of fermions ... "[21]

Appendix A. The Infra-Red Triangle Anomaly and Chirality Violation

It has been known[23] for a long time that the triangle anomaly is not only an ultra-violet phenomena but is also manifest in the infra-red region when the fermions involved are massless. This was elaborated in detail by Coleman and Grossman[1] in the context of establishing 't Hooft's anomaly matching condition for confining theories. Closely related results were also obtained in [25].

In the body of the paper we use the infra-red properties of the anomaly to establish it's presence in very particular reggeized gluon interactions. The Coleman and Grossman analysis establishes that the vertex function for three axial vector currents has a singularity when the quark fields involved are massless. As we describe below, the maximal divergence is obtained when all the spacelike momenta flowing through the vertex are scaled uniformly to zero while a finite light-like momentum remains. The presence of the light-like momentum is a crucial ingredient.

In the notation of Fig. A1, J^a is the axial current and

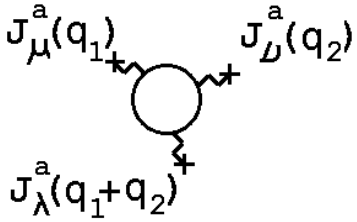

Fig. A1 The Three-point Function

the three current vertex function $\Gamma^{\mu\nu\lambda}$ can be decomposed in terms of invariant amplitudes as follows

$$\Gamma^{\mu\nu\lambda}(\mathbf{q}_1, \mathbf{q}_2) \;=\; A\;\epsilon^{\nu\lambda\alpha\beta}\mathbf{q}_{1\alpha}\mathbf{q}_{2\beta}\mathbf{q}_1^{\mu} \;+\; \cdots \;+\; B\;\epsilon^{\mu\nu\lambda\alpha}\mathbf{q}_{1\alpha} \;+\; \cdots \qquad (A.1)$$

The omitted terms are obtained from those shown explicitly by appropriate permutations. The crucial result from [1] is that the anomaly equation

$$\mathbf{q}_{1\mu}\;\Gamma^{\mu\nu\lambda}(\mathbf{q}_1, \mathbf{q}_2) \;=\; \tilde{A}\;\epsilon^{\nu\lambda\alpha\beta}\mathbf{q}_{1\alpha}\mathbf{q}_{2\beta} \qquad (A.2)$$

implies that, when $\mathbf{q}_1^2 \;\sim \mathbf{q}_2^2 \;\sim (\mathbf{q}_1 + \mathbf{q}_2)^2 \;\sim \mathbf{q}^2 \;\to 0$ the invariant amplitude A has a pole at $\mathbf{q}_1^2 = 0$ with the coefficient $\tilde{A}$ given by the anomaly. Therefore, as $\mathbf{q}^2 \to 0$ we have

$$\Gamma^{\mu\nu\lambda}(\mathbf{q}_1, \mathbf{q}_2) \;=\; \tilde{A}\;\epsilon^{\nu\lambda\alpha\beta}\;\frac{\mathbf{q}_{1\alpha}\mathbf{q}_{2\beta}\mathbf{q}_{1\mu}}{\mathbf{q}_1^2} \;+\; \cdots \qquad (A.3)$$

The ultra-violet anomaly appears also in the vertex function for one axial current and two vector currents and in Ref. [25] it is shown how the corresponding Ward identities similarly imply the presence of the divergence (A.3) when the quarks involved are massless. We also refer to this result in our discussion of reggeon vertices.

If the chiral symmetry associated with the axial current J^a_μ is spontaneously-broken by a quark condensate, the pole at $\mathbf{q}_1^2 = 0$ is associated with the corresponding Goldstone boson. In our case, the anomaly equation (A.2) for the $U(1)$ current is invalidated by non-perturbative, non-trivial topological, gluon field configurations - instantons in particular[‡‡]. However, our initial purpose is to first discover a "perturbative" contribution of the anomaly within reggeon diagrams and only later determine it's dynamical significance. In this case we can use a divergence of the form (A.3) as a signal of the anomaly.

If we simply take all components of $\mathbf{q}_1$ and $\mathbf{q}_2$ to scale with $\mathbf{q}$ then (A.3) gives the (dimensional) result

$$\Gamma^{\mu\nu\lambda} \underset{\mathbf{q} \to 0}{\sim} \mathbf{q} \qquad (A.4)$$

We obtain more singular behavior as follows. First, choose μ to be a light-cone index "+" and choose

$$\mathbf{q}_1^\mu \;=\; \mathbf{q}_1^+ \;=\; \mathbf{q}_{1-} \;=\; \mathbf{p} \not\to 0\;, \quad \mathbf{q}_1^- \;=\; \mathbf{q}_{1+} \;=\; 0 \qquad (A.5)$$

Choosing $\mathbf{q}_2$, and all spacelike momenta flowing through the diagram, to be $O(\mathbf{q})$ and to lie in a spacelike plane orthogonal to the space component of $\mathbf{q}_1^+$, we obtain from (A.3)

$$\Gamma^{++\lambda}(\mathbf{q}_1, \mathbf{q}_2) \underset{\mathbf{q}^2 \to 0}{\sim} \tilde{A}\, \epsilon^{+\lambda-\beta}\, \frac{\mathbf{q}_{2\beta}\; \mathbf{q}_{1-}\mathbf{q}_1^+}{\mathbf{q}^2} \;\sim\; \tilde{A}\, \mathbf{q}_2^\beta\, \frac{\mathbf{p}^2}{\mathbf{q}^2} \;\sim\; \tilde{A}\, \frac{\mathbf{p}^2}{\mathbf{q}} \qquad (A.6)$$

Note that if we leave the spacelike momenta unchanged but instead choose

$$\mathbf{q}_1^\mu \;=\; \mathbf{q}_1^- \;=\; \mathbf{q}_{1+} \;=\; \mathbf{p} \not\to 0\;, \quad \mathbf{q}_1^+ \;=\; \mathbf{q}_{1-} \;=\; 0 \qquad (A.7)$$

then we obtain

$$\Gamma^{--\lambda}(\mathbf{q}_1, \mathbf{q}_2) \underset{\mathbf{q}^2 \to 0}{\sim} \tilde{A}\, \epsilon^{-\lambda+\beta}\, \frac{\mathbf{q}_{2\beta}\; \mathbf{q}_{1+}\mathbf{q}_1^+}{\mathbf{q}^2} \;\sim\; -\,\tilde{A}\, \frac{\mathbf{p}^2}{\mathbf{q}} \qquad (A.8)$$

The change of sign compared to (A.6) has very important consequences for our discussion of the cancellation of the anomaly in Sections 4 and 7. The antisymmetry

[‡‡]In 't Hooft's solution[20] of the U(1) problem, instantons produce a quark interaction (an η' mass term) that moves the "perturbative" η' pole away from $\mathbf{q}_1^2 = 0$. In our regge limit analysis, it is not clear how such an interaction could contribute.

with respect to the light-cone direction of momenta is a consequence of the chirality violation by the anomaly discussed below. Note that the structure of the anomaly divergence involves all four dimensions of Minkowski space. This is, in part, why a triple-Regge limit, which fully utilises all four dimensions, is necessary to see the anomaly appear.

The infra-red behavior (A.6) arises directly from the Landau triangle singularity in the quark triangle diagram shown in Fig. A2, i.e.

$$\Gamma^{\mu\nu\lambda}(\mathfrak{q}_1,\mathfrak{q}_2) = i\int \frac{d^4k\ Tr\{\gamma_5\gamma^\mu\ \not{k})\ \gamma_5\gamma^\nu\ (\not{\mathfrak{q}}_2+\not{k})\ \gamma_5\gamma^\lambda\ (-\not{\mathfrak{q}}_1+\not{k})\}}{k^2(\mathfrak{q}_2+k)^2(k-\mathfrak{q}_1)^2} \qquad (A.9)$$

The triangle diagram singularity can be thought of as a space-time scattering as indicated by the arrows in Fig. A2. $\mathfrak{q}_2$ is a spacelike momentum transfered by the $J^{a\nu}$ current and $\mathfrak{q}_1$ has the light-like component necessary to produce an initial pair of massless particles.

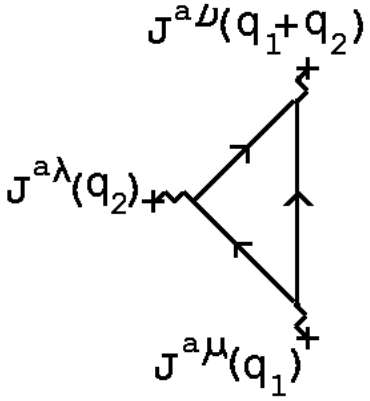

Fig. A2 The Triangle Diagram

Therefore, the vertices where the lightlike momenta enters and leaves are respectively associated with the production and annihilation of a pair of massless fermions. When the helicities of the fermions are determined[1] it is found that in the intermediate states producing the Landau singularity there is a net fermion chirality, i.e. a fermion/antifermion state with the same sign center-of-mass helicities (opposite sign spin components). The axial-vector coupling implies that the contributions of the two states with differing helicity values add rather than cancel, as they would do for a vector coupling (i.e. for a vector coupling the chirality-violating intermediate states are not present). The chirality-violating states are what produce the pseudotensorial asymmetry with respect to light-cone components discussed above. If, as in the main body of the paper, the anomaly singularity is produced by a quark triangle Landau singularity in the midst of a multigluon reggeon interaction (for which there is clearly

no external chirality) then there is a chirality violation involved in producing the divergence. This is the chirality violation that we refer to often in the main text. Clearly the alignment of helicities producing this violation has to be an asymptotic effect of the multi-regge limit, which is not present at finite momentum. The anti-symmetry in going from (A.6) to (A.8) is, of course, a feature that we would expect to lead to cancellation of the anomaly, unless there is some background asymmetry accompanying the reggeon interaction.

Coleman and Grossman also argued for the infra-red equivalent of the "non-renormalization" theorem that holds for the ultra-violet manifestation of the anomaly. They argued that Feynman diagrams with a Landau singularity structure other that that of the triangle diagram, can not reproduce the behaviour (A.6). In our case the reggeon vertices we obtain will not contain the full Lorentz tensor amplitude (A.9) but rather will contain only particular light-cone related momenta and γ-matrix components. We will show, however, that we do have all the necessary components to produce the infra-red divergence (A.6). The argument of Coleman and Grossman then determines that the infra-red divergence we find can not be canceled by the contribution of other diagrams to the reggeon vertices we discuss.

It will also be important for our analysis to discuss the momenta k involved in generating the pole at $\mathbf{q}^2 = 0$ in (A.9). The numerator in (A.9) gives directly the numerator in (A.6) and so we can write

$$\Gamma^{++\lambda}(\mathbf{q}_1, \mathbf{q}_2) \underset{\mathbf{q}^2 \to 0}{\sim} \tilde{A}\, \epsilon^{+\lambda-\beta}\, \mathbf{q}_{2\beta}\, {\mathbf{q}_+}^2 \int \frac{d^4k}{k^4(k^2 - \mathbf{q}_+ k_-)} \qquad (A.10)$$

Superficially this integral depends on $\mathbf{q}_+$ and so might be expected to be $O(1/\mathbf{q}\mathbf{q}_+)$. However, it is straightforward to make the scaling

$$k_+ \;\to\; \Lambda\, k_+ \;, \qquad k_- \;\to\; \Lambda^{-1}\, k_- \qquad (A.11)$$

so that

$$\int \frac{d^4k}{k^4(k^2 - \mathbf{q}_+ k_-)} \;=\; \int \frac{dk_+ dk_- d^2k_\perp}{k^4(k^2 - \mathbf{q}_+ k_-)} \;\to\; \int \frac{d^4k}{k^4(k^2 - \mathbf{q}_+ k_-/\Lambda)} \qquad (A.12)$$

showing that the integral is independent of $\mathbf{q}_+$. (In the limit $\Lambda \to \infty$ the $\mathbf{q}_+$ dependence can be scaled out of the integral altogether, the only trace being the location of the integration contour.) Therefore we can write

$$\int \frac{d^4k}{k^4(k^2 - \mathbf{q}_+ k_-)} \;\sim\; \int \frac{d^4k}{k^6} \;\sim\; \frac{1}{\mathbf{q}^2} \qquad (A.13)$$

and take all components of k to be $O(\mathbf{q})$.

Appendix B. Light Cone Kinematics

Regge limits are conventionally related to light-cone momenta by writing a general 4-momentum $p^\mu = (p_0, p_1, p_2, p_3)$ in the form

$$p^\mu \;=\; \tfrac{1}{2}\, p_{1+}\; \underline{n}_{1+} \;+\; \tfrac{1}{2}\, p_{1-}\; \underline{n}_{1-} \;+\; \underline{p}_{1\perp} \tag{B.1}$$

where $\underline{n}_{1+} = (1,1,0,0)$ and $\underline{n}_{1-} = (1,-1,0,0)$ are and $\underline{p}_{1\perp}$ is a two-dimensional "transverse momentum" orthogonal to both $\underline{n}_{1+}$ and $\underline{n}_{1-}$. It is simple to determine that

$$p_{1+} \;=\; p_0 + p_1 \;,\quad p_{1-} \;=\; p_0 - p_1 \;,\quad \underline{p}_{1\perp} \;=\; (p_2, p_3) \tag{B.2}$$

We regard $\underline{n}_{1+}$ as euclidean vectors and form Minkoski space products by introducing

$$p_\mu \;=\; \tfrac{1}{2}\, p_{1+}\; \underline{n}_{1-} \;+\; \tfrac{1}{2}\, p_{1+}\; \underline{n}_{1-} \;-\; \underline{p}_{1\perp} \tag{B.3}$$

The euclidean product $p^\mu p_\mu$ then, as usual, gives the Minkowski product. Clearly we can similarly define $p_{2+}, p_{2-}, \underline{p}_{2\perp}$ and $p_{3+}, p_{3-}, \underline{p}_{3\perp}$ by, respectively, projecting on vectors $\underline{n}_{2+} = (1,0,1,0)$ and $\underline{n}_{2-} = (1,0,-1,,0)$ or vectors $\underline{n}_{3+} = (1,0,0,1)$ and $\underline{n}_{3-} = (1,0,0,-1,)$.

In this paper we make use of alternative, but formally parallel, decompositions of the form

$$p^\mu \;=\; p_{2-}\; \underline{n}_{1+} \;+\; p_{1-}\; \underline{n}_{2+} \;+\; \underline{p}_{12+} \tag{B.4}$$

where $\underline{p}_{12+}$ is now a two-dimensional vector orthogonal to both $\underline{n}_{1+}$ and $\underline{n}_{2+}$. This determines that

$$\underline{p}_{12+} = \; p_{12-}\; \underline{n}_{12+} + p_3\; \underline{n}_3 \;, \qquad p_{12-} = p_1 + p_2 - p_0 \tag{B.5}$$

where $\underline{n}_{12+} = (1,1,1,0)$ and $\underline{n}_3 = (0,0,0,1)$ are again euclidean vectors. We can also write

$$p_\mu \;=\; p_{2-}\; \underline{n}_{1-} \;+\; p_{1-}\; \underline{n}_{2-} \;+\; p_{12-}\underline{n}_{12-} - p_3\underline{n}_3 \tag{B.6}$$

where $\underline{n}_{1-} = (1,-1,0,0)$, $\underline{n}_{2-} = (1,0,-1,0)$. and $\underline{n}_{12-} = (1,-1,-1,0)$. $p^\mu p_\mu$ is, of course, again the Minkowski product and if $\underline{q}$ is a second four-momentum

$$p \cdot q \;=\; p^\mu q_\mu \;=\; p_{1-} q_{2-} \;+\; p_{2-} q_{1-} \;-\; p_{12-} q_{12-} \;-\; p_3 q_3 \tag{B.7}$$

The analagous decomposition to (B.4) for γ-matrices is

$$\begin{aligned} \gamma^\mu \;&=\; \gamma_{2-}\; \underline{n}_{1+} \;+\; \gamma_{1-}\; \underline{n}_{2+} \;+\; \underline{\gamma}_{12+} \\ &=\; \gamma_{2-}\; \underline{n}_{1+} \;+\; \gamma_{1-}\; \underline{n}_{2+} \;+\; \gamma_{12-}\; \underline{n}_{12-} \;+ \gamma_3\; \underline{n}_3 \end{aligned} \tag{B.8}$$

where

$$\begin{aligned} \gamma_{1^-} &= \gamma_0 - \gamma_1 \ , \quad \gamma_{2^-} = \gamma_0 - \gamma_2 \ , \\ \gamma_{12-} &= \gamma_1 + \gamma_2 - \gamma_0 \end{aligned} \tag{B.9}$$

Similarly

$$\gamma_\mu \ = \ \gamma_{2^-} \ \underline{n}_{1^-} \ + \ \gamma_{1^-} \ \underline{n}_{2^-} \ + \ \gamma_{12-} \underline{n}_{12-} - \gamma_3 \underline{n}_3 \tag{B.10}$$

The γ-matices introduced in this way then satisfy

$$\begin{aligned} &\gamma_{1^-}^2 \ = \ \gamma_{2^-}^2 \ = \ 0 \ , \qquad \gamma_{12-}^2 \ = \ \gamma_3^2 \ = \ -1 \ , \\ &\gamma_{1^-}\gamma_{2^-} \ + \ \gamma_{2^-}\gamma_{1^-} \ = \ 2 \ , \qquad \gamma_3\gamma_{1^-} \ + \ \gamma_{1^-}\gamma_3 \ = \ 0 \ , \\ &\gamma_3\gamma_{2^-} \ + \ \gamma_{2^-}\gamma_3 \ = \ \gamma_{12-}\gamma_{1^-} \ + \ \gamma_{1^-}\gamma_{12-} \ = \ 0 \ , \\ &\gamma_{12-}\gamma_{2^-} \ + \ \gamma_{2^-}\gamma_{12-} \ = \ \gamma_{12-}\gamma_3 \ + \ \gamma_3\gamma_{12-} \ = \ 0 \ . \end{aligned} \tag{B.11}$$

Clearly all the usual algebraic properties of both four-momenta and γ-matrices in terms of conventional light-cone coordinates are the same in the "new light-cone coordinates".

For our discussion of the anomaly it is useful to note that the ϵ-tensor can also be expressed in the new co-ordinates, i.e. we can write

$$\epsilon^{\mu\nu\gamma\delta} P_\mu Q_\nu R_\gamma S_\delta \ = \ p_{2^-} q_{1^-} r_{12-} s_3 \ - \ p_{1^-} \ q_{2^-} \ r_{12-} \ s_3 \ + \ \cdots$$

where there is a term corresponding to each permutation of $(2^-, 1^-, 12-, 3)$, with the sign determined by the usual antisymmetry property of the ϵ-tensor.

Finally we note that we can use any two (non-parallel) light-cone momenta and introduce appropriate "light-cone co-ordinates". In particular we can obviously choose n_{1^+} and n_{3^+}, or n_{2^+} and n_{3^+}, instead of n_{1^+} and n_{2^+} , and trivially repeat all of the above discussion.

Appendix C. Regge Limit Calculations

In this Appendix we discuss some simple Regge limit calculations using the light-cone variables introduced in the previous Appendix. We consider first two quarks scattering via single gluon exchange as illustrated in Fig. C1.

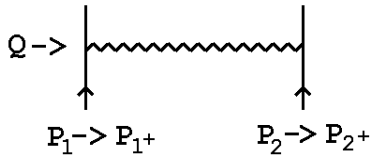

Fig. C1 Single Gluon Exchange

We consider the Regge limit in which

$$\begin{aligned} P_1 \to\ & P_{1+} = p_{12-}\ \underline{n}_{1+}\ , \quad p_{12-} \to \infty \\ P_2 \to\ & P_{2+} = p_{21-}\ \underline{n}_{2+}\ , \quad p_{21-} \to \infty \\ Q \to\ & \underline{Q}_{12+} \end{aligned} \tag{C.1}$$

This is, perhaps, a counter-intuitive way to discuss high-energy forward scattering. Nevertheless, we can proceed in complete parallel with conventional calculations.

The spinor $\psi(P)$ for an on-shell quark satisfies

$$\begin{aligned} m\ \psi(P)\ &=\ (\ p_{2-}\gamma_{1-} + p_{1-}\gamma_{2-} - \underline{p}_{12+}\cdot\underline{\gamma}_{12+})\ \psi(P) \\ &\underset{P \to P_{1+}}{\longrightarrow}\quad p_{2-}\ \gamma_{1-}\ \psi(p) \end{aligned} \tag{C.2}$$

Therefore the vertex for such a fast quark to couple to a single gluon carrying momentum transfer $\underline{Q}_{12+}$ is given by

$$\begin{aligned} \frac{p_{2-}\gamma_{1-}}{m}\ \gamma_\mu\ \frac{(p_{2-}\gamma_{1-} - \underline{Q}_{12+}\cdot\underline{\gamma}_{12+})}{m}\ &=\ \frac{p_{2-}\gamma_{1-}}{m}\left(\frac{p_{2-}}{m}\ \delta_{2^-,\mu}\ -\ \frac{\gamma_\mu\ \underline{Q}_{12+}\cdot\underline{\gamma}_{12+}}{m}\right) \\ &=\ \frac{p_{2-}}{m}\ \delta_{2^-,\ \mu}(1\ +\ O(1/p_{2-})) \end{aligned} \tag{C.3}$$

where we have used the formulae of Appendix B and have reused (C.2) to obtain the last equality. Using this result for the P_1 vertex and the analagous result for the P_2 vertex, we obtain the familiar result for the full amplitude

$$A(s,t) \underset{s\to\infty}{\sim} \frac{p_{12-}\ g^{2^-,1^-}\ p_{21-}}{Q^2}\ \sim\ \frac{s}{t} \tag{C.4}$$

Moving on to the two-gluon exchange diagram illustrated in Fig. C2,

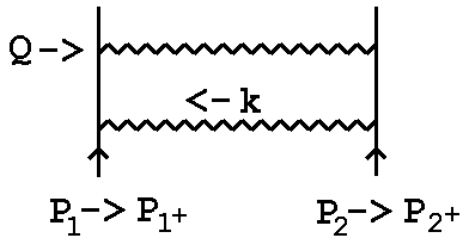

Fig. C2 Two Gluon Exchange

we calculate the imaginary part by first writing

$$\int d^4k \;=\; \int dk_{1^-} dk_{2^-} d^2\underline{k}_{12+} \tag{C.5}$$

Then, for the internal quark propagator along which P_1 flows, we write

$$\begin{aligned} \frac{\gamma\cdot(P+k)+m}{(P+k)^2-m^2} \quad & \overset{\sim}{p_{2^-}\to\infty} \quad \frac{\gamma_{1^-}p_{2^-}+\cdots}{2p_{2^-}k_{1^-}-\underline{k}^2_{12+}-m^2} \\ & \equiv \quad \frac{\gamma_{1^-}+\;0(1/p_{2^-})}{\left[k_{1^-}-(\underline{k}^2_{12+}-m^2)/p_{2^-}\right]} \end{aligned} \tag{C.6}$$

Putting this quark on-shell by performing the k_{1-} integration, the vertex for two gluons to couple to the fast quark is then

$$\frac{p_{12^-}\gamma_{1^-}}{m}\;(\gamma_\mu\;\gamma_{1^-}\;\gamma_\nu)\;\frac{p_{12^-}\gamma_{1^-}}{m} \;=\; \frac{p_{12^-}}{m}\;\delta_{2^-,\mu}\;\delta_{2^-,\nu} \tag{C.7}$$

where we have again used (C.2). The essential feature here, is that the infinite momentum limit leads to the exchange of gluons that will couple to a second scattering quark with a γ_{1^-} -coupling only. Note that this feature would be the same if we had used conventional light-cone co-ordinates (or, in fact, any other light-cone co-ordinates).

Using the analagous result for $P_2 \to P_{2^+}$, to perform the k_{2^-} integration, the kinematic part of the full result, is

$$p_{12^-}\delta_{2^-,\mu}\delta_{2^-,\nu}g^{\mu\alpha}g^{\nu\beta}\delta_{\alpha,1^-}\delta_{\beta,1^-}p'_{21^-}\int\frac{d^2\underline{k}_{12+}}{\underline{k}^2_{12+}(\underline{k}_{12+}+\underline{Q}_{12+})^2} = s\int\frac{d^2\underline{k}_{12+}}{\underline{k}^2_{12+}(\underline{k}_{12+}+\underline{Q}_{12+})^2} \tag{C.8}$$

showing that the familiar tranverse momentum integral is simply replaced by an integral over the new "transverse momentum" $\underline{k}_{12+}$. Since

$$\int \frac{d^2\underline{k}_{12+}}{\underline{k}^2_{12+}(\underline{k}_{12+}+\underline{Q}_{12+})^2} \;=\; J_1(Q^2) \;=\int \frac{d^2\underline{k}}{\underline{k}^2(\underline{k}+\underline{Q})^2} \qquad (C.9)$$

this is a relatively trivial modification. Nevertheless is important for the arguments made in the body of the paper that the same result is clearly obtained whatever light-cone co-ordinates are used.

It is also interesting to calculate the Regge limit of Fig. B2 keeping P_2 finite. In this case the choice of "light-cone co-ordinates" is not determined by the large momenta in the problem, since there is only one. We can equally well use the conventional choice (B.3), or the novel co-ordinates utilised above. In either case we can arrive rapidly at the correct answer by arguing as follows. We again use (C.6) to perform one longitudinal momentum integration (k_{1^-}). The two exchanged gluons then couple to the P_2 quark via

$$\gamma_{1^-}\;\frac{\gamma\cdot(P_2-k)}{(P_2-k)^2-m^2}\;\gamma_{1^-} = \;\gamma_{1^-}\;\frac{\gamma_{1^+}(P_2-k)_{1^-}\;+\;\cdots}{k_{1^+}(P_2-k)_{1^-}\;+\;\cdots}\;\gamma_{1^-}\;=\;\frac{\gamma_{1^-}}{(k_{1^+}\;+\;\cdots)}$$

or

$$=\;\gamma_{1^-}\;\frac{\gamma_{2^-}(P_2-k)_{1^-}\;+\;\cdots}{k_{2^-}(P_2-k)_{1^-}\;+\;\cdots}\;\gamma_{1^-}\;=\;\frac{\gamma_{1^-}}{(k_{2^-}\;+\;\cdots)} \qquad (C.10)$$

in either case, we use this last pole to carry out a second longitudinal momentum integration (k_{1^+} or k_{2^-}) and obtain the corresponding two-dimensional transverse integral. (Whether k_{1^+} or k_{2^-} is used, the exchanged gluon propagators become independent of this variable as $P_1 \to P_{1+}$.) We then use the Dirac equation, as in (C.2), to write either

$$\gamma_{1^-} \;=\; \gamma_{1^-}\;\frac{\gamma\cdot p}{m} \;=\; p_{1^+}/m \;+\; \cdots \qquad (C.11)$$

or

$$\gamma_{1^-} \;=\; \gamma_{1^-}\;\frac{\gamma\cdot p}{m} \;=\; p_{1^-}/m \;+\; \cdots \qquad (C.12)$$

and argue that only the first term, shown explicitly, is capable of forming a Lorentz invariant with the momentum of the fast quark. The result is then either the conventional transverse momentum integral or (C.8). We conclude that when a fast quark scatters off a quark carrying finite momentum we can calculate using any light-cone co-ordinates. The result will be the same, but will be expressed in terms of transverse momenta that depend on the co-ordinates chosen.

We consider next some double-Regge and triple-regge amplitudes. The main results are not used directly in the text but they are instructive and some of the intermediated results are used. We briefly discuss the kinematics of single particle (gluon) production first. We can parallel our elastic scattering discussion using the notation of Fig. C3.

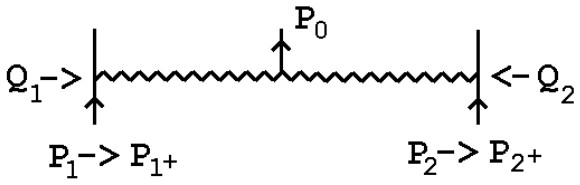

Fig. C3 Double Regge Kinematics

We take $P_1 \to P_{1^+}$ and $P_2 \to P_{2^+}$ as before and also

$$\begin{aligned} Q_1 &\to (q_{11^-}, q_{12^-}, q_{112-}, q_{13}) \equiv (q, 0, \tilde{q}, q_{13}) \\ Q_2 &\to (q_{21^-}, q_{22^-}, q_{212-}, , q_{23}) \equiv (0, q, -\tilde{q}, q_{23}) \end{aligned} \qquad (C.13)$$

with $P_0 = Q_1 + Q_2$. In this notation we have six independent variables, $p_{2^-}, p'_{1^-}, q, \tilde{q}, q_{13}$ and q_{23}. The necessary reduction to five variables is achieved by putting P_0 on mass-shell. This determines q in terms of q_{13} and q_{23}.

Consider now the double-regge amplitude shown in Fig. C4 for producing a quark-antiquark pair via gluon exchange.

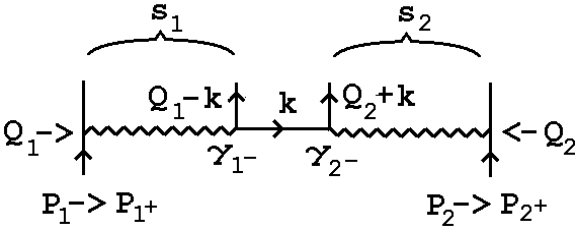

Fig. C4 Quark-antiquark Production in the Double-Regge Limit

We define $\underline{k}$ to be the four-momentum flowing along the exchanged quark propagator and use the same notation for Q_1 and Q_2 as in (C.13), except that we take $q_{11-} \neq q_{22-}$. We can then fix both of q_{11-} and q_{22-} by putting both produced particles on shell.

By applying (C.2) to the fast particles we determine that, as illustrated, the gluons couple to the quark-antiquark pair via γ_{1-} and γ_{2-} couplings. This implies that only the transverse part of the exchanged quark propagator contributes, i.e.

$$\gamma_{1^-} \frac{\underline{k} \cdot \underline{\gamma} - m}{\underline{k}^2 - m^2} \gamma_{2^-} \quad = \quad \gamma_{1^-} \frac{-\underline{k} - 12+ \cdot \underline{\gamma} 12+ - m}{k^2 - m^2} \gamma_{2^-} \qquad (C.14)$$

The full amplitude for Fig. C4 is then

$$A(p_{12^-}, p_{21^-}, \tilde{q}, q_{13}, q_{23}, \underline{k}_{12+}, k_{1^-}k_{2^-}) = \frac{p_{12^-}p_{21^-}\ \gamma_{1^-}\ (-\underline{k}_{12+}\cdot\underline{\gamma}_{12+} - m)\ \gamma_{2^-}}{m^2(\tilde{q}^2+q_{13}^2)(\tilde{q}^2+q_{23}^2)(k^2-m^2)} \quad (C.15)$$

As must be the case, the amplitude is a function of eight independent variables.

To extract an amplitude expressed in terms of invariants consider, in particular, the case in which the produced quark and antiquark spin dependence contributes similarly to (C.2), i.e. we write

$$\begin{aligned} m\ \bar{\psi}(Q_1-k) &= k_{1^-}\ \gamma_{2^-}\ \bar{\psi}(Q_1-k)\ +\ \cdots \\ m\ \psi(Q_2+k) &= k_{2^-}\ \gamma_{1^-}\ \psi(Q_2+k)\ +\ \cdots \end{aligned} \quad (C.16)$$

and keep only the spinor components shown explicitly. In this case the production amplitude of Fig. C4 has the simple form

$$\frac{s\ s'}{m^2Q_1^2Q_2^2}\ \ \frac{-\underline{k}_{12+}\cdot\underline{\gamma}_{12+} - m}{(k^2-m^2)} \quad (C.17)$$

Note that with the polarizations of the produced pair given by (C.16), the diagram of Fig. C5 does not contribute.

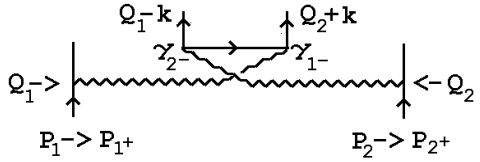

Fig. C5 An Alternative Gluon Coupling

In general a reggeon Ward identity requires that the complete central reggeon amplitude vanish when either Q_1 or Q_2 vanish. This is achieved by adding the three diagrams of Fig. C6.

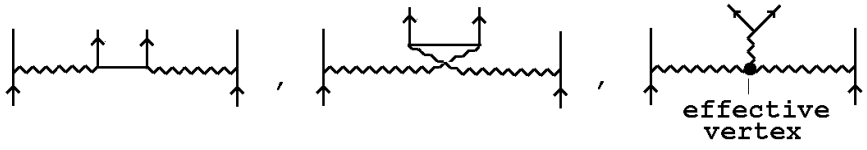

Fig. C6 Diagrams Required for the Reggeon Ward Identity.

For the special polarizations given by (C.16), the last diagram directly cancels the first when Q_1 or $Q_2 \to 0$.

Consider next the diagram of Fig. C7 in which an additional gluon is exchanged in the Q^2 channel.

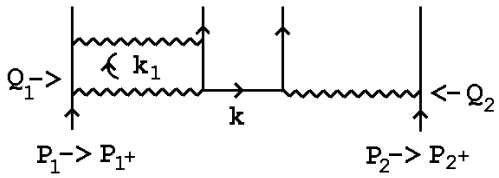

Fig. C7 An Additional Gluon Exchanged

We can calculate the discontinuity in s_1, or simply carry out two longitudinal integrations, by repeating the analysis that we applied to Fig. C2, we obtain

$$A(p_{12^-}, p_{21^-}, \tilde{q}, q_{13}, q_{23}, \tilde{\underline{k}}_\perp, k_{1^-} k_{2^-})$$
$$= \frac{p_{12^-} p'_{21^-}}{m^2 Q_2^2} \int \frac{d^2 \underline{k}_{112+}}{\underline{k}^2_{112+} (\underline{k}_{112+} - \underline{Q}_{12+})^2} \frac{\gamma_{1^-}(-\underline{k}_{12+} \cdot \underline{\gamma}_{12+} - m)\gamma_{2^-}}{(k^2 - m^2)}$$
$$= \frac{p_{12^-} p_{21^-}}{m^2 Q_2^2} J_1(Q_1^2) \frac{\gamma_{1^-}(-\underline{k}_{12+} \cdot \underline{\gamma}_{12+} - m)\gamma_{2^-}}{(k^2 - m^2)} \tag{C.18}$$

Comparing with (C.15), we see that the additional gluon has simply replaced one gluon transverse momentum propagator by a transverse momentum integral. The integral also has a γ_{1^-} "point-coupling" to the central vertex. The pointlike nature of this coupling is, of course, essential if Fig. C7 is to be added to Fig. C3 and the $J_1(Q_1^2)$ is to produce the reggeization of the gluon in the Q_1^2 channel. However, there will also be a pointlike coupling when the quantum numbers in the Q^2 channel are such that each of the two gluons involved in the loop integral in Fig. C7 reggeize separately and the two reggeon cut appears.

If the additional gluon is attached to the outgoing quark as in Fig. C8 (rather than to the antiquark as in Fig. C7) then we no longer obtain a point-coupling for the two-gluon exchange in the Q_1 channel.

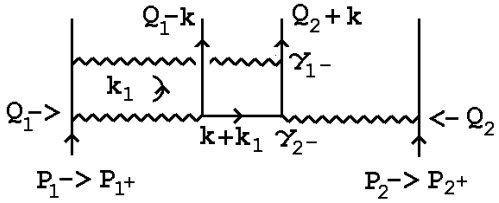

Fig. C8 An Additional Gluon Exchange Giving no Point Coupling.

The contribution of the on mass-shell hatched quark line and the adjacent γ-couplings to the k_1 integral is now

$$\begin{aligned}
&\int dk_{12^-}\ \delta\Big((k_1+k+Q_2)^2-m^2\Big)\gamma_{2^-}\ \Big((k_1+k+Q_2)\cdot\gamma-m\Big)\ \gamma_{1^-}\\
&=\int dk_{12^-}\ \delta\Big(k_{12^-}(k_1+k+Q_2)_{1^-}\ \cdots\Big)\gamma_{2^-}\ \Big(-\ (\underline{k}_{112+}+\underline{k}_{12+}+\underline{Q}_{212+})\cdot\underline{\gamma}_{12+}-m\Big)\ \gamma_{1^-}\\
&=\qquad\frac{\gamma_{2^-}\ \Big(-\ (\underline{k}_{112+}+\underline{k}_{12+}+\underline{Q}_{212+})\cdot\underline{\gamma}_{12+}-m\Big)\ \gamma_{1^-}}{(k_1+k+Q_2)_{1^-}}
\end{aligned}\tag{C.19}$$

We do not obtain a point-like coupling because (unlike in (C.10), for example) the argument of the δ-function contains an integrated longitudinal momentum multiplied by a momentum factor that does not multiply a γ-matrix appearing in the numerator of the propagator. The relevant part of the propagator numerator is eliminated by the surrounding γ matrices.

Finally we move on to the process that is of central interest in the main body of the paper. This is the triple Regge scattering illustrated in Fig. C9.

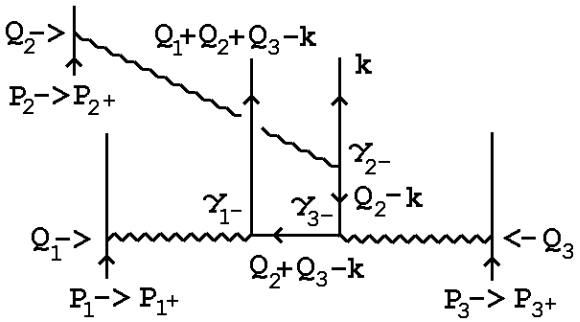

Fig. C9 A Triple Regge Amplitude.

A triple-Regge limit can be defined as $P_i\ \to P_{i+},\ i=1,2,3$ with the Q_i kept finite. We will not give a complete description of the quark-antiquark intermediate state in this limit since it will not be needed in the body of the paper. The important point for our purposes is that to directly obtain the triple discontinuities studied in Sections 5 and 6, the amplitude in Fig. C9 should be combined with another amplitude of the same form and all three of the Q_i integrated over. We do not do this in Section 6 but instead discuss only double discontinuities explicitly. However, we can make the following comment on the direct construction of triple discontinuities.

The reduction of Q_i integrations to two-dimensional integrals is achieved by using all the longitudinal integrations to put on-shell all quark lines involved in the multiple discontinuity. In particular, the internal quark propagator in Fig. C9 carrying

momentum $Q_2 - k$ should be placed on-shell. If we use the Q_2 integration to put this line on-shell, and also use the 1^-,2^-, ... co-ordinates of Appendix B, the combination of the γ_{2^-} and γ_{3^-} factors with the on-shell propagator produces the effective coupling

$$\begin{aligned}
&\int dQ_{21^-}\ \delta\Big(Q_{21^-}(Q_{22^-} - k_{2^-}) \ - \ \cdots\Big)\ \gamma_{2^-}\ (\not{Q}_2 - \not{k})\ \gamma_{3^-} \\
&= \int dQ_{22^-}\ \delta\Big(Q_{22^-}(Q_{21^-} - k_{1^-}) \ - \ \cdots\Big)\ \gamma_{2^-}\ \Big(\gamma_{1^-}(Q_{21^-} - k_{1^-}) \ - \ \cdots\Big)\ \gamma_{3^-} \\
&\qquad = \ \gamma_{2^-}\gamma_{1^-}\gamma_{3^-} \ + \ \cdots
\end{aligned} \tag{C.20}$$

Using the identity

$$\gamma_\alpha\gamma_\beta\gamma_\lambda \ = \ g_{\alpha\beta}\gamma_\lambda \ + \ g_{\beta\lambda}\gamma_\alpha \ - \ g_{\alpha\lambda}\gamma_\beta + i\epsilon_{\mu\alpha\beta\gamma}\gamma^\mu\gamma_5 \tag{C.21}$$

we obtain

$$\gamma_{2^-}\gamma_{1^-}\gamma_{3^-} \ = \ \gamma_0 + \gamma_1 - \gamma_2 - \gamma_3 \ + \ i\gamma_5\ (\gamma_0 + \gamma_1 + \gamma_2 + \gamma_3) \tag{C.22}$$

showing that the coupling (C.20) contains the effective γ_5-coupling shown in Fig. C10

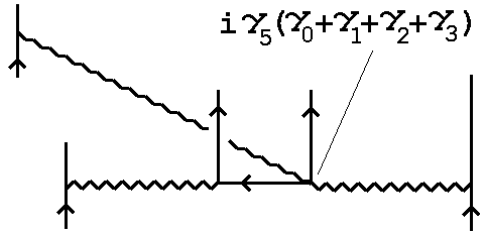

Fig. C10 The γ_5-coupling Generated by Fig. C9

This illustrates how the triple-Regge limit introduces sufficient orthogonality for the large momenta to produce an effective γ_5-coupling.

Appendix D. Angular Variables

To introduce angular variables for a six-particle amplitude it is necessary to define a set of six standard Lorentz frames $\mathcal{F}_1, \mathcal{F}_2, \mathcal{F}_3, \tilde{\mathcal{F}}_1, \tilde{\mathcal{F}}_2, \tilde{\mathcal{F}}_3$. These frames are associated with the vertices of the Toller diagram, as indicated in Fig. D1, by requiring that the momenta meeting at a vertex take a standard form. For each internal vertex there are three frames, in each of which one of the momenta lies either along the t-axis or the z-axis. As we will see, once the standard frames are defined, the angular variables parametrize "little group" Lorentz transformations between the frames.

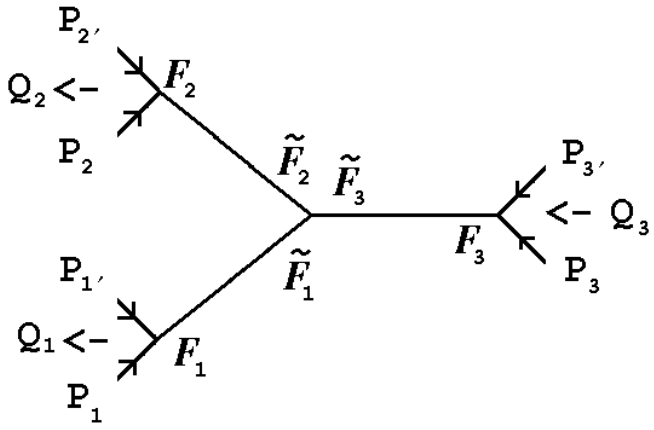

Fig. D1 Special Frames

Not surprisingly, the definition of the standard frames, together with the little groups involved (and their parametrization) depend on the physical region discussed. Since the multi-regge theory we develop in Section 5 effectively moves backwards and forwards between various t and s-channels we need to determine how the variables introduced in different channels are analytically related. For this purpose we explicitly calculate below, expressions for invariants in terms of angular variables in each of the channels we discuss. We take the mass of all external particles to be m. We can then distinguish the three t-channels and four s-channels that we study as follows. In the t_i-channel ($i = 1, 2, 3$), $|Q_i| \geq |Q_j| + |Q_k|$ ($i \neq j \neq k$) with $Q_j^2, Q_k^2 \geq 4m^2$. In the s-shannels the $t_i = Q_i^2$ are all negative. The four channels are that in which the particles with momenta P_1, P_2 and P_3 scatter, with final momenta P_1', P_2' and P_3' respectively, and those in which one of the P_i' is exchanged with the corresponding P_i.

In Fig. D2 we have shown (topographically) the three t_i-channels and one of the s-channels. In this figure, we have also indicated that a single s-channel breaks up

into four distinct sub-regions. There are three "$s-t$" sub-regions in which one of the transverse momenta has longer length than the sum of the other two. In these regions the plane containing the Q_i must have a timelike component. In the "$s-s$" sub-region the Q_i satisfy euclidean inequalities and can be taken to have only spacelike components. We will discuss how the variables introduced in all regions are related by analytic continuation.

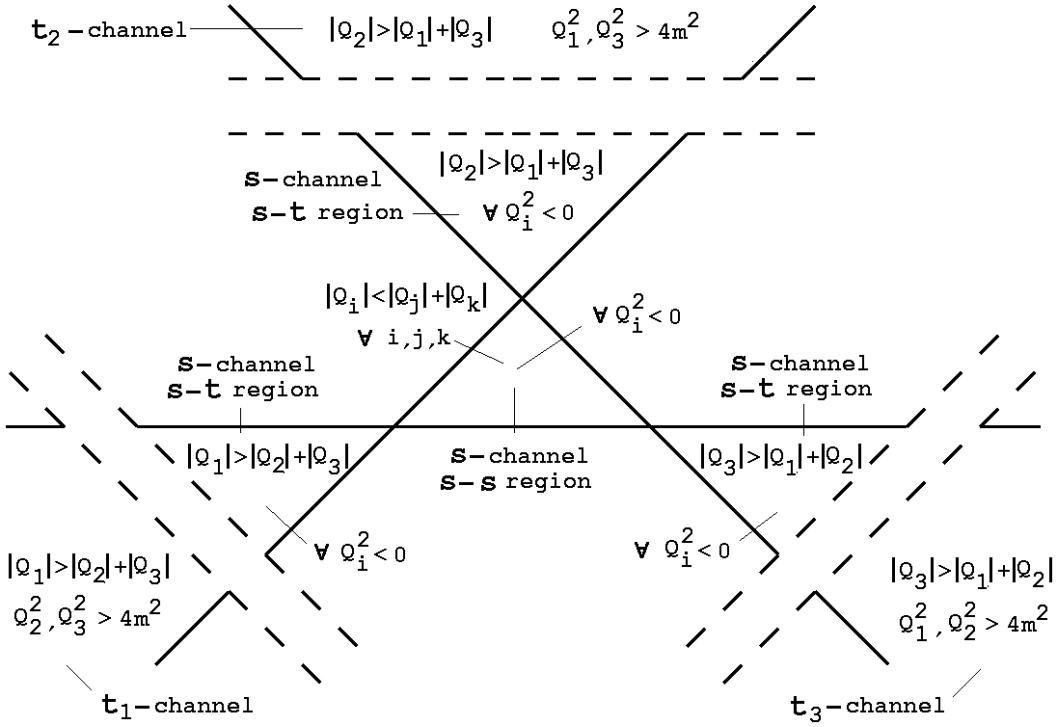

Fig. D2 Physical Regions

We consider first the t_3-channel, illustrated in Fig. D1, in which two initial state particles, 3 and $3'$, scatter into four final state particles $2, 2', 3, 3'$. In this case $Q_1^2, Q_2^2 \geq 4m^2$, $\forall i$, and $|Q_3| \geq |Q_1| + |Q_2|$. The frames $\mathcal{F}_i$, $i = 1, 2, 3$, can be defined by requiring that

$$Q_i = (Q_i, 0, 0, 0) \qquad \begin{aligned} P_i &= (mcosh\xi_i, 0, 0, msinh\xi_i) \\ P_i' &= (mcosh\xi_i, 0, 0, -msinh\xi_i) \end{aligned} \qquad (D.1)$$

where $cosh\xi_i = Q_i/2m$. Clearly we could easily interchange the roles of P_i and P_i' by setting $\xi_i \to -\xi_i$ $\forall i$. As long as the theory is parity invariant, amplitudes can not

depend on this choice. For frame $\tilde{\mathcal{F}}_1$ we require that

$$Q_1 = (Q_1, 0, 0, 0) \qquad \begin{array}{l} Q_2 = (Q_2 cosh\zeta_{21}, 0, 0, Q_2 sinh\zeta_{21}) \\ Q_3 = (Q_3 cosh\zeta_{31}, 0, 0, Q_3 sinh\zeta_{31}) \end{array} \tag{D.2}$$

where

$$cosh\zeta_{21} = \frac{Q_3^2 - Q_2^2 - Q_1^2}{2Q_1Q_2} \ , \qquad cosh\zeta_{31} = \frac{Q_3^2 + Q_1^2 - Q_2^2}{2Q_1Q_3} \tag{D.3}$$

For the frames $\tilde{\mathcal{F}}_2$ and $\tilde{\mathcal{F}}_3$ we make the analagous requirements so that in $\tilde{\mathcal{F}}_3$, for example,

$$Q_3 = (Q_3, 0, 0, 0) \qquad \begin{array}{l} Q_1 = (Q_1 cosh\zeta_{13}, 0, 0, Q_1 sinh\zeta_{13}) \\ Q_2 = (Q_2 cosh\zeta_{23}, 0, 0, Q_2 sinh\zeta_{23}) \end{array} \tag{D.4}$$

where

$$sinh\zeta_{13} \ = \ -sinh\zeta_{31} \ = \ \Big(\frac{(Q_3^2 + Q_1^2 - Q_2^2)^2 - 4Q_1^2Q_3^2}{4Q_1^2Q_2^2}\Big)^{\frac{1}{2}} = \ -\frac{\lambda^{\frac{1}{2}}(t_1, t_2, t_3)}{2\sqrt{t_1}\sqrt{t_3}} \tag{D.5}$$

and

$$sinh\zeta_{23} \ = \ \frac{\lambda^{\frac{1}{2}}(t_1, t_2, t_3)}{2\sqrt{t_1}\sqrt{t_3}} \tag{D.6}$$

where $\lambda(t_1, t_2, t_3)$ is the familiar function

$$\begin{aligned} \lambda(t_1, t_2, t_3) \ &= \ t_1^2 + t_2^2 + t_3^2 - 2t_1t_2 - 2t_2t_3 - 2t_3t_1 \\ &= (\sqrt{t_1} + \sqrt{t_2} + \sqrt{t_3})(\sqrt{t_1} - \sqrt{t_2} - \sqrt{t_3})(-\sqrt{t_1} + \sqrt{t_2} - \sqrt{t_3})(-\sqrt{t_1} - \sqrt{t_2} + \sqrt{t_3}) \end{aligned} \tag{D.7}$$

Clearly we have to take opposite signs for $\lambda^{\frac{1}{2}}(t_1, t_2, t_3)$ in defining $sinh\zeta_{13}$ and $sinh\zeta_{23}$. Conversely we can reverse this sign by interchanging the form of Q_1 and Q_2 in the t_3-channel standard frames. In the next paragraph we will discuss further the ambiguity in making this choice, together with the remaining ambiguity in fixing the frames $\mathcal{F}_i$ and the frames $\tilde{\mathcal{F}}_i$. It is linked, of course, to the ambiguity in the choice of the $sinh\xi_i$.

$\tilde{\mathcal{F}}_1$ and $\mathcal{F}_1$ are related by a Lorentz transformation g_1 that leaves Q_1 unchanged, i.e. g_1 belongs to the little group of Q_1, which is $SO(3)$. We can parametrize $SO(3)$ in the form

$$g_1 = u_z(\mu_1)u_x(\theta_1)u_z(\nu_1) \qquad\qquad 0 \leq \theta < \pi \ , \ \ 0 \leq \nu, \ \mu \leq 2\pi \tag{D.8}$$

where u_z and u_x are, respectively, rotations about the z and x axes. If we take g_1 to transform from $\mathcal{F}_1$ to $\tilde{\mathcal{F}}_1$, g_2 to transform from $\mathcal{F}_2$ to $\tilde{\mathcal{F}}_2$ and g_3 to transform

from $\mathcal{F}_3$ to $\tilde{\mathcal{F}}_3$, then we can absorb the $u_z(\mu_i)$ in our definition of the frames $\mathcal{F}_i$ so that, effectively, we set $\mu_i = 0,\ i = 1, 2, 3$. Apart from the choice of sign for $sinh\xi_i$, this removes the remaining ambiguity in the definition of the $\mathcal{F}_i$ frames after (D.1) is satisfied. Because the $u_z(\nu_i)$ commute with the boosts $a_z(\zeta_{ij})$ along the z-axis, invariants can depend only on differences between the three ν_i - so that only two parameters are actually involved. If we insist on both the parametrization (D.8) and this last commutativity property then the $\tilde{\mathcal{F}}_i$ frames are determined up to a reflection - an overall sign change for all the $sinh\zeta_{ij}$. Again, amplitudes can not depend on this choice of sign because of parity invariance. Nevertheless, the parity transformation that produces this overall sign change plays an important role in the discussion of Section 5.

In general, to calculate invariants we transform all the momenta involved from frames in which they take a simple form to a common frame where the invariant is most easily evaluated. For.example, we transform P_1 from $\mathcal{F}_1$ to $\mathcal{F}_3$ via $\tilde{\mathcal{F}}_1$ and $\tilde{\mathcal{F}}_3$ as follows. In $\tilde{\mathcal{F}}_1$

$$P_1 = (mcosh\xi_1,\ -msinh\xi_1 sin\theta_1 sin\nu_1,\ -msinh\xi_1 sin\theta_1 cos\nu_1,\ msinh\xi_1 cos\theta_1) \quad (D.9)$$

In $\tilde{\mathcal{F}}_3$

$$\begin{aligned} P_1 = (&mcosh\xi_1 cosh\zeta_{31} - msinh\xi_1 cos\theta_1 sinh\zeta_{31},\ \ - msinh\xi_1 sin\theta_1 sin\nu_1, \\ &- msinh\xi_1 sin\theta_1 cos\nu_1,\ msinh\xi_1 cos\theta_1 cosh\zeta_{31} - mcosh\xi_1 sinh\zeta_{31}) \end{aligned} \quad (D.10)$$

In $\mathcal{F}_3$

$$\begin{aligned} P_1 = (&mcosh\xi_1 cosh\zeta_{31} - msinh\xi_1 cos\theta_1 sinh\zeta_{31}, msinh\xi_1 sin\theta_1 sin(\nu_1 - \nu_3), \\ &msinh\xi_1 sin\theta_1 cos(\nu_1 - \nu_3) cos\theta_3 - msinh\xi_1 cos\theta_1 cosh\zeta_{31} sin\theta_3 \\ &- mcosh\xi_1 sinh\zeta_{31} sin\theta_3,\ \ - msinh\xi_1 sin\theta_1 cos(\nu_1 - \nu_3) sin\theta_3 \\ &+ msinh\xi_1 cos\theta_1 cosh\zeta_{31} cos\theta_3 - mcosh\xi_1 sinh\zeta_{31} cos\theta_3) \end{aligned} \quad (D.11)$$

Alternatively we can transform P_1 to $\tilde{\mathcal{F}}_2$ and to $\mathcal{F}_2$ as follows. In $\tilde{\mathcal{F}}_2$

$$\begin{aligned} P_1 = (&mcosh\xi_1 cosh\zeta_{21} - msinh\xi_1 cos\theta_1 sinh\zeta_{21},\ \ - msinh\xi_1 sin\theta_1 sin\nu_1, \\ &- msinh\xi_1 sin\theta_1 cos\nu_1,\ msinh\xi_1 cos\theta_1 cosh\zeta_{21} - mcosh\xi_1 sinh\zeta_{21}) \end{aligned} \quad (D.12)$$

In $\mathcal{F}_2$

$$\begin{aligned} P_1 = (&m cosh\xi_1 cosh\zeta_{21} + m sinh\xi_1 cos\theta_1 sinh\zeta_{21}, \;\; - m sinh\xi_1 sin\theta_1 sin(\nu_1 - \nu_2), \\ &m sinh\xi_1 sin\theta_1 cos(\nu_1 - \nu_2) cos\theta_2 + m sinh\xi_1 cos\theta_1 cosh\zeta_{21} sin\theta_2 \\ &- m cosh\xi_1 sinh\zeta_{21} sin\theta_2, \;\; - m sinh\xi_1 sin\theta_1 cos(\nu_1 - \nu_2) sin\theta_2 \\ &+ m sinh\xi_1 cos\theta_1 cosh\zeta_{21} cos\theta_2 - m cosh\xi_1 sinh\zeta_{21} cos\theta_2) \end{aligned} \tag{D.13}$$

From the above expressions for P_1 we can already calculate several invariants. In $\tilde{\mathcal{F}}_1$, for example, Q_3 has the form (D.2) and so

$$P_1.Q_3 \;=\; m Q_3 \; [cosh\xi_1 cosh\zeta_{31} - sinh\xi_1 sinh\zeta_{31} cos\theta_1] \tag{D.14}$$

In $\mathcal{F}_3$, similarly, P_3 has the form (D.1) and so

$$\begin{aligned} P_1.P_3 \;=\; & m^2 \; [cosh\xi_1 cosh\xi_3 cosh\zeta_{31} - sinh\xi_1 cosh\xi_3 sinh\zeta_{31} cos\theta_1 \\ & - sinh\xi_1 sinh\xi_3 sin\theta_1 sin\theta_3 cos(\nu_1 - \nu_3) - sinh\xi_1 sinh\xi_3 cosh\zeta_{31} cos\theta_1 cos\theta_3 \\ & + cosh\xi_1 sinh\xi_3 sinh\zeta_{31} cos\theta_3] \end{aligned} \tag{D.15}$$

while, in $\mathcal{F}_2$, P_2 has the form (D.1) and so

$$\begin{aligned} P_1.P_2 \;=\; & m^2 \; [cosh\xi_1 cosh\xi_2 cosh\zeta_{21} - sinh\xi_1 cosh\xi_2 sinh\zeta_{21} cos\theta_1 \\ & - sinh\xi_1 sinh\xi_2 sin\theta_1 sin\theta_2 cos(\nu_1 - \nu_2) - sinh\xi_1 sinh\xi_2 cosh\zeta_{21} cos\theta_1 cos\theta_2 \\ & + cosh\xi_1 sinh\xi_2 sinh\zeta_{21} cos\theta_2] \end{aligned} \tag{D.16}$$

(D.15) and (D.16) differ only by the interchange of 1 and 2. It is straightforward to calculate all other invariants in a similar manner. If we write $z_i = cos\theta_i$ and $u_{ij} = e^{i(\nu_i - \nu_j)}$ then we can take any two of the u_{ij}, together with the z_i and the t_i, as eight independent variables.

We see from the above formulae that a change of sign of $sinh\xi_1$ is equivalent to a change of sign of both $cos\theta_1$ and $sin\theta_1$ ($\theta \to \theta + \pi$). A change of sign of the $sinh\zeta_{ij}$ is equivalent to a change of sign of all the $cos\theta_i$ which, in turn, is equivalent to a change of sign of all the $sinh\xi_i$. It is also interesting to write (D.14) and (D.15) explicitly in terms of the t_i and z_1, i.e.

$$4 \; P_1.Q_3 \;=\; t_3 + t_1 - t_2 \;-\; \left(\frac{t_1 - 4m^2}{t_1}\right)^{\frac{1}{2}} \lambda^{\frac{1}{2}}(t_1, t_2, t_3) \; z_1 \tag{D.17}$$

and

$$8\ P_1.P_3\ =\ t_3+t_1-t_2\ -\ \lambda^{\frac{1}{2}}(t_1,t_2,t_3)\Big[\frac{(t_1-4m^2)^{\frac{1}{2}}}{\sqrt{t_1}}z_1\ -\ \frac{(t_3-4m^2)^{\frac{1}{2}}}{\sqrt{t_3}}z_3\Big]$$
$$-\ (t_1-4m^2)^{\frac{1}{2}}(t_3-4m^2)^{\frac{1}{2}}\Big[(1-z_1^2)^{\frac{1}{2}}(1-z_3^2)^{\frac{1}{2}}\Big(u_1+\frac{1}{u_1}\Big)+\frac{t_3+t_1-t_2}{\sqrt{t_1}\sqrt{t_3}}z_1z_3\Big] \tag{D.18}$$

From these expressions we see that we will encounter analytic continuation problems at the thresholds $t_i = 4m^2$, at $t_i = 0$, and at $\lambda(t_1, t_2, t_3) = 0$. In particular, when $t_i < 0$ and also $\lambda(t_1, t_2, t_3) < 0$ the real relationship between the z_i and the invariants is necessarily lost.

Consider now the s-channel in which $1, 2$ and 3 are the three initial state particles and consider the $s - t$ region in which $Q_i^2 < 0, \forall i$ and $|Q_3| \geq |Q_1| + |Q_2|$. The frames $\mathcal{F}_i$, $i = 1, 2, 3$ are now defined by requiring that

$$Q_i = (0, 0, 0, q_i) \qquad \begin{aligned} P_i &= (mcosh\xi_i, 0, 0, msinh\xi_i) \\ P_i' &= (-mcosh\xi_i, 0, 0, msinh\xi_i) \end{aligned} \tag{D.19}$$

where $sinh\xi_i = q_i/2m$ and $q_i = |Q_i| = [-t_i]^{\frac{1}{2}}$ (so that $sinh\xi_i \equiv i\ cosh\xi_i$ if we consider the analytic continuation of $cosh\xi_i$ defined by (D.1)). The obvious redefinition of the frame $\tilde{\mathcal{F}}_1$ is to require

$$Q_1 = (0, 0, 0, q_1) \qquad \begin{aligned} Q_2 &= (q_2 sinh\zeta_{21}, 0, 0, q_2 cosh\zeta_{21}) \\ Q_3 &= (q_3 sinh\zeta_{31}, 0, 0, q_3 cosh\zeta_{31}) \end{aligned} \tag{D.20}$$

where

$$cosh\zeta_{21} = \frac{q_3^2 - q_2^2 - q_1^2}{2q_1q_2}\ , \qquad cosh\zeta_{31} = \frac{q_3^2 + q_1^2 - q_2^2}{2q_1q_3} \tag{D.21}$$

These last expressions are simple analytic continuations of the expressions given in (D.3). The frames $\tilde{\mathcal{F}}_2$ and $\tilde{\mathcal{F}}_3$ are redefined analagously. Note, however, that there is again an overall ambiguity in the choice of sign for the $sinh\zeta_{ij}$. Now the reflection involved is not a parity transformation since it applies to the time axis. If any of the Q_i were timelike and associated with a particle state (as in a normal multi-regge production process) this sign would be determined. In the present case we will see that we must use both signs to fully cover the physical region.

$\tilde{\mathcal{F}}_i$ and $\mathcal{F}_i$ are again related by a Lorentz transformation g_i that leaves Q_i unchanged, but now $g_i \in SO(2, 1)$. Since the Q_i triangle has a timelike component it

is simplest to use the parametrization of $SO(2,1)$ that is closely related to that used above for $SO(3)$, i.e.

$$g_1 = u_z(\mu_1)a_x(\beta_1)u_z(\nu_1) \qquad -\infty \leq \beta < \infty \quad 0 \leq \nu,\ \mu \leq 2\pi \tag{D.22}$$

where $a_x(\beta_1)$ is a boost along the x-axis. With this parametrization, we can again choose the $\mathcal{F}_i$ such that $\mu_i = 0,\ i = 1,2,3$ and the $u_z(\nu_i)$ commute with the boosts $a_z(\zeta_{ij})$.

Repeating the transformation of P_1 from $\mathcal{F}_1$ to $\mathcal{F}_3$ gives the following. In $\tilde{\mathcal{F}}_1$

$$P_1 = (mcosh\xi_1 cosh\beta_1,\ mcosh\xi_1 sinh\beta_1 cos\nu_1,\ -mcosh\xi_1 sinh\beta_1 sin\nu_1,\ msinh\xi_1) \tag{D.23}$$

In $\tilde{\mathcal{F}}_3$

$$\begin{aligned} P_1 = (&mcosh\xi_1 cosh\beta_1 cosh\zeta_{31} - msinh\xi_1 sinh\zeta_{31},\ mcosh\xi_1 sinh\beta_1 cos\nu_1, \\ &-mcosh\xi_1 sinh\beta_1 sin\nu_1,\ msinh\xi_1 cosh\zeta_{31} - mcosh\xi_1 cosh\beta_1 sinh\zeta_{31}) \end{aligned} \tag{D.24}$$

In $\mathcal{F}_3$

$$\begin{aligned} P_1 = (&mcosh\xi_1 cosh\beta_1 cosh\beta_3 cosh\zeta_{31} - msinh\xi_1 sinh\zeta_{31} cosh\beta_3 \\ &-mcosh\xi_1 sinh\beta_1 sinh\beta_3 cos(\nu_1 - \nu_3),\ -mcosh\xi_1 cosh\beta_1 sinh\beta_3 cosh\zeta_{31} \\ &msinh\xi_1 sinh\zeta_{31} sinh\beta_3 + mcosh\xi_1 sinh\beta_1 cosh\beta_3 cos(\nu_1 - \nu_3), \\ &-mcosh\xi_1 sinh\beta_1 sin(\nu_1 - \nu_3),\ msinh\xi_1 cosh\zeta_{31} - mcosh\xi_1 cosh\beta_1 sinh\zeta_{31}) \end{aligned} \tag{D.25}$$

Calculating in $\tilde{\mathcal{F}}_1$, we now obtain

$$P_1.Q_3 \ = \ mq_3\ [cosh\xi_1 sinh\zeta_{31} cosh\beta_1 - sinh\xi_1 cosh\zeta_{31}] \tag{D.26}$$

and in $\mathcal{F}_3$ (arranging terms to compare with (D.15))

$$\begin{aligned} P_1.P_3 \ = \ m^2\ [&-sinh\xi_1 sinh\xi_3 cosh\zeta_{31} + cosh\xi_1 sinh\xi_3 sinh\zeta_{31} cosh\beta_1 \\ &- cosh\xi_1 cosh\xi_3 sinh\beta_1 sinh\beta_3 cos(\nu_1 - \nu_3) \\ &+ cosh\xi_1 cosh\xi_3 cosh\zeta_{31} cosh\beta_1 cosh\beta_3 - sinh\xi_1 cosh\xi_3 sinh\zeta_{31} cosh\beta_3] \end{aligned} \tag{D.27}$$

Comparing (D.26) and (D.27) with (D.14) and (D.15) we see that, if we identify $cos\theta_i \leftrightarrow cosh\beta_i = z_i$, the two sets of formulae are directly related by analytic continuation. All terms have changed sign as a result of $cosh\xi_i/sinh\xi_i \ \rightarrow \ i\ sinh\xi_i/cosh\xi_i$ and $Q_i \rightarrow i\ Q_i$, apart from that containing $sin\theta_1 sin\theta_2$, which contains an extra minus sign via $sin\theta_i \rightarrow i\ sinh\beta_i$.

In this last discussion we have effectively made the analytic continuation choice that the $sinh\zeta_{ij}$ do not change sign, yet we have emphasized that there is an overall sign ambiguity for these quantities. To see the significance of this ambiguity we note that (calculating in frame $\tilde{\mathcal{F}}_3$ for simplicity)

$$P_3.Q_1 \;=\; mq_1\,[cosh\xi_3 sinh\zeta_{13} cosh\beta_3 - sinh\xi_3 cosh\zeta_{13}] \qquad (D.28)$$

and

$$P_3.Q_2 \;=\; mq_2\,[cosh\xi_3 sinh\zeta_{23} cosh\beta_3 - sinh\xi_2 cosh\zeta_{23}] \qquad (D.29)$$

where if we choose $sinh\zeta_{13}$ to be positive then we must choose $sinh\zeta_{23}$ to be negative. This in turn will imply that, for large $cosh\beta_3$, $P_3.Q_1$ is positive, while $P_3.Q_2$ is negative. However, the part of the physical region we are discussing is completely symmetric with repect to 1 and 2. Therefore, to cover the full physical region, we must take both sign conventions for the $sinh\zeta_{ij}$. This would appear to prevent the full description of s-channel physical regions using angular variables defined by analytic continuation from the t_i-channels since it implies, in particular, that we must choose both signs for $\lambda^{\frac{1}{2}}(t_1,t_2,t_3)$ z_1 in (D.17). Fortunately, as we remarked earlier, and can be seen directly from (D.26),(D.27),(D.28), and (D.29), changing the sign of the $sinh\zeta_{ij}$ is equivalent to changing the sign of the three $z_i = cosh\beta_i$. Therefore, to cover the $s-t$ part of the s-channel that we are discussing, using z_i variables defined by anaytic continuation from a t-channel, we must use both $z_1, z_2, z_3, \geq 1$ and $z_1, z_2, z_3, \leq -1$. This is a very important point for the discussion of dispersion theory and signature in the body of the paper.

Finally we consider the $s-s$ region of the same s-channel. In this case the three Q_i lie entirely in a spacelike plane so that $Q_i^2 < 0, \forall i$ and $|Q_i| \leq |Q_j| + |Q_k| \;\; \forall\; i,j,k$. The $\mathcal{F}_i$ frames are again defined so that

$$Q_i = (0,0,0,q_i) \qquad \begin{aligned} P_i &= (mcosh\xi_i, 0, 0, msinh\xi_i) \\ P_i' &= (-mcosh\xi_i, 0, 0, msinh\xi_i) \end{aligned} \qquad (D.30)$$

with $sinh\xi_i = q_i/2m$. However, the frame $\tilde{\mathcal{F}}_1$ is now defined so that

$$Q_1 = (0,0,0,q_1) \qquad \begin{aligned} Q_2 &= (0, 0, q_2 sin\zeta_{21}, q_2 cos\zeta_{21}) \\ Q_2 &= (0, 0, q_3 sin\zeta_{31}, q_3 cos\zeta_{31}) \end{aligned} \qquad (D.31)$$

where

$$cos\zeta_{21} = \frac{q_2^2 + q_1^2 - q_3^2}{2q_1q_2}\;, \qquad cos\zeta_{31} = \frac{q_3^2 + q_1^2 - q_2^2}{2q_1q_3} \qquad (D.32)$$

Now there is a change of sign of $cos\zeta_{21}$ compared to the definition of $cosh\zeta_{21}$ in (D.3). Also the ambiguity in the choice of sign for the $\sin\zeta_{ij} = i\lambda^{\frac{1}{2}}(t_1,t_2,t_3)/2q_iq_j$ persists. The frames $\tilde{\mathcal{F}}_2$ and $\tilde{\mathcal{F}}_3$ are redefined analagously.

$\tilde{\mathcal{F}}_i$ and $\mathcal{F}_i$ are again related by a Lorentz transformation $g_i \in SO(2,1)$. However, to proceed as in the previous cases, we have to use a different parametrization of $SO(2,1)$, i.e.

$$g_i = u_z(\mu_i)a_y(\beta_i)a_x(\gamma_i) \qquad -\infty < \beta_i,\, \gamma_i < \infty \quad 0 \le \mu_i \le 2\pi \qquad (D.33)$$

where a_x and a_y are boosts in the $x-t$ and $y-t$ planes respectively. With this parametrization (provided we take g_i to transform from $\mathcal{F}_i$ to $\tilde{\mathcal{F}}_i$) we can once again absorb the $u_z(\mu_i)$ in our definition of the frames $\mathcal{F}_i$ and also have the $a_x(\gamma_i)$ commute with the rotations $u_x(\zeta_{21})$ and $u_x(\zeta_{31})$.

Repeating, for a final time, the calculation of P_1 in the various frames.
In $\tilde{\mathcal{F}}_1$

$$P_1 = (mcosh\xi_1 cosh\beta_1 cosh\gamma_1,\ mcosh\xi_1 cosh\beta_1,\ mcosh\xi_1 sinh\beta_1 sinh\gamma_1,\ msinh\xi_1) \qquad (D.34)$$

In $\tilde{\mathcal{F}}_3$

$$\begin{aligned} P_1 = (&mcosh\xi_1 cosh\beta_1 cosh\gamma_1,\ mcosh\xi_1 cosh\beta_1 sinh\gamma_1,\ mcos\zeta_{31} cosh\xi_1 sinh\beta_1 \\ &- msin\zeta_{31} sinh\xi_1, msin\zeta_{31} cosh\xi_1 sinh\beta_1 sinh\gamma_1 - mcos\zeta_{31} sinh\xi_1) \end{aligned} \qquad (D.35)$$

In $\mathcal{F}_3$

$$\begin{aligned} P_1 = (&mcosh\xi_1 cosh\beta_1 cosh\beta_3 cosh(\gamma_1-\gamma_3) - msinh\beta_3 cos\zeta_{31} cosh\xi_1 sinh\beta_1 \\ &+ msinh\beta_3 sin\zeta_{31} sinh\xi_1,\ mcosh\xi_1 cosh\beta_1 sinh(\gamma_1-\gamma_3), \\ &- mcosh\xi_1 cosh\beta_1 sinh\beta_3 cosh(\gamma_1-\gamma_3) + mcosh\beta_3 cos\zeta_{31} cosh\xi_1 sinh\beta_1 \\ &- mcosh\beta_3 sin\zeta_{31} sinh\xi_1,\ msin\zeta_{31} cosh\xi_1 sinh\beta_1 - mcos\zeta_{31} sinh\xi_1) \end{aligned} \qquad (D.36)$$

The evaluation of invariants now gives, using $\tilde{\mathcal{F}}_1$,

$$P_1.Q_3 \ = \ mq_3\ [-sin\zeta_{31} cosh\xi_1 sinh\beta_1 - cos\zeta_{31} sinh\xi_1] \qquad (D.37)$$

and in $\mathcal{F}_3$,

$$\begin{aligned} P_1.P_3 \ = \ m^2\ [&cosh\xi_1 cosh\xi_3 cosh\beta_1 cosh\beta_3 cosh(\gamma_1-\gamma_3) \\ &- cosh\xi_1 cosh\xi_3 cos\zeta_{31} sinh\beta_3 sinh\beta_1 + msinh\xi_1 cosh\xi_3 sin\zeta_{31} sinh\beta_3 \\ &- cosh\xi_1 sinh\xi_3 sin\zeta_{31} sinh\beta_1 + sinh\xi_1 sinh\xi_3 cos\zeta_{31} \end{aligned} \qquad (D.38)$$

Now we see some more significant changes. Comparing (D.37) with (D.14) and (D.26) we see that $cosh\beta_1$ has been replaced by $sinh\beta_1$ (in conjunction with

$sinh\zeta_{31} \rightarrow sin\zeta_{31}$). We recognize that the change of sign of $\lambda(t_1, t_2, t_3)$ produced by going from the $s-t$ to the $s-s$ region has, as anticipated, destroyed the real relationship between the z_i defined in the t_i channels and invariants of the form $P_i.Q_j$, so that now $z_i \leftrightarrow isinh\beta_i$. In Fig. D3 we have shown the location of the relevant physical regions in the z_i-planes, for the various values of the t_i. The $s-s$ part of one physical region fills the complete imaginary axis in each of the z_i-planes. However, the invariants also depend on $cosh\beta_i = \sqrt{z_i^2 - 1}$, which should change sign as we go from one s-channel physical region to a crossed physical region. This implies that, in the $s-s$ region, there are two physical sheets for each z_i-plane separated by branch-cuts connecting the branch-points at $z_i = \pm 1$. Crossing an incoming particle into an outgoing particle takes us from one sheet to the other in the corresponding z_i plane. Note that the same crossing can also be achieved by changing the sign of u_{ij} and u_{ik}, while leaving $\sqrt{z_i^2 - 1}$ unchanged. Therefore the second z_i-planes can alternatively be identified as the original z_i-plane but with a change of sign for u_{ij} and u_{ik}. (Note that if we have chosen $u_1 = u_{31} = u_{13}^{-1}$ and $u_2 = u_{23}$ as independent variables then changing the sign of u_{13} and $u_{12} = u_2/u_1$ corresponds to changing the sign of u_1 but not u_2.) This is important, of course, for the introduction of signature for complex helicity continuations. Finally we note that changing the signs of all the $sin\zeta_{ij}$ again corresponds to changing the signs of all the $cosh\beta_i$.

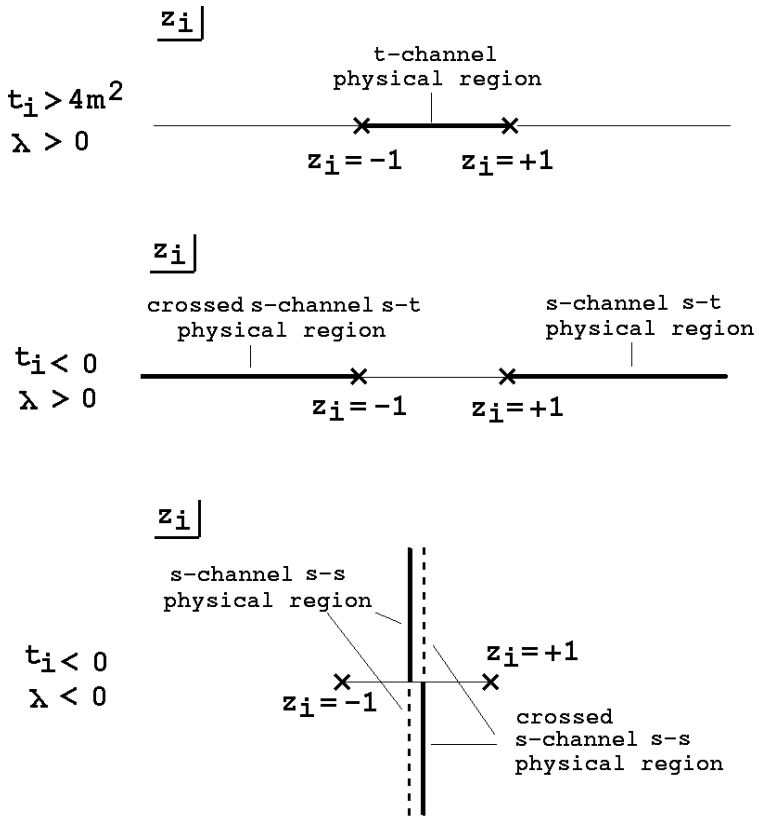

Fig. D3 Physical Regions in the z_i-planes

As we stated in Section 5, the asymptotic dispersion relation that we use should be initially written in an $s - t$ region of the s-channels. It is straightforward to continue it directly to any of the t_i channels. In the $s - s$ region it corresponds to using a combination of the upper and lower z_i half-planes (from the two sheets). Of course, that the $s-s$ physical region lies along the imaginary z_i-axes is very important for discussing the phases obtained from the S-W representation, particularly since it is only in this region that limits in which the u_{ij} are taken large (whether or not the z_i are large) are physical region limits.

References

[1] S. Coleman and B. Grossman, *Nucl. Phys.* **B203**, 205 (1982).

[2] P. Goddard and A. R. White, *Nucl. Phys.* **B17**, 1, 45 (1970).

[3] A. R. White, *Phys. Rev.* **D58**, 074008 (1998), see also Lectures in the Proceedings of the Theory Institute on Deep-Inelastic Diffraction, Argonne National Laboratory (1998).

[4] A. R. White, ANL-HEP-PR-99-108.

[5] A. R. White, Int. J. Mod. Phys. **A11**, 1859 (1991); A. R. White in *Structural Analysis of Collision Amplitudes*, proceedings of the Les Houches Institute, eds. R. Balian and D. Iagolnitzer (North Holland, 1976); H. P. Stapp ibid.

[6] H. P. Stapp and A. R. White, *Phys. Rev.* **D26**, 2145 (1982).

[7] V. N. Gribov, I. Ya. Pomeranchuk and K. A. Ter-Martirosyan, *Phys. Rev.* **139B**, 184 (1965).

[8] E. A. Kuraev, L. N. Lipatov, V. S. Fadin, *Sov. Phys. JETP* **45**, 199 (1977).

[9] J. B. Bronzan and R. L. Sugar, *Phys. Rev.* **D17**, 585 (1978). This paper organizes into reggeon diagrams the results from H. Cheng and C. Y. Lo, Phys. Rev. **D13**, 1131 (1976), **D15**, 2959 (1977).

[10] V. S. Fadin and V. E. Sherman, Sov. Phys. JETP **45**, 861 (1978).

[11] V. S. Fadin and L. N. Lipatov, *Nucl. Phys.* **B406**, 259 (1993)

[12] V. S. Fadin and L. N. Lipatov, *Nucl. Phys.* **B477**, 767 (1996) and further references therein.

[13] J. Bartels, *Z. Phys.* **C60**, 471 (1993) and references therein.

[14] A. R. White, *Int. J. Mod. Phys.* **A8**, 4755 (1993).

[15] A. A. Migdal, A. M. Polyakov and K. A. Ter-Martirosyan, *Zh. Eksp. Teor. Fiz.* **67**, 84 (1974); H. D. I. Abarbanel and J. B. Bronzan, *Phys. Rev.* **D9**, 2397 (1974).

[16] I. Halliday and C. T. Sachrajda, *Phys. Rev.* **D8**, 3598 (1973).

[17] R. C. Brower, C. E. DeTar and J. H. Weis, *Phys. Rpts* **14C**, 257 (1974), C. E. DeTar and J. H. Weis, *Phys. Rev.* **D4**, 3141 (1971).

[18] J. Berges and K. Rajagopal, *Nucl. Phys.* **B538**, 215 (1999) and references therein, see also G. W. Carter and D. Diakonov, hep-ph/9905465 (199) and references therein.

[19] V. V. Khoze, M. P. Mattis and M. J. Slatere. *Nucl. Phys.* **B536**, 69 (1998) and references therein.

[20] G. 't Hooft, *Phys. Rpts.* **142**, 357 (1986).

[21] D. J. Gross, hep-ph/9809060, *Nucl. Phys. Proc. Suppl.* **74**, 426 (1999).

[22] G. 't Hooft, *Nucl. Phys.* **B33**, 173 (1971).

[23] A. D. Dolgov and V. I. Zakharov, *Nucl. Phys.* **B27**, 525 (1971)¿

[24] G. 't Hooft, in Recent Developments in Gauge Theories, ed. G. 't Hooft et al. (Plenum, N.Y., 1980)

[25] T. Banks, Y. Frishman, A. Schwimmer and S. Yankielowicz, *Nucl. Phys.* **B177**, 157 (1981).